UNIVERSITÀ DEGLI STUDI DI PADOVA

Sede Amministrativa: Università degli Studi di Padova

Dipartimento: Territorio e Sistemi Agro - Forestali

SCUOLA DI DOTTORATO DI RICERCA IN:
"TERRITORIO, AMBIENTE, RISORSE E SALUTE"
INDIRIZZO:
"IDRONOMIA AMBIENTALE"

CICLO XXI

FLASH FLOOD ANALYSIS AND MODELLING IN MOUNTAIN REGIONS

Direttore della Scuola: Ch.mo Prof. VASCO BOATTO

Supervisore: Ch.mo Prof. MARCO BORGA

Dottorando: **MARCO SANGATI**

TABLE OF CONTENTS

ABSTRACT: "Flash flood analysis and modelling in mountain regions"

Flash flood are rare and localized phenomena, triggered by meteorological event with a pronounced spatial variability, with a precipitation gradient, at event scale, up to 20-50 mm/km. The consequences of these features is that the scientific and operational communities working on flash flood analysis have to deal with an impressive lack of data. Even a dense raingauge network may not be able to represent spatial variability of rainfall patterns associated with convective storms that trigger flash floods. Radar rainfall estimations, when correctly elaborated, are able to represent spatial patterns, but quantitative precipitation volume estimations need to be validated. In addition, concerning discharge data, the majority of the upstream and larger catchments affected by flash floods are not gauged and stream gauges, where present, are often damaged, so that peak discharge distribution along main and secondary river network is even less known than precipitation fields.

This study aims at covering the gap between needed and available data for flash flood event analysis, combining different methodologies. An *Intense Post Event Campaign* (*IPEC*) may be very useful to collect peak discharge estimations and time sequence of the flood in ungauged sections. Simplified hydrological model, based on rough runoff excess computation and set velocity propagation, can be used to cross validate quantitative distributed precipitation data from weather radar and peak discharge estimations collected during an *IPEC*. More complex and detailed model may help to improve the knowledge about flash flood associated phenomena, like debris flow.

Another objective of this thesis is to investigate the role of rainfall spatial variability in flash flood triggering. First a standard procedure to describe the variability catchment scale is needed. It will be so possible to study the relationship between rainfall input distribution and flood propagation dynamics. Then a simplified hydrological model is used to investigate the role of spatial variability in precipitation patterns: systematic studies are carried to describe the accuracy of rainfall volumes at basin scale and the effect of spatial variability within the basin.

Often the studies about flash flood dynamics are slow down or stopped because no measured data are directly to hand, or, if so, because they are not considered sufficiently

accurate. This work shows the possibility to combine together data with an assured degree of uncertainty, the only available or collectable existing data, and processed them with simple statistical and hydrological tools to obtain a more precise knowledge about past flash floods.

The remainder of this dissertation is organised as follows.

Chapter 1 "*Introduction*". The work starts with the aim to define what a "flash flood" is, underlying the importance to characterize such event according spatial and temporal proprieties. From this definition it follows that a generic flood can be classified according its own spatial and temporal proprieties and located in a specific point of a segment delimitated by the two ideal cases of "flash flood" and "flood at large scale".

Chapter 2 "*Literature review*". Spatial and temporal characterization leads to describe typical features of flash flood in different climates. Meteorological conditions able to trigger this kind of events are described and analyzed, with particular care about convective cells system organized in mesoscale structures. Finally some literature examples are reported to show different possible approach and to underline usual uncertainty when dealing with flash flood.

Chapter 3 "*Materials and methods*". This chapter summarizes and describes the tools used in this thesis to carry on flash flood analysis.

3.1 Weather radar data are used to describe rainfall spatial distribution and obtain quantitative estimations of rainfall patterns. Data acquiring and processing are described and most common errors are summarized along with most common procedures and algorithms to avoid and correct them. It is finally shown how merging radar and conventional raingauge network information can provide a more exhaustive description of rainfall fields, with quantitative estimation. This data processing is very useful for further characterization and analysis of past flash flood events.

3.2 Post event surveys are presented as an essential tool to collect the richest possible documentation. Measure campaigns are valorised to obtain qualitative and quantitative description of past floods. The goal is to complete the spatial and temporal precipitation knowledge and dynamic description, focusing on discharge estimation along hydrological network in term of peak values and timing.

3.3 Hydrological models can be routed for a better comprehension of flood dynamics at event scale. Two hydrological models, then used for flash flood analysis, are described in detail. The first one is applied at large event scale and starts from a distributed precipitation input. Hortonian runoff generation is applied punctually and superficial flood propagation is computed basing on fixed hillslope and channel velocity. The second model is built to be applied at very small catchment scale and simulate infiltration and transport processes for surface and subsurface flow through uniform hypothesis equations.

Chapter 4 "*Analysis of past flash flood events*". Some specific post flood analyses are collected in three sections.

4.1 Five flash flood events occurred in Romania are analysed with *HYDRATE* European project contribution. This study shows that even if the conventional hydrometeorological data are poor, weather radar information and hydrological modelling can help in understanding specific past flood dynamics.

4.2 *HYDRATE* project was also involved in the analysis of a flash flood occurred in Slovenia in September 2007, including radar processing and post event surveys. It is shown how this approach, characterize by time and cost significant efforts, is a precious tool to collect data and information for a detailed description that would be not possible through traditional hydrometeorological network.

4.3 A detailed model is used to describe surface and subsurface flow dynamics during the debris flow occurred in two small subcatchments in Fella river valley (North East of Italy), hit by a flash flood on August 29, 2003. The study mainly consists on liquid and solid mass balance during the different phases of the event.

Chapter 5 "*Spatial variability in flash flood events*". An analysis on rainfall spatial distribution is carried with the same tools on two different basin interested by flash flood event. The studies include a fist detailed analysis on rainfall spatial variability within selected subcatchments at different scales: spatial variability is described through time distance calculated in base of hydrological network. Then a simplified hydrological model is used to investigate spatial aggregation effects on mean areal rainfall and peak discharge value at subcatchment scale.

5.3 For Fella river basin (in Friuli Venezia Giulia region), ten subcatchments from 10.5 and 623km² are chosen.

5.4 For Cervo River (Piomente region, North West Italy) the study is applied to three flood events characterized by different rainfall spatial variability, and focused on four subcatchments (from 75 to 983km²).

Chapter 6 "*Conclusions*". Are here reported and summarized the main observations coming from the specific studies describe in the two previous chapters as long as recommendation for future research.

RIASSUNTO: "Analisi e modellazione di piene improvvise in zone montane"

Le piene improvvise sono fenomeni rari e localizzati, causati da eventi meteorologici caratterizzati da una spiccata variabilità spaziale, con gradienti di precipitazione che possono raggiungere, a scala di evento, i 20-50 mm/km. La conseguenza di ciò è che la comunità scientifica e gli enti operativi interessati nell'analisi dei fenomeni di piena si relazionano quotidianamente con una carenza di dati. Anche una fitta rete di pluviometri non è in grado di rappresentare la variabilità spaziale dei campi di precipitazione associati a fenomeni convettivi che innescano piene improvvise. Le stime di precipitazione ottenute attraverso il radar meteorologico, opportunatamente elaborate, sono in grado di rappresentare i *pattern* spaziali, ma i valori di volumi di pioggia necessitano di essere validati. Inoltre, per quanto riguarda i dati di portata, la maggior parte dei bacini colpiti da piene improvvise non sono strumentati e gli strumenti, dove presenti, risultano spesso danneggiati, cosicché la conoscenza della distribuzione delle portate al picco, lungo la rete idrologica principale e secondaria, è persino più approssimativa di quella della distribuzione spaziale della precipitazione.

Questo studio si prefigge di colmare la distanza tra i dati disponibili e quelli richiesti per un'analisi a scala di evento con riferimento a fenomeni di piena improvvisa. Un'approfondita campagna di rilievi post evento (in inglese *Intense Post Event Campaign, IPEC*) può risultare estremamente utile per raccogliere le stime di portate al picco e la sequenza cronologica dello svilupparsi della piena in sezioni non monitorate. Modelli idrologici semplificati, dotati di metodi elementari per la separazione dei deflussi e predeterminate velocità di propagazione, possono essere utilizzati per una validazione incrociata tra una descrizione quantitativa della distribuzione di precipitazione ottenuta attraverso il radar meteorologico e le stime di portate al picco raccolte durante un *IPEC*. Modelli più complessi e dettagliati possono migliorare il livello di conoscenza riguardo fenomeni associati alle piene improvvise, come le colate detritiche.

Un altro obiettivo di questa tesi è quello di investigare il ruolo della variabilità spaziale della precipitazione nei fenomeni di piena improvvisa. In primo luogo è necessario impostare una procedura che permette di caratterizzare tale variabilità all'interno di un particolare bacino idrografico, mettendo in relazione la distribuzione degli apporti meteorici con le modalità di

propagazione della piena. In secondo luogo si vuole indagare, attraverso l'applicazione di modelli idrologici semplificati, il ruolo della risoluzione spaziale della precipitazione. A questo fine è necessario separare due aspetti: l'accuratezza della stima dei volumi piovuti a scala di bacino e l'influenza della variabilità spaziale all'interno del bacino stesso.

Spesso gli studi che si concentrano sulle dinamiche delle piene improvvise sono rallentati o resi impossibili per il fatto che nessun dato misurato risulta utilizzabile così come disponibile, oppure perchè i dati di partenza non sono ritenuti sufficientemente accurati. Questo lavoro si prefigge di mostrare come sia possibile, partendo dai soli dati esistenti, disponibili o recuperabili, caratterizzati da un certo grado di incertezza, passare attraverso un'elaborazione tramite semplici strumenti statistici e idrologici al fine di ottenere una conoscenza più precisa riguardo passati eventi di piena improvvisa.

Si riporta una breve descrizione del contenuto dei capitoli della tesi, che sarà elaborata in lingua inglese.

Capitolo 1 "*Introduction*". Introduzione alla tematica che comprende una definizione del termine "piena improvvisa", convenendo sulla necessità di caratterizzare tali eventi in termini di proprietà spazio-temporali. Si nota che, a partire da questa definizione, è possibile classificare una generica piena in un punto di un segmento ai cui estremi ci sono i casi ideali di "piena improvvisa" e "piena a larga scala".

Capitolo 2 "*Literature review*". Partendo dalla caratterizzazione spazio temporale si descrivono le caratteristiche tipiche delle piene improvvise nei diversi tipi di clima, si individuano le condizioni meteorologiche in grado di innescare tali fenomeni, quali le celle convettive organizzate in strutture di mesoscala. Si riportano, infine, alcuni esempi di studi in letteratura che mostrano diverse tipologie di approcci e che sono indicativi dell'incertezza in cui si è soliti lavorare quando si approfondiscono questi temi.

Capitolo 3 "*Materials and methods*". In questo capitolo sono presentati i principali strumenti comuni a tutte le analisi di fenomeni di piena improvvisa presentati in questa tesi.

3.1 L'utilizzo del radar meteorologico per studiare, dal punto di vista quantitativo, la distribuzione spaziale della precipitazione. Vengono approfondite la modalità di acquisizione del dato, sottolineando le possibili fonti di errore ed i metodi più comuni per ovviare a questi inconvenienti. Viene anche mostrato come l'utilizzo

combinato di radar e tradizionali pluviometri renda più completa la caratterizzazione della precipitazione ai fini di un'analisi di una piena improvvisa.

3.2 Le indagini post evento, necessarie per raccogliere la maggior documentazione possibile, sono valorizzate al fine di una ricostruzione, anche qualitativa, delle dinamiche caratteristiche di una specifica piena. Queste, attraverso diverse metodologie, devono aiutare a descrivere la struttura spazio temporale della precipitazione e la stima di portata, distribuita lungo la rete idrica, in termini di valore al picco e di tempistica.

3.3 L'uso della modellistica idrologica applicata ad una miglior comprensione delle dinamiche a scala di evento. In particolare sono descritti i due modelli idrologici utilizzati. Il primo, da applicare a larga scala, parte da un input di precipitazione spazialmente distribuito e, attraverso un meccanismo *hortoniano* di separazione dei deflussi applicato puntualmente, propaga la piena in base a fissate velocità di versante e di canale. Il secondo, da applicare a bacini di piccolissima dimensione, simula i processi di trasporto superficiale e sottosuperficiale integrando le note equazioni di moto uniforme.

Capitolo 4 "*Analysis of past flash flood events*". Vengono qui presentate alcune analisi di eventi, distinte in tre sezioni.

4.1 Analisi di cinque eventi di piena improvvisa avvenuti in Romania nell'ambito del progetto europeo *HYDRATE.* Da questo studio risulta che, pur in presenza di scarsi dati provenienti dalle tradizionali fonti di monitoraggio idro-meteorologico, l'informazione proveniente da radar meteorologico e la modellistica idrologica possono aiutare nella ricostruzione delle dinamiche dell'evento preso in considerazione.

4.2 Analisi di una piena improvvisa avvenuta in Slovenia nel settembre 2007 per la quale, attraverso il progetto *HYDRATE* si è condotta un'indagine post evento. La ricchezza di questo approccio, pur dispendioso in termini di tempo, mostra un possibile percorso per recuperare le maggior informazioni possibili per eventi di piena che non sono ricostruibili solo attraverso le normali reti di monitoraggio idrometeorologico.

4.3 Analisi attraverso un modello dettagliato di deflusso superficiale e sottosuperficiale della colata detritica avvenuta in due piccoli sottobacini nella valle del fiume Fella, colpita da una piena improvvisa il 29 agosto 2003. Lo studio consiste

essenzialmente nel bilancio di massa liquida e solida durante le diverse fasi dell'evento.

Capitolo 5 "*Spatial variability in flash flood events*". Questa analisi sulla distribuzione spaziale della precipitazione è stata condotta con le medesime metodologie in due diversi bacini. Gli studi comprendono un primo approfondimento della variabilità spaziale della precipitazione all'interno di sottobacini di diversa estensione: la variabilità è descritta in funzione del reticolo idrografico del bacino preso in considerazione. Successivamente, attraverso un modello idrologico semplificato, si è valutata l'influenza della variabilità spaziale della precipitazione analizzando gli effetti dell'aggregazione spaziale in termini di precipitazione media su bacino e di portata al picco simulata.

5.3 Per l'analisi nel bacino del fiume Fella (FVG), colpito da una piena improvvisa il 29 agosto 2003, si sono scelti dieci sottobacini di dimensione variabile tra i 10.5 e i 623km².

5.4 Nel caso del fiume Cervo (Piemonte) lo studio ha riguardato tre eventi di piena con diversa variabilità spaziale della precipitazione e si è concentrato su quattro sottobacini (tra i 75 e i 983km²).

Capitolo 6 "*Conclusions*". Vengono riassunte le principali osservazioni ricavate dalle analisi descritte nei due capitoli precedenti e indicazioni per possibili future linee di ricerca.

Chapter 1 - INTRODUCTION

1.1 Definition of flash flood

FLOODsite, in its Language of Risk document [Gouldby et al., 2007], defines flooding as the inundation of a normally dry area caused by high flow or overflow of water in an established water channel (e.g., river, stream, drainage ditch) or the ponding of water at or near the location where substantial rainfall is experienced. Flooding occurs whenever a drainage system receives more water than it can handle. Flash flood is a specific form of flooding. Scientific and technical literature offers several definitions for flash flood. Most of them refer to the short time lapsing between the rainfall causative event and the flood peak: "A flash flood is a flood that rises and falls quite rapidly with little or no advance warning, usually the result of intense rainfall over a relatively small area" [AMS, 2000].

The short time scale of occurrence of flash floods has several implications, in term of definition. According to Kelsch et al. [2000]: "Flash floods are phenomena in which the important hydrologic processes are occurring on the same spatial and temporal scales as the intense precipitation". The short occurrence time implies also a short lead time for forecasting the flood event, as stressed by ACTIF (2004): "A flash flood can be defined as a flood that threatens damage at a critical location in the catchment, where the time for the development of the flood from the upstream catchment is less than the time needed to activate warning, flood defence or mitigation measures downstream of the critical location. Thus with current technology even when the event is forecast, the achievable lead-time is not sufficient to implement preventative measures (e.g. evacuation, erecting of flood barriers)."

In line with the definitions given before, in this study flash floods are defined according to their scales in space and time. A flash flood is a flood characterised by a rapid response, with water levels in the drainage network reaching a crest within minutes to six (USA conventional threshold) or ten hours (UE) after the onset of the rain event, leaving extremely short time for warning. Owing to the short response time, flash floods are localized phenomena that occur in basins up to few thousands km² [Hirschboeck, 1987; Gruntfest and Huber, 1991; Creutin and Borga, 2003; O'Conner and Costa, 2004; Borga et al., 2008]. Most flash floods occur in streams and small river basins with a drainage area of a few hundred square kilometres or less [Gaume et al., 2007]. Such basins respond rapidly to intense rainfall

rates because of steep slopes and impermeable surfaces, saturated soils, or because of human (i.e., urbanization) or fire induced alterations to the natural drainage.

Distinction between large floods (meaning: large spatial and temporal scales) and flash flood is important to capture typical features of a given flood and to improve a specific alert system for each of the two category of flood. Quantitative forecast are possible in the first case and the operational forces can follow the flood from upstream to downstream sections. Flash floods need real time weather observation system and detection of the possible risk area; people must be trained and informed about flood evolution since wrong personal behaviour (e.g., driving) can sensibly increase risk level. From a scientific point of view runoff generation may be quite different in the two cases: larger flood may be more sensible to cumulated rainfall while intense precipitation rate is the main needed ingredient to produce flash floods. This distinction is not that sharp: in a large scale flood, some small watersheds may be affected by flash flood dynamic due to local intense rainfall or particular hydrological basin features, so that any flood can be positioned in a specific point of a segment where the two ends are the ideal case of large and flash flood. Also from an operational point of view many mitigation procedures that aim to reduce damage risk are common for any kind of flood.

1.2 Flash floods as ungauged extremes

Owing to their characterising space and time scale, flash flood events are difficult to monitor. These events generally develop at space and time scales that conventional measurement networks of rain and river discharges are not able to sample effectively [Creutin and Borga, 2003] (see Tab. 1.I).

Physiologic unit	**Minimum density per station [area in km² per station]**		
	Raingauge (non recording)	Raingauge (recording)	Streamgauge (recording)
Costal	900	9000	2750
Mountainous	250	2500	1000
Interior plains	575	5750	1875
Hilly/undulating	575	5750	1875
Small islalnd	25	250	-
Urban areas		10-20	300
Polar/arid	10000	100000	20000

Table 1.I. Typical raingauge and streamgauge density in European countries [WMO, 1994].

As these events are locally rare, they are also difficult to capture during classical field-based experimentation, designed to last a few months over a given region, or on experimental catchments with drainage areas of a few km². This explains why the investigation of flash flood events is by necessity event-based and opportunistic as opposed to driven by observations from carefully designed field campaigns. Post-event surveys play therefore a critical role in gathering essential observations concerning flash floods.

Traditionally, indirect peak discharge estimates and collection of rainfall maxima have been used to document these events, as well as to provide an answer to the questions that are invariably asked after a major flood: why did such a major flood occur? and how frequently might such a flood be expected to occur? Collection of these studies contributed to the establishment of regional peak discharges envelope curves and to the development of more understanding of regional behaviour of extreme floods. However, focusing just on peak discharges and point rainfall maxima alone provides limited insight into the hydrological controls of flash flood response.

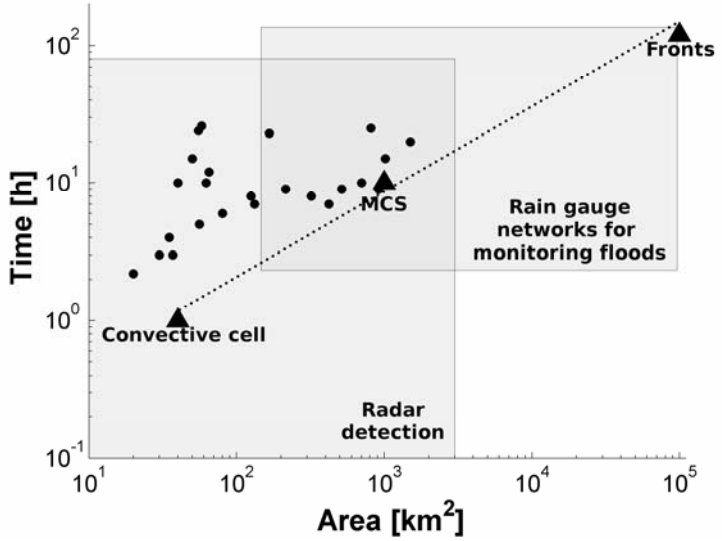

Figure 1.1. Schematic of flash-flood space-time scale versus monitoring capabilities of weather radar and raingauge networks. Dots represent time and space scales of a number of flash flood generating storms observed in Europe in the last 15 years [Borga et al., 2008]. Scales of convective cells, Mesoscale Convective Systems (MCS) and fronts are taken from Orlanski [1975].

Flash flood monitoring requires rainfall estimates at small spatial scales (1 km or finer) and short time scales (15-30 minutes, and even less in urban areas). These requirements are generally met by weather radar networks. This is shown schematically in Fig.1.1, which reports typical monitoring scales of weather radar systems and raingauge networks together with the time and space scales of a number of flash flood generating storms observed in Europe in the last 15 years [Borga et al., 2008].

Rapidly increasing availability of good quality weather radar observations is greatly expanding our ability to measure and monitor the rainfall distribution at the space and time scales which characterise the flash flood events [Borga et al., 2007]. These technical advances have the potential to enhance the information content of post-event surveys. Realising this potential calls for the development of a methodology for flash flood response survey which goes beyond the collection of indirect peak discharge estimates with the aim of rebuilding the

flood time sequences (in term of local intense precipitations as well as of hydrograph peak in distributed cross section along river network) and of collecting observation about phenomena (i.e., debris flow, landslides, woody debris) related to the flood.

1.3 Problem statement

Whereas progress has been made in the last decade in the integration of meteorological forecasts and radar observations in flash flood surveillance, lack of observations hamper advances on understanding the hydrological processes at work during flash floods, and, consequently, on forecasting the stream response to extreme precipitations.

Process understanding is required for flash flood forecasting, due to the fact that the small basins prone to flash-floods are rarely gauged and must be modelled without prior calibration. Furthermore, the dominant processes of runoff generation may change with the increase of storm severity, and therefore the understanding based on analysis of moderate flood events may be questioned when applied to forecast the response to extreme storms. In this sense, flash flood forecasting exemplifies the ungauged basin problem under extreme conditions.

Observational limitations mainly stem from the fact that flash floods develop at space and time scales that conventional observation systems of rain and river discharges are not able to monitor. Due to these limitations existing knowledge on flash flood events is relatively sparse. Improvement of understanding of rainfall-runoff dynamics during flash flood requires the development of an observational strategy capable to provide high-resolution data on storm and stream/landscape response during flash floods.

Hydrologic models are simplified, conceptual representations of a part of the hydrologic cycle; in particular they have as input rainfall data and as output discharge data. They are primarily used for hydrologic prediction and for understanding hydrologic processes. In the last decades several models with different complexity levels has been developed for different aims. Models are generally divided in two conceptual steps: the first is the rainfall-runoff generation and the second is water transport (on surface and in the ground). Each step may be lumped (averaged answer of the watershed) or distributed (computed in each cell with a certain resolution, in witch the basin is divided) and have coarser of finer assumptions. More complex models are theoretically closer to reality, but they need a greater number of calibration parameters, that means heavier terrain survey and long series of hydrological data [Sivapalan, 2006].

Flood modelling requires knowledge about terrain feature and initial moisture condition. These two aspects are crucial to simulate a correct runoff generation dynamic, but often in flash flood cases, it is not easy to collect this kind of data. Soil classification requires time and often uncertainties and lack of time suggest to use a simple sorting based on land use maps. In addition a solid scientific modelling should compare simulations of different flood in the same basin using the same calibration parameters. For flash floods it is uncommon to have significant historical flood data beside the analyzed case and so the only solution is to calibrate the model at the event scale.

The choice of a distributed input is needed for the high spatial gradient of rainfall fields during flash flood events. In this study a simpler model is used for cross checking rainfall and discharge data and a finer model, that includes a DEM based surface and subsurface propagation computation is used to analyse a specific debris flow phenomenon.

1.4 Purpose and objectives of study

The aim of this study is to contribute to a better understanding of the dynamics of flash flood triggered by intense rainfall; the analysis is extended to associated phenomena as debris flow and woody material transport. The first step consist in developing an integrated observation and modelling strategy that will allow to advance our capability to forecast flash floods in small and medium size humid catchments.

Several flash flood past event has been analyzed by collecting available data. Data collection and cross validation are used to analyze the common and different dynamics of past flash flood events occurred in different climatic region. The study is based on experimental data provided from the *HYDRATE* (HYdrometeorological Data Resource And Tecnology for Effective flash flood forecasting): a European Project, funded under the Sixth Framework Programme of the European Union. The idea of the project in based on sharing data from different European meteorological observatories (see Fig.1.2) to overcame the problems due to the fact that flash flood are rare and localized phenomena. In particular, flash flood events observed in the Piemonte and Friuli regions of Italy, in Slovenia and Romania provide the fundamental observations used in this study.

The event analysis is focused into the rainfall-runoff processes that are relevant to the production of flash flood on small and medium size humid catchments. The objectives of this study are:

- identifying common features of watershed that have experienced flash flood;

- recognizing meteorological structures able to generate flash flooding in different mountain regions;
- developing common procedures to describe space and time scales typical of meteorological events that trigger flash flood;
- giving suggestion to scientific community to develop a common strategy to share data and strategy for flash flood modelling;
- helping local alert and recovering technical service by describing typical flash flood dynamics.

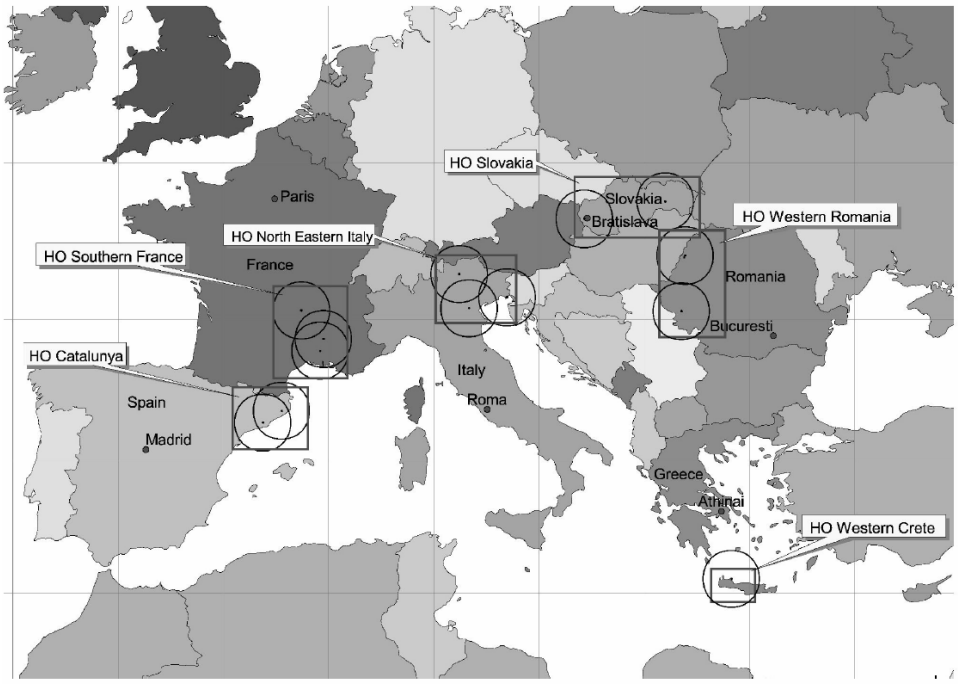

Figure 1.2. Meteorological observatories of the *HYDRATE* project.

Chapter 2 - LITERATURE REVIEW

2.1 General remarks

A flash flood is a localized phenomenon, it is generally caused by heavy or excessive rainfall in a short period of time and it is characterized by a rapid occurrence, often with little or no warning; usually it has a single, very high, peak discharge and total volume flow is not necessary important. Flash flooding occurs when the ground under a storm becomes saturated with water so quickly that it cannot be absorbed. The runoff collects in low-lying areas and flows rapidly downhill: rising water along drainage network is a suddenly result. Georgakakos and Hudlow [1984] state that in the UK flash floods have a time to peak of less than 3 hours within catchments of 5-10 km², whereas in the USA times to peak of up to 6 hours for basins of 400km². Gaume et al. [2007], analysing data for different hydro-climatic regions and for the last decades, show that in Europe flash floods are generated by intense rainfall that trigger the dispersed response of watersheds of some tens to some hundred km² and occur suddenly, with water levels in the drainage network reaching a crest within 1 to 10 hours after the onset of the rain event, leaving extremely short time for warning.

A particular case are flood waves caused by the collapse of a human made or a natural dam that realises huge amount of stored water (and materials) in a short period of time. On may 31 1898, after several day of heavy storms over a large region between Nebraska and Kansas the Lake Conemaugh rise until overflowing the South Fork Dam, that burst, allowing 20 million cubic meter of water to flow in that downstream river. The flood wave reached Johnstown, situated 23 km downstream the dam, less than one hour later; the disaster caused 2209 causalities: 99 entire families died, including 396 children [Rosental 1993]. A similar dynamic may occur when during a flood caused by intense precipitation wood logs and debris collect in a narrow stream cross section and form a temporary blockage.

Snow melting process is generally too slow to produce a fast hydrological answer, but, in some particular conditions, it can contribute to generate flash flood. Bonacci [2004] shows that Cetinje Polje flood (Montenegro) was a coincidence of rainfall and snowmelt extremes and bad human intervention. The Polje catchment between February 16 and 20 1986 experienced 670mm of cumulated precipitation and in the same period the sudden rise of air

temperature caused by warm southern wind led to a rapid melting of about 80cm thick snow cover. The flood was mostly caused by groundwater discharge due to artificial access tunnel to Cetinje karst Cave.

Flash floods are considered one of the most dangerous kinds of natural hazards because they combine the destructive power of a flood with incredible speed. They are extremely dangerous because of their sudden nature. The prediction and forecasting of flash floods is an extremely difficult and unreliable issue as explained by Lin [1999]: time intervals between the causative event and the flood peak is few hours; this leads to the fact that the standard and conventional flood warning techniques, models and organisation are not suitable for use with flash floods.

2.2 Space and time scales: meteorological and hydrological dynamics

The two necessary ingredients to produce fast hydrological answer are high runoff rate and fast superficial water propagation. These two aspects can be due to different combination of meteorological conditions and basin features.

High runoff rates can be produced only by intense rainfall storm. From a synoptic viewpoint, precipitation is produced by lifting moist air to condensation. The instantaneous rainfall rate at a particular point is assumed to be proportional to the magnitude of vertical moisture flux [Doswell, 1996]. Substantial water vapour content and rapid ascendant air are the ideal conditions to produce a heavy rainfall event. Large space-time metrological features, as stratiform structures, may cover a several thousands km² region for several days with low intensity and widespread precipitation, but doesn't produce intense precipitation rates.

A single convection cell is a common meteorological structure with a central area of 1 to 5km with approximately uniform rainfall rate, that reduce to zero within a distance less than 10km from the core. Rainfall intensity in the cell core is generally more than 90mm h^{-1} [Lin, 1999]. The life duration of a single cell cycle is about 20 minutes [http://www.mcwar.org] If the cell is in an active state, moisture and wind distribution may contribute to a regeneration process, where the downdraught of the decaying cell forces the uplift of a new one: convection storm may last up to few hours containing several rain-forming cells, building up and decaying within a matter of minutes. Single convective cell has not the water volume to produce a cumulated precipitation able to trigger a flash flood.

Multi convective cells can be organized with different spatial structures [Marwitz, 1972]. Supercells are features with a deep, continuously rotating updraft; supercells are usually found isolated from other thunderstorms, have strong updrafts and significant low

moisture associated with their environment. The first aspect is related to the high wind speed and the latter one limit the precipitation rate of supercells; heavy precipitations are possible when the structure evolves in a mesoscale convective system [Doswell, 1996]. When convective cells evolution brings to continuative moisture recharge and they are organized on the mesoscale, the whole structure may last for more than 3 hours and is called mesoscale convective system (MCS). MCS are the most common flash flood triggering storm since they produce high intensity rate and high cumulated precipitation. Sometimes initial convection is organized (due to fronts, drylines or orography) along lines; this feature can produce a pool of precipitation-cooled air, that tends to be the place for development of new cells, forming a succession of cell that pass repeatedly over the same location.

Although most flash flood events are produced by deep, moist convection, there are situations where high rate and cumulated rainfall are produced in a nonconvective situation. This may happen when strong updrafts are forced, leading to heavy precipitation: the most common way in which this dynamic occurs is caused by presence of vertical motion forced by orography [Doswell, 1996].

Runoff rate and flood propagation velocity depends, beside on rainfall intensity, on soil characteristic and antecedent moisture condition. Hydrological process in arid zones differs substantially from that in better documented humid environments. In arid or semi arid environments, marked by sparse vegetation cover and thin soil, the ponding point for infiltration is reached within few minutes from the first rain and overland flow forms the major component of basin runoff [Foody et al, 2004]. Drainage densities during intense storms are high, maximising the opportunity for water to reach the channel in a short time followed by a rapid propagation along the river network, due to smooth terrain especially if the basin is characterized by steeply sloping ground [Reid and Frostick 2006]. In arid region flash flood events are typically driven by intense convective thunderstorm cells with limited areal extent, usually less than 10–15km in diameter [Yatheendradas et al, 2008]. Intense runoff rate don't need in this climate high value of initial moisture condition and of cumulated precipitation and the dominant triggering variable is rainfall intensity. Important flash flood are experienced even with low value of total precipitation just in a portion of the entire catchment with important runoff coefficient (>0.5).

Humid climate in natural condition is associated with rich vegetation cover. Form the hydrological point of view it causes important initial losses in term of leaves interception and soil infiltration. In humid region elevated values of runoff rates and cumulated rainfall are needed to generate a flash flood events and runoff rate are not very high (generally less than

0.4). Borga et al. [2007] for a major flash flood in Northern Italy (a rainfall peak of 400mm in six hours, see Chapter 4.3 and 5.4 for more details) found initial abstraction up to 150mm and runoff coefficient between 0.05 and 0.25. Steep terrains favour flash flood generation both for a thinner soil and for faster superficial transport. Flash flood in humid climates commonly occurs in mountain regions, where great spatial variability is present and rainfall patterns are generally strongly influenced by orography. In these cases the scale of small basin is the one at witch the most devastating effects are produced.

Michaud et al. [2001], analyzing data from 130 steam gauging stations with a 30 year recording period and from 90 reports of exceptional floods in ungauged sections in small basin of United States, found that flash floods occurred in semiarid regions were caused by as little as 50-100mm of rain in 30-60 minutes, while in humid areas they were triggered by precipitation of 130-320mm in 1-12 hours.

Urbanization typically results in increasing flood peak magnitudes and major sensitivity of basin response to short-term rainfall rates [Smith et al., 2005]. Urbanized catchments, due to the impermeable and smooth terrain, answer with elevate runoff coefficient and fast propagation to storm. In addition people and building high density in villages and town increases the risk in term of human life and of economical losses, both in the case the runoff is generated in town and if the urban area is just along the drainage network.

Wildfire alters the hydrologic response of watersheds, including the peak discharges resulting from subsequent rainfall. The main hydrological consequences that fire produces are in decreasing the canopy interception, in reducing the average watershed infiltration rate and in consuming ground cover [Moody and Martin, 2001]. Infiltration rates have been shown to decrease by a factor of two to seven after wildfires, so that ingredients for flash flood generation may occur even with low values of return time precipitation.

Precipitation values are indicatory to understand the intensity related to extreme event and they are able to amaze also people used to relate with rainfall intense phenomena. Liljequist and Cehak [1984] reported world collected records: 31.2 mm in 1 minutes (Unionville, USA, 1 July 1956), 126.0mm in 8 minutes (Füssen, Germany, 25 May 1920) and 304.8mm in 42 minutes (Holt, USA, 22 June 1947).

As previously described, multi cell storm is the prevalent meteorological feature that triggers flash floods. Convective precipitations lead to an elevated spatial variability, emphasized where important orography is present. One of the most recent flash flood event reported by Rosso and Serva [1998] involved Versilia and Garfagnana regions in central Italy on June 19, 1996; it caused 14 causalities and was characterized by a strong rainfall spatial

variability: near the cost at Ponte delle Tavole (Forte dei Marmi) just 21 mm were measured while in the mountain gauges within 7km, 400mm were registered at Retignano and 440 at Pomezzano [www.meteogiornale.it].

The result of high spatial rainfall gradient is that just a small portion of the area hit by the storm experiences a precipitation with elevated cumulated and rate values. This is a limiting factor for the extension of the catchment hit by flash flood: the range varies between 10 km² or less to few hundreds of square kilometres. Adequate representation of this extreme rainfall variability even over small watersheds requires high-resolution rainfall estimates obtained from dense rain gauge networks, high resolution radar, or possibly even high-resolution numerical weather prediction models [Yatheendradas et al, 2008].

The capability to describe rainfall spatial variability is essential for hydrological modelling of flash flood events in small or larger basins. During a convective storm, the smaller is the basin, the stronger is the dependence from the estimated rainfall volume and the knowledge of the spatial precipitation fields. Some studies found that in small size basin the primary reason for evaluating spatial variability is the estimation of the total water volume of the model input; but, beyond this aspect, rainfall spatial patterns doesn't influence much the hydrological modelling [Shah et al., 1996]. These results may be model dependent, but it seems that often spatial variability is not sufficiently organized to overcome the smoothing effects due to the hydrological processes present in a real or modelled basin [Obled et al., 1994]. On the other side, Milly and Eagleson [1988] described the effect of rainfall spatial variability on runoff generation processed, considering relatively large catchments and modelled areas greater than the storm size, founding that a fixed volume of precipitation produce more runoff when it is concentred over a smaller area: runoff generation is characterized by a nonlinear behaviour, with threshold dependent response to rainfall.

Several studies analyzed the relation between maximum peak discharge and watershed area founding weak but statistically significant regressions and envelope rising curves enclosing the exceptional floods [Michaud et al., 2001]. It is quite common to normalize the peak discharge with the basin area, obtaining the specific peak discharge, with the purpose of comparing the severity of different floods in similar meteorological environment. Results differ according the climatic region considered but show specific discharge values grater than 20 m³/s/km² for small size catchments (<20km²) and up to 2-5 m³/s/km² for larger basin (>500km²).

The selected datasets for each *HYDRATE* observatory and an Austrian database have been plotted with their envelope curves as shown in Fig.2.1. The envelope curves, that

represent the bound of extreme flood events that have occurred in a given region, have been drawn using equation:

$$Q_s = aA^b \tag{2.1}$$

where Q_s is the specific discharge [m³/s/km²], a is a coefficient indicating the specific discharge theoretically associated to a unit area of the basin, A [km²] is the catchment area and b is the specific peak flow scaling exponent. This power law shape was theoretically justified by Gupta et al. (1996). For this analysis a value of b=-0.4 has been employed for all regional samples. Although Spanish and Greek datasets are represented by a small number of floods, it appears quite evident that flooding in the Mediterranean region is generally more extreme than in inland European regions.

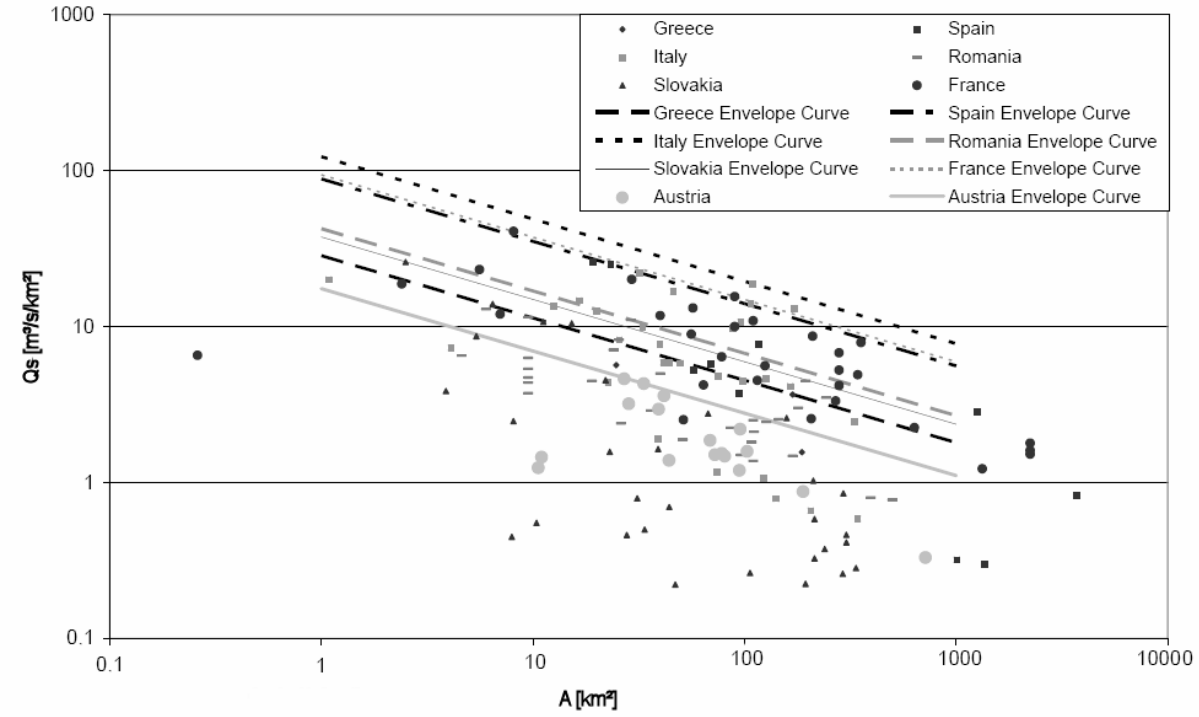

Figure 2.1. Data and envelope curves relative to the six *HYDRATE* observatories and Austrian database

2.3 Data sources: weather radar observation and survey campaign

Even a dense raingauge network may not be able to represent spatial variability of rainfall patterns associated with convective storms. It is quite common to have flash flood event in an anthrop zed region were none of the present gauges records a significant amount of rainfall. A correct use of weather radar information can provide rainfall patterns helpful for a better understanding of precipitation distribution, especially in mountain areas (where raingauge network is generally rarefied) and in urban catchments (where the hydrological answer is strongly dependent form rainfall spatial distribution) [Anidreu et al., 1996]. High spatial (1km²) and temporal (5 minutes) resolution would make of the weather radar the best

hydrological instrument to describe distributed precipitation fields. Radar data processing has considerably improved in the last decades, but uncertainties due to lack of electronic stability and miscalibration, ground clutter, beam blockage effects and fluctuations of the atmospheric conditions [Borga et al., 2002] limit the employment of wheatear data for real time applications. Post event processing is able to produce a detailed, realistic and robust spatial and temporal description of a storm event, especially when availability of raingauges data is copious. Rain gauge data can be useful both for calibration and for validation of processing parameters, needed to model attenuation and intensity to reflectivity relationship. A detailed analysis of radar data processing is described in the next chapter of this work.

Beside rainfall description also other hydrological values (e.g., soil characterization parameters) have problems due to uncertainties and lack of data sources. Discharge is the most important hydrological variable, but water level gauges are sparsely distributed along main and secondary drainage system. The majority of the upstream and larger catchments affected by flash floods are not gauged and often gauges are damaged during extreme floods. In any case rating curves that describe the relationship between the water level and the section discharge are never calibrated for extreme values. For this last reason the peak discharge data are affected, when gauges work correctly, by an error ranging between 20 and 50%. On the other hand gauges are extreme precious to reconstruct the timing of the flood.

In addition, the peak discharges appear to be spatially highly heterogeneous, even within small catchments. A detailed flash-flood study should not be limited to the few gauged river cross-sections if some exist. Flash-floods are by definition rare events and they are ranked as the most destructive process among weather-related hazards in many parts of the world. Not studying these extreme events because no measured data are directly to-hand, or if so, because they are not considered as sufficiently accurate, or even because it is time consuming, and limiting the hydrological analysis to moderate events on gauged watersheds, would be focussing on the trivial while skipping the essential [Gaume, 2006].

Since areas involved by flash flood are not predictable, the only possibility to have an exhaustive description of the flood dynamic is to conduct an *Intense Post Event Campaign* (*IPEC*). Indicators of the peak discharge values, mainly cross-section surveys based on flood marks, can be recognized even several months and up to some years after an extreme flood. Other important notions to rebuild the flood dynamic are indicators of the time sequence of the flood: mainly eyewitness accounts where no stream gauge measurements are available.

2.4 Risk management and literature examples

The management improvement of flash flood risk is delayed compared to other natural or anthropoid disasters as floods, tornado or fire. Until few decades ago the term "flash flood" had not a specific definition from an operational point of view. Often damages and causalities were computed in other categories (e.g., generic flood, car accident) [Burrell et al. 2002]. The fast moving and violent features, the short lead time and the long return period are the main limiting factors for an improvement of forecasting and alert system. Flash floods usually affect small areas and regional and national media treats each disaster as a unique and non predictable one. Target and victim are not located in expectable area: they are often just a car travelling along a road or a hiking group of tourists in the mountains. Flash flood management requires long term decision as an accurate study of past event, a preparation of the population to this kind disaster, and a specific training for the alert system. Modelling and understanding past event dynamic can help and strengthen the effort for a better risk management.

As referring point it is useful to resume some results on past flash flood study. Here we present two well known typical flash floods in small (<100km²) mountain catchments: the first in humid climate and the second in arid one; the latter case is also interesting to highlight potential uncertainties regarding peak discharge estimation for extreme floods. The third case consists in an intense rainfall event that affected a large area (several thousands km²) with many victims and huge damages.

- The Avene watershed is located in the French Mediterranean area. It is a rural watershed of 57 km². The downstream part is covered by agricultural lands and scrub. Forested areas are predominant in its upstream part. Two thirds of the Avene river watershed is composed of a limestone plateau covered by 1 or 2 m deep sandy soils. The upstream part of the catchment is mountainous (culminating point at 695 m), with a diverse geology (limestone, schist and sandstone) and shallow soils. In 1997 a flood was caused by a very heavy rainfall event: in the night between October 6 and 7 over 300 mm of rain in six hours have been measured at some private rain gauges. The French technical services estimated, on the basis of the Manning–Strickler formula applied on various river sections, which the maximum downstream discharge was between 600 and 900 m³/s. With a specific discharge of 10–15 m³/s/km², the Avene flood is one of the most important floods ever reported in France for similar catchment areas [Gaume et al., 2003]. The interviews and the flood marks inventory were conducted in October 1998: one year after the flood. The event had left traces in the

landscape (flood level and erosion marks) and witnesses had a clear recollection of it, many of them having their lives been threatened.

- The 49 km² Bronco Creek watershed is located in west-central Arizona, an arid region, near the southerner end of the Hualapai Mountains. The mean annual precipitation is 240mm and the highest topographic relief in the basin is 950m above sea level [House and Pearthree, 1995]. On August 19, 1971 three separate convective thunderstorms hit the Bronco Creek catchment and a total precipitation between 76 and 89 mm was registered by an unofficial gauge within the basin. The discharge estimate, based on critical depth calculation, was carried by the US Geolocical Service. The value of 2080 m³/s makes it virtually the world's largest known rainfall generated flood to come from a 50 km² basin [Costa, 1987]. The estimation was rated as "poor" meaning a possible error of ±25%. House and Pearthree [1995] states that the original estimation did not considered the changes that the flood debris produced in the channel. Using historical areal photographs they reconstruct pre and post flood geometry, estimating the peak in 750-850 m³/s.

- The 8–9 September 2002 catastrophic event resulted in 24 casualties and an economic damage evaluated at 1.2 billion euros in the Gard region, France, with a humid climate. A description of the synoptic meteorological situation shows that no particular precursor indicated the imminence of such an extreme event. Radar and rain gauge analyses are used to assess the magnitude of the rain event, which was particularly remarkable for its spatial extent with rain amounts greater than 200 mm in 24 h over 5500 km² [Delerieu et al, 2005]. The maximum values of 600–700 mm observed locally are among the highest daily records in the region. The preliminary results of the postevent hydrological investigation show that the hydrologic response of the upstream watersheds of the Gard and Vidourle Rivers is consistent with the marked space–time structure of the rain event. It is noteworthy that peak specific discharges were very high over most of the affected areas (5–10 m³/s/km²) and reached locally extraordinary values of more than 20 m³/s/km².

Chapter 3 - MATERIALS AND METHODS

3.1 Radar rainfall estimation

3.1.1 Weather radar fundamental

RADAR is an acronym of RAdio Detection and Ranging and it is essentially a tool able to generate and detect electromagnetic waves that are reflected by objects hit by the radar beam. After World War II radarmeteorology had an intense impulse due to the surplus of war radar working in frequencies adequate to detect rain drops in atmosphere. Several researchers realized that radars are able to describe meteorological features with spatial and temporal scales much more resolute than any other tools. Since late 50's radars have been used to follow convective cell systems and cyclone evolution and, in some counties, they have been employed to alert authorities and population. With computer evolution in the 70's radar potential were amplified by the possibility of storing and elaborating great amount of data.

Weather radar antenna used for specific meteorological objectives have a circular-parabolic shape that permit to focus the radar signal in a specific direction. Radars are able to move in two orthogonal directions: azimuthally and vertically. Consequently, different ways to detect atmospheric condition are possible (see Fig.3.1).

- PPI (Plan Position indicator) when elevation angle is constant and radar can rotate around it vertical axis; this procedure allows to screen a conical area that is then projected in a horizontal plane.
- RHI (Range Height Indicator) when azimuth direction is constant and detection is limited to a vertical profile.
- CAPPI (Constant Altitude Plan Position Indicator) is a complex procedure that allows to map the atmosphere at a constant planes level; this result is possible when the entire volume is already scanned, and so just in post analysis phase, while the other procedures can be obtained in now casting.

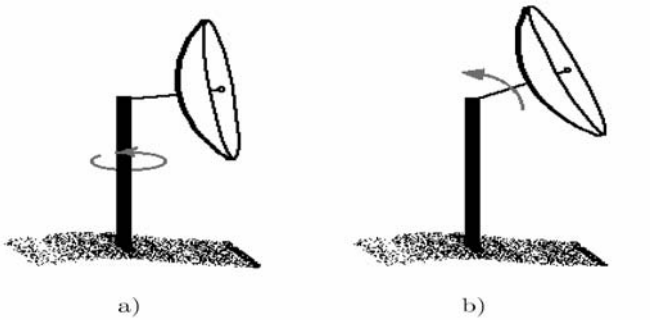

Figure 3.1. Representation of the two radar working procedure: a) PPI and b) RHI.

Electromagnetic waves interact with objects when their length is comparable with object dimension. Wavelength is tied to frequency so that the product of the two values give the propagation velocity (c=3 x 10^8 m/s). The ideal wavelength for rainfall detection is a compromised between rainfall drop size (up to few millimetres) and the will to minimizes attenuation process (due to interaction with rainfall and other particles), so that weather radars usually work in microwaves range in X, C and S bands (see Tab.3.I). X band radars have the advantages that they need quite small antenna so that they are quite cheep to be build and there is the chance locate them in mobile structures; on the other hand short X band microwaves actively interact with atmospheric particles and are affected by strong attenuation so that these tools work well only in a 50km range. On the other extreme S band antenna need big structures where to be installed, they are more expensive, but are less affected by attenuation, since they work with longer wavelengths, and they are able to give information about rainfall spatial distribution up to 200km. C band radars behave in intermediate way and are the most common tools used by public administration and are able to provide good precipitation estimation in a 120km range.

band	**frequency [GHz]**	**wavelength [cm]**
S	2 – 4	15 – 8
C	4 – 8	8 – 4
X	8 – 12	4 - 2.5

Table 3.I. Typical wavelengths and frequencies for weather radar.

When a radar beam hits an object in its propagation path, the electromagnetic wave is scattered so part of its energy returns back to the receiver. This back-scattering radiation has much less power of the transmitted one and the total power return signal increases with the number of the detected objects and with their dimension. The double of the distance (direct and return paths) of the hit object is obtained by multiplying velocity c by the time that the signal needs to arrive back to the receiver. Spatial resolution depends on beam wideness, object distance and impulse duration: typical values of 1μs leads to 150m length resolution; a beam 0.2° wide means 350m at 100km distance. Final spatial data are then elaborated and stored in square pixel raster format with resolution of about 250m-1km. Temporal resolution is function of the antenna rotation velocity and it is generally around few minutes. Whether radar theory is based on the assumption that most of the scattering in atmosphere is due to raindrops so the power of the return signal is an indicator of rainfall intensity.

The power of the return signal P_r is measured by the receiver and converted in the reflectivity Z according to Eq.3.1, where C depends on radar proprieties (i.e., power, wavelength) and it is constant, r is the distance from the radar to the targets (i.e., rainfall drops) while k is the imaginary part of the refraction index and depends on target surface: $|K|^2$ is about 0.93 for rainfall drops at 0°C and 0.176 for ice particles.

$$Z = \frac{P_r r^2}{C|K|^2} \tag{3.1}$$

Electromagnetic scattering have been studied exhaustively by Mie, but in case the dimension of the targets D are smaller that the wavelength (specifically $D<0.16\lambda$), as for whether radar, Rayleigh simplifications (early 1900) are used. These lead to the reflectivity dependency on the drop size distribution $N(D)$ as:

$$Z = \int_0^\infty D^6 N(D) dD \tag{3.2}$$

This last equation shows that reflectivity is very sensible to the dimension of the raindrops, since there is a 6 power factor in the relationship: an adequate study of drop size distribution (DSD) is needed before starting with quantitative rainfall estimation. Since Z varies in a wide range reflectivity value is usually reported in a logarithmic scale:

$$dBZ = 10 \log_{10} Z \tag{3.3}$$

DSD is usually modelled according predefined distribution equation. The simplest is the one-parameter exponential model, but its assumption lead to overestimation the number of both smallest and biggest drops [Joss and Gori, 1978; Waldvogel, 1974]. Ulbric [1983] proposed the three parameter (N_0, μ, and Λ) gamma function:

$$N(D) = N_0 D^{\mu} e^{-\Lambda D} \tag{3.4}$$

that is capable of describing a broader range of raindrop size distributions than an exponential distribution (a special case of the gamma distribution with $\mu=0$ and N_0 tied to Λ). The three parameters of the gamma DSD can be obtained from three independent remote measurements such disdrometer or vertical reflectivity profile measurement (see later).

3.1.2 Z-R relation for rainfall estimation

The main objective of weather radars, from hydrological point of view, is providing spatially distributed quantitative estimations on rainfall rate. The reflectivity maps have to be converted in rainfall fields, but this is a process that contains different types of uncertainties and error sources. In general reflectivity up to 15-20 dBZ means no or light rainfall (higher no rainfall values correspond to cloud reflectivity), and reflectivity values between 40 and 50 dBZ generally means convective precipitation. Reflectivity value grater than 60 leads to assumption of hail presence, due to the fact that ice reflects much more than water surface. The conversion from reflectivity to rainfall rate can be accomplished using many different approaches, the most popular, however, is the use of power type function with two coefficients a and b.

$$Z = aR^b \tag{3.5}$$

Relationship of this type should be regarded as empirical although strong theoretical justification exists for this choice. The justification is the fact, that both radar reflectivity and rainfall rate can be expressed as moments of drop size distribution within a radar sampling

volume. This is where the first problem appears with using raingauge observations for parameter estimation of *Z-R* relationship. Most rain gauges do not measure rainfall rate but rather, rainfall accumulation. The radar sampling volume is often located at elevation as high as 1-2 km, with potentially significant time displacement (up to several minutes) which creates difficulties in time and space synchronization of the two measurements [Krajewski, 1995]. Also, the radar sampling volume is much larger than the raingauge one. These problems, when combined with extremely high space and time variability of rainfall, indicate that one should not expect high correlation between raingauge observed rainfall and radar-estimated rainfall at short time scales.

Researchers	a	b
Marshall and Palmer, 1948	200	1.6
Joss and Waldvogel, 1968	300	1.5
Sekhon and Srivastava, 1970	300	1.35

Table 3.II. Different empirical parameterizations for *Z-R* power relationship: R in mm h^{-1} and Z in mm^6m^{-3}.

The idea of a relation between reflectivity Z and rainfall rate R started with early weather radar studies [Marshall and Palmer, 1948], but that relation is not unique, but is event (mainly due to different DSD) dependent so that many other empirical parameterisation of the same equation are commonly used. Tab 3.II shows different sets of parameters find by other researchers [Joss and Waldvogel, 1968], the third one calibrated specifically for convective precipitation [Sekhon and Srivastava, 1970]. Fig.3.2 reports 69 empirical parameterizations collected by Battan [1973] in a logarithmic graph, and indicate the ideal goal to have a specific parameter estimation for each studied event. This would be theoretically possible if disdrometer network would be denser, but since these instruments are quite costly it is not practically reliable.

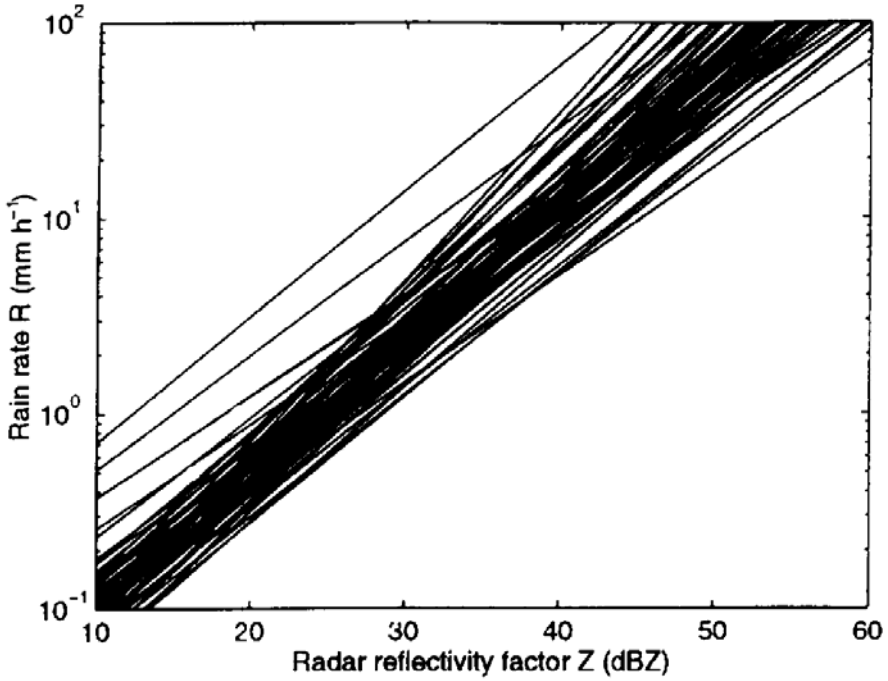

Figure3.2. 69 Z-R relation collected by Battan [1973].

Since DSD is not constant in the same event some studies suggest spatially and temporally distinction inside the same event: Steiner et al. [1995] proposed a storm classification method to separate convective and stratiform regions within the rainfall event basing on the basis of the intensity and sharpness of the peaks to echo intensity. Good results are found using different methodologies in different events, but complex procedures that perfectly fit in one case may not provide satisfying rainfall fields in other cases. In this study (Chapter 4 and 5) physically based assumption are considered and parameter calibration is done, where possible, with punctual comparison between raingauge and radar precipitation values. This technique is the oldest one and probably sill the most common. Even with limitation due to comparison between punctual (raingauge) and mean volumetric (radar) data, this procedure provides a simple tool to validate precipitation fields from radar processing. Radar and raingauge data can be displayed (as shown in Chapter 4) in a dispersion graph at the event scale or at finer ones (e.g., hourly). When data are linearly well correlated with unitary slope, it mean that raingauge and radar give coherent spatial data; if correlation is good but slope scientifically differs from 1 radar overestimation or underestimation is probable: all rainfall fields can be multiplied by a factor to reduce or eliminate bias between radar and raingauges; if the graph shows no correlation it should lead to consider different hypothesis (e.g., parameters, physical correction, raingauge errors) and hopefully to conclude with more coherent results.

The quality of final radar rainfall estimates can be evaluated by comparison between hourly rainfall estimates obtained from radar observations and from raingauges, and summarised by means of three statistics:

1) the fractional standard error (FSE)

$$FSE = \frac{\left[\frac{1}{N_t N_s}\sum_{i,j=1}^{N_t N_s}\left(R_{i,j} - G_{i,j}\right)^2\right]^{0.5}}{\frac{1}{N_t N_s}\sum_{i=1}^{N_t} G_{i,j}} \tag{3.6}$$

2) the mean relative error (MRE)

$$MRE = \frac{\frac{1}{N_t N_s}\sum_{i,j=1}^{N_t N_s}\left(R_{i,j} - G_{i,j}\right)}{\frac{1}{N_t N_s}\sum_{i=1}^{N_t} G_{i,j}} \tag{3.7}$$

and

3) the correlation coefficient,

where N_t is the number of hours in the storm event, N_s is the number of raingauge station used in the evaluation, $G_{i,j}$ and $R_{i,j}$ are the raingauge measurement and the corresponding radar estimate at time step *i* and for the raingauge station *j*.

3.1.3 Error sources and advances in radar research

Beside errors due to Z-R miss calibration other typical problems are found when using weather data for rainfall estimations. To avoid them there are some recommendations during volume scanning performance. Other improvements can be obtained in post processing phase with appropriate algorithms and procedures.

Most error sources derive from radar physics and atmospheric or terrain features. Since radars are continually rotating during data acquirement it is important that the azimuth position is always better known; in general automatic procedures check the North position during rotation, but periodically manual checking can avoid difficult post processing corrections.

Ground clutter can disturb the radar measure, since fixed objects, as an orographic relief, cause back radiation that receiver is not able to distinguish from rainfall drop scatter signal. Since the velocity of fixed objects is null they can be detected by Doppler methodology, searching pixels with no velocity and removing those data from rainfall estimation fields. Ground clutter at a certain elevation can also be detected by using radar maps obtained with observations in dry condition: when terrain echo is not important (up to 10dBZ) ground reflectivity can be subtract to total one before proceeding with data elaboration; for local and sharp clutter pixel reflectivity can be substituted by interpolation of near values. Ground clutter corrections are generally taken in account by the agency that provides radar data, which generally keeps also raw reflectivity fields.

Radar beam, along its propagation path, can be partially or totally occluded by orography. This problem can be avoided or reduced when radar location is decided. When working in mountain regions total occlusion often reduces radar visibility, while partial beam occlusion can be corrected modifying assumption in using Eq3.1, and specifically the parameter C should varies according to occlusion maps: with no occlusion the total wave power hit atmospheric particles; when part of the beam propagation is interrupted by orography only the not occluded portion of beam power must be taken in account, so C parameter is reduced by the occlusion factor [Vivekanandan et al., 1999]. Occlusion maps can be derived by DEM elaboration for the used radar angle elevations [Anagnostou et al., 2008]. In general data with different elevation are available so occlusion decreases when considering higher radar elevation. Choosing best elevation is a compromising procedure to minimize beam blockage and errors due to vertical profile reflectivity variations (see further). Increasing the elevation angle leads also to scan meteorological event at a major distance from terrain; the higher part of the atmosphere displays greater difference when compared with terrain rainfall estimations.

One of greater problem in radar data accuracy is that reflectivity is not homogeneous at different altitudes. Several factors contribute to this feature: evaporation, air turbulence and, above all, water changing from liquid to solid form or vice versa. Despite the fact that radar

observations in rain show considerable variety in the shape of echoes, the various reflectivity profiles can be grouped in five classes [Fabry, 1995].

1) Low level rain, that includes all stratiform rain or drizzle echoes when precipitation forms directly in the liquid form: reflectivity decreases very rapidly with height.
2) Rain with bright band, that it is the most common profile in temperate latitudes and at low to moderate rain rates (Fig.3.3 from Fabry and Zawadzki [1995]): reflectivity is roughly constant from the ground up to the level of the melting layer where is found an enhancement of the reflectivity, the bright band; above the melting layer, the reflectivity of snow decreases on average at a rate of about 6 to 7 dB/km in the first kilometre above the bright band.
3) Rain from compact ice: this profile is similar to the previous one except that no clear bright band can be found and the profile undergoes a quick transition from the rain regime to the ice regime through a sudden decrease of *Z*.
4) Showers: as in case 1 the precipitation forms directly in the water phase isolated showers and convective rainbands, which are indistinguishable in terms of vertical reflectivity profiles: reflectivity is generally constant from the ground up to 1 km from the echo top beyond which the reflectivity rapidly decreases.
5) Deep convection, exclusively generated by thunderstorms: this type of echo displays the most significant variability in time and strong reflectivities extend several kilometres above the level of the 0°C isotherm.

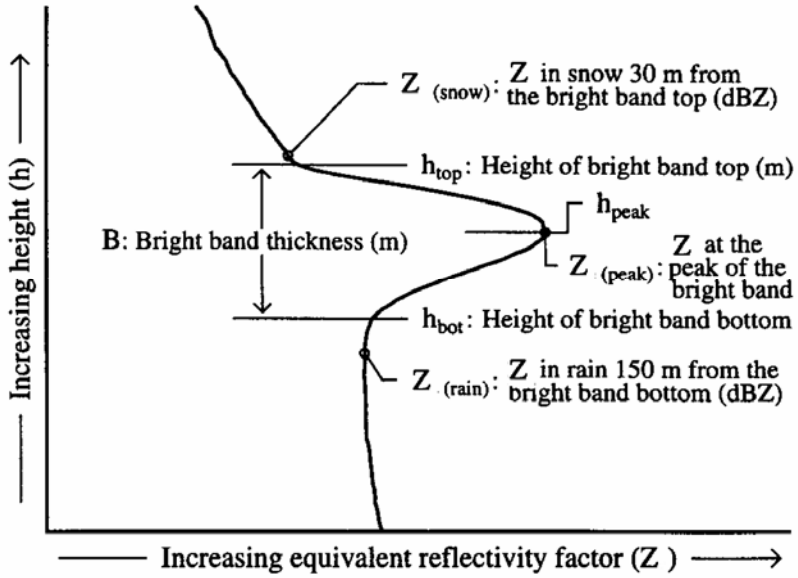

Figure3.3. representation of reflectivity profile of rain with bright band [Fabry and Zawadzki, 1995]

When radar beam intersects the melting layer, correctly describing the rate of decrease of reflectivity with height above the bright band can have a considerable impact on the quantitative accuracy of rainfall estimates at longer range [Lewis et al, 2007]. Several correction schemes have been developed to prescribe the observed profile shape above the bright band using radar data from multiple elevation scans; most methods are based on

assuming that the reflectivity expressed in dBZ decreases linearly with height and decreasing slope is found by vertical profile of reflectivity (VPR) scansion from the radar. In the events studied in this thesis VPR is not considered since they consist on convective events in summer period: combination of high melting layer and choosing low elevations avoids significant variation in VPR. Hail presence is another source of intensity and can lead to local overestimation; when solid precipitation is present or presumed a threshold for *Z* is chosen to limit overestimation due to high ice surface reflectivity.

Attenuation is another common problem in analyzing reflectivity fields since electromagnetic waves interact with atmospheric gases, clouds and rainfall drops and loose part of their power along the propagation path due to scattering and absorption. Hitschfeld and Bordan [1954] studying attenuation for different wavelength show that at 10cm or longer length attenuation is almost negligible, while its effect become increasingly more serious as the wavelength is reduced. In standard radar equation (Eq.3.1) no attenuation effect is taken in account. If the thickness of the absorbing medium to be traversed is *dr*, the drop in the power received, dP_r, may be written as:

$$\mathrm{dP_r} = -2\Lambda' \mathrm{P_r dr} \tag{3.8}$$

where Λ' is the attenuation constant of the medium; the factor 2 arises from the fact that, in case of weather radar, each element of the path is traversed twice: from antenna to the target and then back to the receiver. Attenuation increases with distance from radar and varies according to medium characteristic. Integrating Λ' along the path the attenuation effect can be divided in three different components:

$$\int \Lambda' \mathrm{dr} = \int \mathrm{k_1 dr} + \int \mathrm{k_2 M dr} + \int \mathrm{k R^{\alpha} dr} \tag{3.9}$$

respectively due to atmospheric gases, clouds and precipitation. The three parameter k, k_1 ,k_2 and α exponent can be derived by past studies or calibrated for the specific studied event, while *M* depends cloud density.

The first two terms are negligible for convective storm occurring not too far from the radar, as in the past event studies presented in this work, while the dominant attenuation phenomena are due to rainfall. Hildebrand [1978] presents a method where the attenuated radar reflectivity measurements at distance *r* are converted to attenuated rainfall rates and to attenuation estimates k_a (express as the drop in *Z* due to attenuation across the pixel transport). With appropriate assumptions concerning DSD and temperature a new estimate of reflectivity fields can be produced with the relation:

$$\log Z'(\mathrm{r}) = \log Z(\mathrm{r}) + 2\sum_{\mathrm{x}=1}^{\mathrm{r}-1} \mathrm{k_a(x)} \tag{3.10}$$

and new reflectivity Z' is used to derive revised attenuation estimates $\mathrm{k'_a(r)}$. This procedure can be repeated iteratively repeated until a further step doesn't produce any significant changes in reflectivity fields and final *Z* is used to calculate rainfall rates corrected for attenuation.

Modern weather radars have the possibility to distinguish the received electromagnetic signal between horizontal and vertical polarisation, Z_{hh} and Z_{vv}. These two values differ since rainfall drop are not spherical. A new parameter, named differential reflectivity, is defined as:

$$Z_{DR} = 10\log_{10}\left(\frac{Z_{hh}}{Z_{vv}}\right) \tag{3.11}$$

that is less affected from attenuation than standard Z. Differential reflectivity can be used to distinguish intense ($Z_{hh}>>Z_{vv}$) from weak ($Z_{hh}\approx Z_{vv}$) rainfall rates. Bringi et al. [1998] proposed:

$$R = 0.0017 Z_{hh}^{\ 0.91} Z_{DR}^{\ -4.03} \tag{3.12}$$

and this type of equation seems to be less fluctuating than usual Z-R relation. Z_{DR} is also used to detect hail: solid precipitation has a quasi spherical shape and so it result that Z_{DR}=0. In addition some polarimetric radar may measure also differential phase from horizontal and vertical component:

$$\phi_{DP} = \phi_{hh} - \phi_{vv} \tag{3.13}$$

and it is found [Hubbert and Bringi] that its spatial differential, called K_{DP}, is linearly correlated to rainfall intensity; filtering techniques must be considered in the analysing since measured are affected by noise. These two techniques are here presented for a complete picture on actual radar research and potential, but they are not used in the analysis.

3.2 Post flash flood survey

3.2.1Purpose of post event surveys

Flash-floods are rank as the most destructive process among weather-related hazards in many parts of the world. Not studying these extreme events because no measured data are directly to-hand, or if so, because they are not considered as sufficiently accurate, or even because it is time consuming, and limiting the hydrological analysis to moderate events on gauged watersheds, would be focussing on the trivial while skipping the essential [Gaume, 2006].

The analysis of the past experiences shows that two main types of post-flood investigations can be distinguished in base of their objectives and contexts. The first type is generally commissioned by the local or national authorities after a major catastrophe. The main objective is to answer questions raised by the public opinion and the local stakeholders on the causes of the floods, the possible human impacts on the flood magnitude and frequency, but also on the management of the crisis, the efficiency of the flood mitigation measures and the solutions to recover from the flood and to limit the future risks. A second type of post-flood investigations is conducted by technical services like the U.S. Geological Survey or the IRPI in Italy (Istituto di Ricerca per la Protezione Idrogeologica) for instance or by research institutions. In these cases the aim is documentation of extreme events. Most of the past works have been limited to a description of the event through the available measured data (rain gauge or river gauge measurements) and some field observations as cross-section surveys and corresponding peak discharge estimates. Sometimes the description of the mass transfer processes, of their localisation and the estimation of the transferred volumes is provided. A detailed rainfall-runoff analysis of the event is rarely done due to the lack of measured rainfall and discharge data.

The inventory of the extreme events and their peak discharge values is of course important to define the range of the possibilities, to built envelope curves and to study the regional patterns of the river flood extreme peak discharges, or to reduce the uncertainties in flood frequency analysis [Payrastre et al., 2005]. The recent developments of the measurement networks, especially the weather radar networks, open new perspectives for the analysis of flash-floods. The weather radar provides rainfall estimates at appropriate space and time resolutions. It seems therefore now possible to get deeper into the analysis of the rainfall-runoff dynamics of the watersheds.

Due to the time-space characteristic scale of flash-flooding, the majority of the upstream catchments affected by these floods are not gauged. In addition, the peak discharge appears to be spatially highly heterogeneous, even within small catchments. A detailed flash-flood study should not be limited to the few gauged river cross-sections if some exist. Flash-floods are by definition rare events. If an intensive research activity is to be set up on these hydrological events, it is necessary to develop specific methods to collect and analyse the

existing information about the floods when and where they occur and not to limit the analysis to the few events affecting gauged watersheds.

For a flash flood post event investigation there are three main types of data that the analysis must consider:

1) Indicators of the peak discharge values: mainly cross-section surveys based on flood marks but also clues of flow velocities (video movies, witness observations, water super-elevations in river bends or in front of obstacles). The following sections present and criticize various indirect postflood peak discharge estimation methods and put the emphasis on the cross-validation procedures.
2) Indicators of the time sequence of the flood: mainly eyewitness accounts where no stream gauge measurements are available. Accounts from eyewitnesses are occasionally cited in flash-flood studies, but they have seldom been systematically collected and analysed.
3) Mass transfer processes (erosion and deposits on the slopes and in the river bed, hyperconcentrated, mud or debris flow) as the main focus of the post-flood investigation but also as an indication of the local flow energy and velocity.

Other secondary aspects that a post event survey should consider are: information on socio-economical aspects, qualitative description of public behaviour, effectiveness of warning broadcasts, nature and extension of the damages caused to bridges, roads and buildings, …

3.2.2 Peak discharge estimation

The existence of a streamflow measuring station that remained undamaged during the flood does not mean that an accurate discharge value is available. The short duration of rainfall able to produce floods in small watersheds and the danger associated with accompanying high-water velocity, sediment and debris, preclude the possibility of obtaining direct measurements for extremely large floods. The river stage measurements themselves may also be dubious even if the gauging station has not been damaged during the flood. Last but not least we have to remember that gauging stations directly measure the water level and then the corresponding discharge values is calculated by means of the rating curve equation. One first approximation is that, due to the highly transitional conditions, the stage-discharge relation may not be unique. It is well known that for a given river stage, the discharge is higher during the rising limb of a hydrograph than during a decreasing limb. This effect, called hysteresis, depends on the rating-curve, the shape of the cross-section and the gradient of evolution of the discharge with time. It can generally be neglected but may become important in highly non-stationary conditions and when the water flows in a large floodplain. In addition rating curve are calibrated with discharge and level values corresponding to a return period of few years; values much lower than the one experienced during flash flood: this add some uncertainties in the discharge values estimated from water level since extrapolating the rating curve equation to levels much higher than the calibrations ones adds approximation. Taking these precautions, stage measurements are very precious to know the

hydrograph timing at the section even if the rating curve is not available or if it has some uncertainties.

One or more cross sections may be surveyed and along with bed slope estimation they can be used in hydraulic simulation to calibrate a rating curve and obtain a discharge hydrograph. The uncertainties concerning the riverbed position during the flood and the solid transport still remains, but if several discharge values are available along the main river and the tributary some coherence reasoning can be helpful to validate the estimations or to indicate that in some of the surveyed sections a deeper investigation is needed.

Peak discharge estimation is a key issue of post-flood studies. The most important peak discharge values are gathered to establish flood catalogues. Moreover, estimations of runoff discharges and volumes are necessary for any further hydrological analysis. Erroneous values will lead to false conclusions. Various discharge estimation methods have been developed in the past, especially by the U.S. Geological Survey, to homogenise the procedures and to share the experience gained by the hydrological community; experience summarized in empirical formulas to compute the Manning-Strickler roughness coefficient. The hope was that the use of these formulas would reduce the necessarily large discharge estimation uncertainties when no current-metre measurements are available. An estimate is rated as good if the calculated peak is believed to be within 10% of the true peak discharge; fair if the difference could be as much as 15%; and poor when the error could be 25% or greater. This is a very optimistic point of view, and this rating is probably better adapted to direct measurements of large discharge values.

Moreover, no real technical breakthrough has been achieved in the field of indirect discharge estimations. The most probable explanation of this discrepancy between the highest estimated discharge values during various periods, is that the same estimation methods were used but with different reference values, especially as far as the Manning-Strickler roughness coefficient or the mean flow velocities are concerned [Jarrett, 1987]. The main conclusion is that, estimating peak discharges when no direct current-metre measurement is available is, above all, a question of sound engineering judgment and experience. Empirical relations must be used with caution, as guidelines, and their systematic use may have led in the past to systematic over-estimations of the largest flash-floods. A corollary to this conclusion is that large efforts must also be put on the critics of the estimated values during the field investigation. It is useful to estimate discharges for a minimum of two or three cross-sections for the same river reach to reduce or be aware of uncertainties. The cross-sectional flow area may vary significantly between sections, and a discharge estimate made for one section may imply an unrealistic velocity value for another section and, consequently, be rejected. Uncertainties can also be reduced by testing the upstream-downstream coherence of the estimates and their coherence with the rainfall data. More accurate discharge or velocity estimates - critical depth estimates, super-elevation in bends, velocity estimated from films - are sometimes available to adjust the Manning roughness coefficients. Solid transport, erosion,

deposition clues may also be used to validate the estimated velocity values. However, the accuracy of the single peak discharge estimates remains highly dependent on the experience of the expert: in the best case it is probably within 30-50% [Gaume, 2006].

The first pitfall in peak discharge estimation lies in the identification of the mean high water levels in river cross-sections where no measurement is available. Much evidence of levels reached by the water can be found after an exceptional event. Vegetation fragments, silt or fuel marks on walls can be preserved over several years. But, they are not necessary representative of the mean water level. They can result from projections due to the presence of an obstacle or be settled on vegetation temporarily bent by the flow. High water marks in still water areas, such as inside houses, are preferable. But, here again, there is a need for caution. Due to the short duration of flash-floods, the water level inside closed houses may never reach the maximum level of the water outside. However, it would be difficult for the margin of error on the high water levels estimated on the basis of marks left by the flood to be less than 10-20 centimetres. It can be concluded that it is actually impossible to identify water surface slopes much lower than 1%. This of course limits the accuracy of the discharge estimation methods based on the longitudinal water surface or energy line profile.

3.2.3 One-dimensional steady state hydraulic theory

Two-dimensional hydraulic models have been used in some recent studies for estimating peak discharges, but most of the hydraulic post-flood discharge estimations are based on one-dimensional models.

In steady state conditions, when the derivatives with time are equal to zero, the Barré de Saint Venant system of equations is reduced to the well-known Bernoulli equation.

$$\frac{d}{dx}\left(\frac{Q^2}{2gA^2}+y\right)=S-S_f=\frac{dHs}{dx} \tag{3.14}$$

Where x is the longitudinal coordinate, Q is the discharge, A is the wetted cross-sectional area, y is the flow depth, g is the gravitational acceleration, S is the river bed longitudinal slope and S_f is the friction slope. The quantity H_s is called the specific flow head. We will call the quantity $V=Q/A$ the mean flow velocity. Empirical formulas have been proposed to relate the friction slope S_f to the characteristics of the flow and of the channel cross-section. The Manning-Strickler formula is the most popular one:

$$Q=KAR_h^{2/3}S_f^{1/2} \tag{3.15}$$

Where R_h is the hydraulic radius ($R_h=A/P$, with P the wetted perimeter), and K known as the Manning-Strickler roughness coefficient depending on the river cross-section characteristics. The parameter $n=1/K$ is also often used in the technical and scientific literature. These two equations control the shape of the longitudinal water surface profile in river reaches. The simplifications done (one-dimensional flow hypothesis, synthesis of the friction effects into

the empirical Manning-Strickler equation) have proven to lead to very satisfactory results in most of the situations.

Two particular values of the water depth y can be defined on the basis of these equations. The normal water depth y_n, when $S_f = S$, is solution of the following equation:

$$Q = KA(y)Rh(y)^{2/3} S^{1/2} \tag{3.16}$$

In a uniform channel, with constant cross-section shape and roughness, y_n corresponds to an equilibrium value. This value is observed in cross-sections located in a relatively straight and uniform reaches and far enough upstream and downstream from hydraulic singularities (bends, dams, bridges, confluences). During cross section survey, especially in mountain region where the big dimension of gravel and rocks present in streambed and the irregular morphologic shape, a careful estimation of k parameter is needed. The choice of an appropriate roughness coefficient has discussed for decades: Chow [1959] proposed to use empirical equations, while Benson and Dalrymple [1967] tabulated values. More recently, Jarrett [1990] argued that the tabulated roughness coefficient values had been determined in cases of moderate floods and low-gradient streams; velocity and turbulence increases with discharge, and so change in energy loss lead to variable k parameter for the same cross section. This led Jarrett and other authors to propose empirical equations to predict the value of the Manning roughness from S and R_h but presence of vegetation, streambed sediment size, torrent morphology need to be considered for the final k evaluation. Finally, the estimation of the roughness coefficient requires a certain know-how, but even the experts can wrongly evaluate a situation. It is absolutely necessary to cross-compare various estimations carried on different sites, to limit the risks of wrong estimations.

The second particular value is the critical water depth y_c. It is the value for which the derivative of the specific flow head H_s with y is equal to zero. This means that y_c is solution of the equation:

$$F(y) = \frac{Q^2}{gA(y)^3}\frac{dA(y)}{dy} = 1 \tag{3.17}$$

The left hand term of this equation is the well-known Froude number $F(y)$. Note that y_c does not depend on the roughness coefficient which is one of the main sources of uncertainties in indirect discharge estimations. It is therefore appealing to try to find cross-sections in river reaches where the critical state may have been reached during the peak of the flood. Apart from the specific case of a critical flow regime ($y_c = y_n$), the critical depth can only be observed in particular cross-sections: contraction in the channel cross-section, flow over a dam across the river bed. If this kind of situation is combined with some information on maximum level, as floodmarks or witnesses report, the corresponding cross section is ideal for peak discharge estimation since, at least, the uncertainty derived from the roughness parameter is not present under this hypothesis.

3.2.4 Eyewitnesses interview

A methodological report on post flood investigations [Gaume, 2006] outlines the importance of interviews to eyewitnesses of the floods. Witness interviews are carried out in order to understand the timing of the rise and fall of the flood and the nature of the flood water. This methodology helps to construct the hydrograph of the event and can also help in understanding flow patterns for hydrodynamic modelling. Witnesses can also provide useful information on the rainfall runoff processes (e.g, observation of surface runoff, origin of this runoff, groundwater levels observed in wells, soil saturation observed by farmers…) and the local flow characteristics (e.g., whether water flow or debris flow, presence of woody debris in the flow, approximated surface water flow velocities, blockages formed during the flood, timing and influence of the collapse of bridges or dykes …). Finally, witnesses are often able to give information on previous floods, including dates and severity: cross checking accounts of previous events with historical archives is important to verify these data.

Information concerning the chronology of a flood is essential for analysing the rainfall-runoff dynamics. The peak duration and the discharge during the recession limb are indicator on the influences of direct and subsurface flow during the flood; the response delay time to rainfall provides information concerning infiltration and water storage capacities. Accounts of eyewitnesses are the only alternative source of information about the time sequence of floods when no direct stage measurements exist. Accounts of witnesses are sometimes mentioned in post flood survey reports, but seldom collected with systematic procedures: if so they could increase the ability to cover the gap between needed information and available conventional data to describe flood dynamics.

The main objective of the interviews is to collect data on the time sequence of the flood in areas where no direct river stage measurements are available: typically indications of water levels and the corresponding times. Direct interview are preferable than second-hand accounts, since the level of accuracy of the latter ones can hardly be tested. Witnesses and inhabitants can also provide useful information on rainfall, runoff process and the local flow characteristics. Pictures (and movies) of the flood may help to estimate the surface water level (and velocities).

Ideally, the interviews should be conducted just after the event. Nevertheless, it is often not possible or even “decent”. People are fully occupied by recovery actions during the weeks after the flood and hydrological studies are clearly not considered, for the moment, as the first priority [Gaume, 2006]. A rapid intervention after a flood event is certainly preferable, but it is yet not always possible, and is not absolutely necessary. Collecting interviews together with cross section surveys, one or two month after the flood, when people are already back to quotidian lives, can be a valid alternative able to minimize survey cost and have a complete pictures of the flood.

Before starting with interviews and cross section surveys, a journey to identify areas where to focus with the post event campaign can help the further organisation. It is also the

moment for establishing the work plan, deciding how many interviews are necessary. Then a visit to the city hall is preferable to inform local authorities about the investigation and to have suggestions about possible witness willing to give details of the flood. Generally people have not been informed of the investigation so the person conducting the survey must rapidly create a confidence atmosphere with them: few sentence to expose the aim of the interview and than explain some specific features about the flood; in this way generally people, helped by open and general questions, spontaneously tell what they know about the flood; at the end some specific question (e.g., about water level or timing) may be asked to have quantitative evaluation from the witness. Every information given by the population must be collected, but from each interview there also must be an evaluation of the level of accuracy of the witness' account. The reliability and the accuracy of the collected accounts are, of course, extremely variable, but in most cases, the witnesses themselves are quite aware of where to draw the line. One of the most important results of the previous surveys is that it is generally possible to collect accurate information concerning the time sequencing of a flood event by interviewing witnesses. The time of the peak discharge could often be determined to within quarter of an hour.

3.3 Hydrological modelling of flash flood events

3.3.1 Purposes of hydrological models

Modelling is a widely discuss theme in scientific hydrological community and this section doesn't aim to give a complete view about it. Anyway a brief description on main steps of a generic hydrological model is needed before the presentation of the two different models used in this study. Numerical modelling starts from observations on how a process occurs in natural condition and passes though the formulation of some simplified assumptions. Even more complex models can not simulate real word with perfect results, since most of the equations used in models have empirical origin and they work correctly only under certain assumptions; in addition, equation parameters quantify real word proprieties, which are not usually known in details. In hydrology, as in numerous other natural sciences, often researchers aim to add complexity to new models and present them as a more complete representation of reality; in any case researchers should be aware of the model limitations and underline the uncertainties of results obtained by using models. Complexity increases with the increasing of the number of parameters that the model uses to simulate real processes, but the problem is then shifted to parameter calibration since any set of parameters represents a different world condition, so that more parameters the model has more efforts are needed in term of knowledge of the reality (i.e., field survey).

Hydrological models, presented in this chapter and then used to carry on the study, are very simple and they are not considered able to simulate correctly hydrological processes in details. This choice is done first because uncertainty related to flash flood data acquirement procedures is still a big problem and quantitative data are affected by a great error sources; from this point of view to improve flash flood simulation one should start first from reducing observation uncertainty and only in a second step eventually from modifying model algorithms, adding complexity to approach model steps to real processes. In addition the aim of this study is not to simulate reality, but understand real processes, so it is necessary to screen each model step and compare it with field evidences. Finally models are thought as an additional tool to validate field observation.

There is a theoretical distinction between physical and empirical models. The first type should use parameter that can be directly measured by hand in the field. The fact is that in any case parameter calibration is needed when a comparison between simulated and measured data is scheduled. Hydrological models can be classified as lumped, where the computation is carried on average values at basin scale or distributed, when process simulation is calculated at point (pixel) scale and then results are integrate to the required catchment or subcatchment scale.

Most hydrological models are divided in two main steps. The first one, where big uncertainties still remain, is the separation of water input in the different path of transport that it can follows: surface and subsurface flow. The second one is water transport from the

different part of the basin to its outlet at witch scale simulation results are computed. Water input considered in this study is just meteorological precipitation, while in general it could consist also from snowmelting process or specific water incoming due to particular geology. This simplification is not a strong assumption since flash flood cases (see Chapter 2) where snow melting produces significant runoff amount, even if existing, are quite rare.

3.3.2 Infiltration and runoff generation processes

An important question in hydrology is how much stream flow occurs in a river in response to a given amount of rainfall [Tarboton, 2003]. In this prospective the first important step of an hydrological model consists in separating infiltration from runoff: these two terms are the main inputs to subsurface and surface simulations. Infiltrated water can follow different pathways. It can percolate to deep groundwater, which may sustain the steady flow in streams (baseflow) or may rise outside the river basin. Infiltrated water can also remain in the soil to later evaporate. These fractions just described are not very important to simulate the event hydrograph, but may become interesting for other applications (carsick phenomena, water spring, land stability, seasonal water balance…). Finally infiltrated water can flow downhill until it reaches, after a subsurface path, a saturated zone and exfiltrates back to surface flow.

Infiltration is the most crucial element of the description of the transformation of rainfall into streamflow [Bras, 1990]. Infiltration process is ruled mainly by two factors: rainfall rate and the top soil layer behaviour. The thickness of this layer varies between some centimetres and few meters and it is influenced by depth of vegetation roots and geological characteristics; this layer is generally inferior limited by an impermeable layer (rock, fine clay). The relationship between rainfall and runoff rate is highly nonlinear: at the beginning of a storm event in humid climate, in dry condition of soil, most of the precipitation is captured in the soil and it contributes to the rise of water table and to ground water flow; with the increasing of the soil moisture the infiltration capacity of the ground decrease, due to the saturation of the pores. In arid climate soil with no vegetation cover may be impermeable at the beginning of the event since dry condition can cause soil crust at the contact with atmosphere.

Continuity 3D equation for groundwater can be derived by imposing the increasing of subsurface volume storage in an infinitesimal cube of soil to be equal to the difference between input and output discharge [Fiedler, 2004].

$$\frac{\mathrm{d}\theta}{\mathrm{dt}} = -\left(\frac{\mathrm{dq_x}}{\mathrm{dx}} + \frac{\mathrm{dq_y}}{\mathrm{dy}} + \frac{\mathrm{dq_z}}{\mathrm{dz}} \right) \tag{3.18}$$

where θ is the volumetric moisture content (volume of water / total volume), variable between 0 and the soil porosity n, and q_i is the discharge per unit area in the i direction. Assuming infiltration as a one-dimensional process the conservation equation it is commonly considered just in term of the vertical direction z.

Another fundamental equation for groundwater is Darcy's law that assumes the velocity of water movement in saturated soil to be proportional to the energy slope:

$$q_z = -k_z \frac{dh}{dz} \tag{3.19}$$

Combining the two we obtain Richard's equation, that it the fundamental governing equation for subsurface flow:

$$\frac{d\theta}{dt} = \frac{d}{dz}\left(k_z \frac{dh}{dz} \right) \tag{3.20}$$

where k_z is the hydraulic conductivity in the vertical direction and h is the hydraulic head, given by:

$$h = \psi + z \tag{3.21}$$

where ψ is the soil suction head and z is elevation. Replacing the latter equation in Eq.3.18 we finally obtain a more useful form of Richard's equation:

$$\frac{d\theta}{dt} = \frac{d}{dz}\left(k_z \frac{d\psi}{dz} + k_z \right) \tag{3.22}$$

There are two different ways to interpret this equation, depending of the meaning that we want to give to the relationship θ, K_z and ψ [Tarboton, 2003]. The first is considering the soil moisture θ as independent variable. Calling diffusivity

$$D = k_z(\theta) \frac{d\psi}{d\theta} \tag{3.23}$$

Richard's equation can be rewritten as:

$$\frac{d\theta}{dt} = \frac{d}{dz}\left(k_z(\theta) \frac{d\psi(\theta)}{dz} + k_z(\theta) \right) = \frac{d}{dz}\left(D \frac{d\theta}{dz} + k_z(\theta) \right) \tag{3.24}$$

The second case is to consider ψ as independent variable. Defining soil moisture capacity as

$$C(\psi) = \frac{d\theta(\psi)}{d\psi} \tag{3.25}$$

we can obtain

$$C(\psi) \frac{d\psi}{dt} = \frac{d}{dz}\left(k_z(\psi) \frac{d\psi}{dz} + k_z(\psi) \right) \tag{3.26}$$

These differential equations, combined with specific initial and boundary condition, can be solved analytically. A common initial assumption for Eq.3.24 is to ignore gravitational term, assuming $K_z(\theta)$ to be constant along the vertical direction or that the potential term is so large to dominate the equation: those condition will be more easily met with low level of saturation (beginning of infiltration or end of exfiltration) [Bras,1990]. The equation can be further simplified if the diffusion term is assumed to be constant:

$$\frac{\mathrm{d}\theta}{\mathrm{dt}} = \mathrm{D}\frac{\mathrm{d}^2\theta}{\mathrm{dz}^2} \tag{3.27}$$

When the initial and the boundary (on the surface) condition of Eq.3.27 are:

$$\theta = \begin{cases} \theta_\mathrm{i}\,\mathrm{z} \le 0; \mathrm{t} = 0 \\ \theta_0\,\mathrm{z} = 0; \mathrm{t} > 0 \end{cases} \tag{3.28}$$

the solution of the simplified differential equation is:

$$\frac{\theta - \theta_0}{\theta_\mathrm{i} - \theta_0} = \mathrm{erf}\left[\frac{|\,\mathrm{z}\,|}{2\sqrt{\mathrm{Dt}}}\right] \tag{3.29}$$

where *"erf"* represent the increasing monotonic error function (*erf*(0)=0; *erf*(+∞)=1 and in general *erf(x)*= $\sqrt{\frac{4}{\pi}}\int_0^{\mathrm{x}} \mathrm{e}^{-\mathrm{y}^2}\,\mathrm{dy}$) [Bras, 1990].

The solution of equation (3.26) requires $k(\psi)$, $C(\psi)$ and $\theta(\psi)$ to be known. For saturated condition, $C(\psi)$ is zero and $k(\psi)$ is constant and equal to the saturated hydraulic conductivity [Fiedler, 2003]. In this case the equation reduces to:

$$\frac{\mathrm{d}}{\mathrm{dz}}\left(\mathrm{k}_\mathrm{z}\left(\frac{\mathrm{d}\psi}{\mathrm{dz}} + 1\right)\right) = 0 \tag{3.30}$$

Hydrological models general use a simplified equation or empirical equation to compute infiltration and runoff. A first formula comes from Darcy's law, approximating that water infiltrates as a sharp wetting front with saturated condition above the latter [Fiedler, 2004]. Considering a wet top soil layer characterized by depth *L* and neglecting the pressure applied by ponded water, the infiltration capacity can be calculated by Darcy's law written for the vertical direction:

$$\mathrm{f} = \mathrm{k}_\mathrm{z}\frac{\psi + \mathrm{L}}{\mathrm{L}} \tag{3.31}$$

remembering that ψ is the soil suction head and k_z is the hydraulic conductivity in the vertical direction in saturated condition. Considering cumulative infiltration (*n* is porosity, θ_i is the initial moisture):

$$\mathrm{F} = \mathrm{L}\left(\mathrm{n} - \theta_\mathrm{i}\right) = \mathrm{L}\Delta\theta \tag{3.32}$$

and substituting *L* in Eq.3.31 we obtain:

$$\mathrm{f} = \mathrm{k}_\mathrm{z}\frac{\psi\Delta\theta + \mathrm{F}}{\mathrm{F}} = \mathrm{k}_\mathrm{z}\left(1 + \frac{\psi\Delta\theta}{\mathrm{F}}\right) \tag{3.33}$$

This equation, first proposed by Green and Ampt [1911], simulates correctly the soil behaviour in vegetated areas: at the beginning of the rainfall ($F \approx 0$) the infiltration capacity result very high and the entire precipitation infiltrates. As long as the rainfall goes on *F* increase, *f* decreases until it reaches (if the event lasts enough) the value of the rainfall rate *p*. From this point just a fraction of the rainfall (*f*) will infiltrate and the reaming part (*p-f*) will

generate runoff. The decreasing of the infiltration capacity goes on toward the value in saturated soil condition K_z.

Soil conservation Service (SCS) of the United States suggested in 1968 a method based on the dimensionless curve number CN. It has become very popular since there has been a great effort to classify with good definition various region. The procedure gives as output the volume of runoff in the case that cumulated precipitation P is greater than initial retention volume I_a:

$$R_s = \frac{(P - I_a)^2}{P - I_a + S} \tag{3.34}$$

Where S is available subsurface volume. Commonly the initial abstraction is taken as I_a = 0.2S, which leads to:

$$R_s = \frac{(P - 0.2S)^2}{P + 0.8S} \tag{3.35}$$

The available volume is calculated through the parameter CN

$$S = \frac{25400}{CN} - 254[\text{mm}] \tag{3.36}$$

$$0 \le CN \le 100$$

CN=100 leads to S=0 that means to consider no infiltration and that the entire precipitation contributes to the surface flow (impermeable soil hypothesis). CN=0 brings to infinite available volume and to the consequence that the entire rainfall volume infiltrates generating no runoff. The advantage of this approach is that SCS collected a rich literature to obtain a very detailed table to derive CN value of a soil with from hydrologic characteristic and land use.

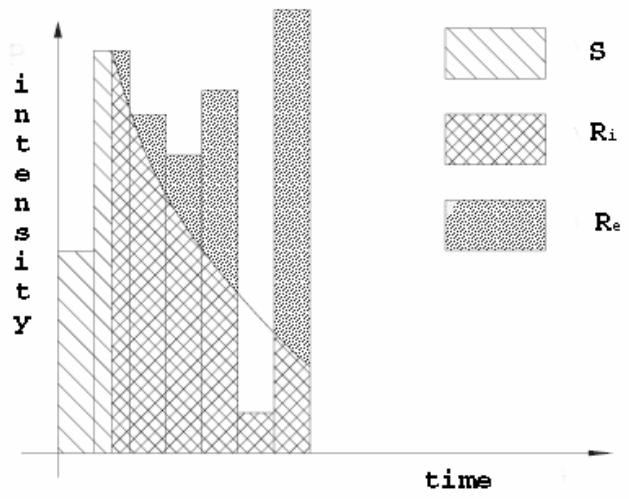

Figure 3.4. Runoff generation according to SCS.

3.3.3 Subsurface and surface water transport

Once water infiltrates in the ground it can follow different paths. In most studies infiltration is treated separately from lateral movement. This is possible because the soil, due to its geological history, has strong anisotropy. Thinking about a flat region infiltration direction is vertical, while lateral flow is horizontal. For a sloping bed infiltration remains vertical, while water moves downhill parallel to slope direction. Darcy's law states that the velocity of flow through a porous media is directly proportional to the gradient of piezometric head [Bras, 1990]; thinking about a monodimensional movement in the *x* direction:

$$q_x = -k_x \frac{dh}{dz} \tag{3.37}$$

The conductivity *k* in saturated condition is function of the size and the tortuosity of the pores and it varies from 10^{-9} m/s for fine clay to 10^{-3} m/s for sand and gravel soil. For unsaturated condition hydraulic conductivity decreases with decreasing of volumetric soil moisture θ. Since a certain amount of water can not be drained from the soil, it is common to work with effective porosity n-θ_r; where θ_r is the residual soil moisture, the lower limit of the possible range of moisture content. The upper limit for moisture content is instead the porosity *n*. For practical purpose this range is referred to the effective saturation (s=0 → $\theta = \theta_r$; s=1 → θ=n)

$$s = \frac{\theta - \theta_r}{n - \theta_r} \tag{3.38}$$

A rigorous approach to subsurface flow results very complex from a computational point of view, but it requires also an exhaustive knowledge of soil proprieties. Soil in fact may be very heterogeneous and water flow can often be determined by preferential paths. The alternative choice is to use simplified equation to simulate the average behaviour of the water. Boussinesq [1877] developed a mono-dimensional hydraulic theory for unconfined groundwater, based on Darcy's law applied to a sloping aquifer:

$$q = -kh\left[\frac{\partial h}{\partial x}\cos i + \sin i\right] \tag{3.39}$$

where *q* is the discharge per unit width in the *x* direction, which is parallel to the slope and *h* is the depth of the water table perpendicular to the slope. This equation neglects the effect of capillary rise above the water table and assumes hydraulic head to be independent from the depth. Combining it with continuity equation, in the hypothesis of no spatial variability of *k*, *n* and *i* we obtain:

$$\begin{aligned} &\frac{\partial h}{\partial t} = -\frac{1}{n}\frac{\partial q}{\partial x} = \\ &= \frac{k}{n}\left[\frac{\partial h}{\partial x}\left(\frac{\partial h}{\partial x}\cos i + \sin i\right) + h\frac{\partial^2 h}{\partial x^2}\cos i\right] = \frac{k}{n}\left[\cos i\frac{\partial}{\partial x}\left(h\frac{\partial h}{\partial x}\right) + \sin i\frac{\partial h}{\partial x}\right] \end{aligned} \tag{3.40}$$

usually referred as the Bussinesq equation, that relates the temporal to the spatial changing of the phreatic water surface elevation.

Overland flow, both in hillslope and in channel, can be described by mass and momentum continuity one-dimensional equations:

$$\begin{cases} \dfrac{\partial Q}{\partial x} + \dfrac{\partial A}{\partial t} - q = 0 \\ \dfrac{1}{g}\dfrac{\partial v}{\partial t} + \dfrac{v}{g}\dfrac{\partial v}{\partial x} + \dfrac{\partial y}{\partial x} + s_f - s_0 - vq = 0 \end{cases} \tag{3.41}$$

where g is gravitational acceleration, v is the average velocity in the considered cross section, s_f and s_0 are friction and riverbed slope and q is lateral inflow per length unit. The hypotheses under which the equations are valid are the following: flow is one-dimensional, hydrostatic pressure prevails and vertical accelerations are negligible, streamline curvature is small, bottom slope of the channel is small and the fluid is incompressible. This formulation is used when both inertial and pressure forces are important and backwater effects are not negligible (mild slope channels with downstream control).

These equations must be combined with a uniform motion equation, which can have a laminar form for the hillslope or a turbulent as the Gauckler-Stickler one for open channel [Moody, 2005]:

$$Q = k_s R_h^{2/3} s_f^{1/2} \tag{3.42}$$

For practical use momentum Eq.3.41 can be simplified under the assumption of no lateral contributes (q=0). The first two terms, that represent local and convective acceleration, can be neglected, since $\dfrac{\partial v}{\partial t}$ and $\dfrac{\partial v}{\partial x} << \dfrac{\partial y}{\partial x}$. In this way substituting the simplification

$$\frac{\partial y}{\partial x} + s_f - s_0 = 0 \tag{3.43}$$

in the continuity equation we obtain for large rectangular channel:

$$\frac{\partial y}{\partial t} + a\frac{\partial y}{\partial x} - \frac{\partial^2 y}{\partial x^2} = 0 \tag{3.44}$$

where a represents the peak propagation celerity and D is the diffusivity term that produce an attenuation of the wave as it proceeds along the reaches. When gravity forces and friction forces balance each other (steep slope channels with no back water effects) kinematic wave assumption is consider $\dfrac{\partial y}{\partial x} \approx 0$ and so $s_f \approx s_0$.

An analytical solution to kinematic wave for hillslope has been proposed and developed by Rose et al. [1983] and Moore [1985]. Considering a rectangular plane hillslope of unit width, length L with spatially constant soil characteristic and a stationary effective rainfall of intensity r, uniformly distributed over the area, the kinematic equation for an infinitesimal element of the hillslope of length dx can be expressed (see Fig.3.5) as:

$$r(t)dx - \frac{\partial Q(t)}{\partial x}dx = \frac{\partial h(t)}{\partial t}dx \tag{3.45}$$

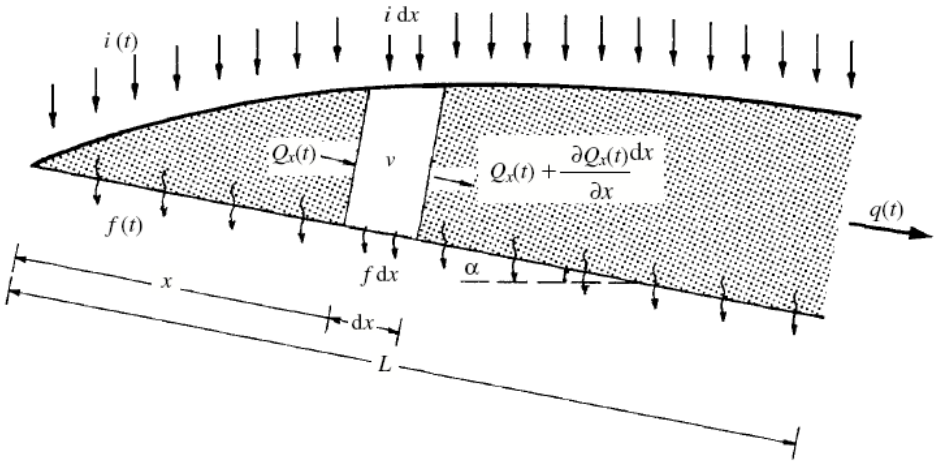

Figure 3.5. Sketch of overland flow model [Agnese et al., 2001]

Rose's approximation consist in assuming at any time t $\frac{\partial Q(t)}{\partial x} = q(t)$: the rate of change of the discharge per unit width along the plane is considered to be constant and equal to the outflow rate at the bottom of the plane, *q(t)*. This assumption is equivalent to approximating the overland flow process by a continuous sequence of stationary states. Although this simplified approach does not capture the complete hydraulics of the motion, as will be shown later, it does lead to an analytical solution [Agnese et al., 2001].

The discharge Q can be related to the local depth of flow h, through a uniform motion equation:

$$h(t) = \left(\frac{Q(t)}{k\sqrt{\sin\alpha}}\right)^{1/m} \tag{3.46}$$

where k is a roughness parameter and m is a flow parameter (m=3 for laminar flow and $m = \frac{5}{3}$ for turbulent flow, as in Gauckler-Strickler equation). By differentiating Eq.3.46 with respect to t and by substituting the result in Eq.3.45, we obtain:

$$r(t)dx - q(t)dx = \left(\frac{x}{k\sin\alpha}\right)^{1/m}\frac{dq(t)}{dt}\frac{1}{m}q(t)^{\frac{1-m}{m}}dx \tag{3.47}$$

Finally integrating the latter equation with respect to x, from 0 to L, and assuming $k_* = \frac{k\sqrt{\sin\alpha}}{L}$, a parameter that synthetically accounts for the hillslope geometry (length, slope and roughness), it follows the differential flow equation:

$$\frac{1}{(1+m)k_*^{1/m}}\frac{q(t)^{\frac{1-m}{m}}}{r(t)-q(t)}dq(t)=dt \tag{3.48}$$

Three different cases can be distinguished; for *m*=2 (transitional flow regime) the Eq.3.48 can be integrated in the close interval $[t_0,t]$ by fixing the initial condition $q=q_0$ for $t=t_0$:

- r = 0: this case consider the recession of the hydrograph at the end of the rainfall. In this case in literature is available in literature is available an analytical solution [Horton, 1938; Robinson and Sivapalan, 1996]:

$$q=q_0\left[1+\frac{3}{2}\sqrt{q_0k_*}(t-t_0)\right]^{-\frac{1}{2}} \tag{3.49}$$

- 0 < r < q0: in this case a close analytical solution, corresponding to a decreasing hydrograph is:

$$q=r\left[\coth\left(\operatorname{arcoth}\sqrt{\frac{q_0}{r}}+\frac{3}{2}\sqrt{k_*r}(t-t_0)\right)\right]^2 \tag{3.50}$$

- r > q0 >0: this is the most interesting case for hydrological simulation, since it corresponds to a increasing hydrograph; the explicit analytical solution is:

$$q=r\left[\tanh\left(\operatorname{arctanh}\sqrt{\frac{q_0}{r}}+\frac{3}{2}\sqrt{k_*r}(t-t_0)\right)\right]^2 \tag{3.51}$$

3.3.4 The KLEM model

Hydrologic response is analysed in this study by using a simple spatially distributed hydrologic model: KLEM, Kinematic Local Excess Model [Cazorzi and Dalla Fontana, 1992]. The distributed model is based on availability of raster information of the landscape topography and of the soil and vegetation properties. In the model, the SCS-Curve Number (SCS-CN) procedure [US SCS, 1986] is applied on a grid-by-grid way for the spatially distributed representation of runoff generating processes, while a simple description of the drainage system response [Da Ros and Borga, 1996; Giannoni et al., 2003] is used to represent runoff propagation.

The SCS-CN method is chosen because it can be applied by specifying a single parameter called the curve number, CN and spatial distribution of the CN values is easily estimated from technical maps and field observations on the study area [Cazorzi and Bincoletto, 2005]. Following Ponce and Hawkinks [1996], the value of S_0 for a given soil is related to the curve number as

$$S=S_0\left(\frac{100}{CN}-1\right) \tag{3.52}$$

where S is a calibration parameter, called infiltration storativity. The use of the parameter S_0 allows one to use the spatial distribution of CN values, which represents an input data in this work, and to simulate correctly, at the same time, the observed flood water balance. In the original SCS-CN equation (Eq.3.36) the value of S_0 is 254 mm and the initial abstraction is specified as a percentage of S. Calibration parameters for the runoff generation process are the S_0 and I_a/S values at subbasin scale, that are calibrated using manual and automatic procedures based on field observations and discharge hydrograph information.

The distributed runoff propagation algorithm is based on the identification of drainage paths, and requires the characterization of hillslope paths and channelled paths. A channelization support area is used and considered constant at the subbasin scale, to distinguish hillslope elements from channel elements. Discharge at any location along the river network is represented by

$$Q(t) = \int_A q[t - \tau(x), x]dx \tag{3.53}$$

where A indicates the area draining to the specified outlet location, $q(t,x)$ is the runoff at time t and location x, and $\tau(x)$ is the routing time from x to the outlet of the basin specified by the region A. The routing time $\tau(x)$ is defined as

$$\tau(x) = \frac{L_h(x)}{v_h} + \frac{L_c(x)}{v_c} \tag{3.54}$$

where $L_h(x)$ is the distance from the generic point x to the channel network following the steepest descent path, $L_c(x)$ is the length of the subsequent drainage path through streams down to the watershed outlet, and v_h and v_c are two invariant hillslope and channel velocities, respectively. The propagation model is so characterised by three calibration parameters: the channelization support area and two kinematic parameters (v_h and v_c). The model includes also a linear conceptual reservoir for base flow modelling: the reservoir input is provided by the infiltrated rate computed based on the CN-SCS method and this method is applied at the subbasin scale, where it is possible to calibrate the reservoir empting constant.

3.3.5 The GRISS-2D model

Hydrological model GRISS-2D has been developed to be applied at the very small scale (up to few km²) to improve the understanding, through process simulation, on geomorphologic dynamic related to flash flood (e.g., debris flow). It is a process-based, distributed-parameter, finite-difference hydrologic model that simulates stream flow generated by both infiltration-excess and saturation-excess mechanisms, as well as exfiltration, and subsurface storm flow to streams. The model operates on a raster-based digital elevation model of the catchment and it is applied at very small scale, so precipitation is considered with uniform spatial distribution (using mean area rainfall data). The subsurface storm flow component provides a mechanism that allows saturated soil water flow to move within a soil horizon overlying impermeable bedrock toward a receiving stream channel. This component

generates return flow from the soil subsurface to the land surface that feeds sheet overland flow. Since the location of land surface saturation by subsurface storm flow evolves in time and space, this saturated land area becomes a "variable source area" for water flow toward a receiving stream. The GRISS-2D model conceptualises the water contribution from a hillslope into a neighbouring stream channel in terms of overland flow, and seepage from subsurface storm flow (which may lead to return overland flow) following the maximum slope direction propagation (derived from DEM) both for surface and for subsurface flow.

The vertical unsaturated flow component is simulated according to Kavvas et al. [2004]. The model is based upon the Green-Ampt infiltration equation and links the overland flow and the subsurface storm flow components of GRISS-2D. It is capable of estimating the vertical soil water flow rate: this capability enables the model to simulate the build up of the groundwater flow above the impeding layer. The rainfall excess becomes the lateral inflow flux to the hillslope overland flow model. A portion of the infiltrated water becomes subsurface storm flow and the remaining portion is stored within the soil column.

The saturated subsurface flow is simulated according to Wigmosta et al. [1994] by using a kinematic wave model [Beven, 1981]. The effects of topography on flow routing are obtained through the direct use of DEM data. Local hydraulic gradients are approximated by local ground surface slopes (kinematic approximation). Thus a given grid cell receives water from its upslope neighbours and discharges to its downslope neighbours. Rise and fall of the subsurface storm flow is taken into account by the unsaturated zone model. In extreme cases, the saturated zone may rise to the soil surface; in these cases the unsaturated zone disappears and only the saturated flow equations are solved.

The overland flow is routed using Gauckler-Strickler equation with the kinematic wave assumption. When overland flow reaches a cell that contains a defined channel, the flow is passed into the channel and routed using a one dimensional kinematic wave model for surface runoff.

The numerical model here proposed for the simulation of subsurface flow is based on continuity equation (Eq.3.55) and Darcy's law (Eq.3.56). Using the apex to indicate the spatial position and the subscript to describe the time step, the two equations may be express as:

$$H_{(t)} = H_{(t-\Delta t)} + \frac{r_i \Delta t}{n} + \frac{(Q_{in(t)} - Q_{out(t)})\Delta t}{n \Delta x^2} \tag{3.55}$$

$$Q^{x}_{out(t)} = k \Delta x \frac{H^{x}_{(t)} + H^{x+\Delta x}_{(t)}}{2} s_b \tag{3.56}$$

where H is the water table thickness, r_i is the infiltration rate, n is effective porosity and Q_{in} is the sum of the incoming discharge of the given pixel. The scheme has been implemented in the following way: first Darcy's law is applied from the divide to the outlet (following and increasing upslope area order); for better numerical convergence this value is combined with

the incoming discharge with using as weight parameter θ_p an 1-θ_p (where $0<\theta_p<1$, but $\theta_p=0.5$ is generally assumed); second the continuity equation is applied to get H in each pixel. Surface water is routed with the same scheme, substituting Darcy's law with Gauckler Strickler (Eq.3.42) and infiltration with sum of runoff and infiltration rate.

Numerical methods require discretization in both space and time. The space element dimension is generally given by the grid resolution and the time step choice is crucial to the stability and the accuracy of the numerical scheme used. Courant has shown that the actual time step used in the time integration scheme must not be longer than the time during which a front of a kinematic wave may propagate through spatial element. For each time step of the simulation the minimum crossing-cell time has been calculated for the entire grid; that value is used to determinate the following time step duration. When both subsurface and surface flow occurs the Courant condition for the second one results much more restricted.

In the model the conductivity k used in Darcy's law is considered a separated parameter from the vertical conductivity k_z used in Green-Ampt (Eq.3.33). Another important parameter of the model is permeable soil depth. This parameter is important because when the entire soil is saturated no more water can infiltrate in the soil. In addition due to slope variation (i.e. in correspondence of the bottom of a valley) water can exfiltrate from the soil to overland flow. These processes are determined from continuity equation for the soil (Eq.3.55).

GRISS-2D model have been applied for both surface and subsurface flow in different standard and simple hillslope and compared with analytical solution. Seven different hillslope geometries tested with constant rainfall inputs of different duration (up to slope concentration time) has been used for comparison: three concave, three convex and one constant slopes. Results show very good agreement in every case but in the most concave slope where numerical solution anticipate flow peak from analytical solution. These observations lead to the fact that the model should be improved for a systematic analysis, but it is enough realistic for a first estimation of flood dynamic simulation, that is the aim of this thesis.

Chapter 4 - ANALYSIS OF PAST FLASH FLOOD EVENTS

4.1 Analysis of flash flood events in Romania

4.1.1 Romanian Climate and meteorological network

Romania, due to its geographic location, has a climate that is characterized by a mixture of temperate and continental features. The Carpathians mountains restrict the Atlantic influences to the western and central part of the country. The Mediterranean and Bleak Sea are the main moisture sources for costal and continental regions and their influences determine a milder climate in the Southerner and the Eastern plain.

An important characteristic of the Romanian climate is the wide variability of the meteorological phenomena, first of all precipitation, mostly imposed by the peculiarities of the relief. Precipitation is characterized through large time and space variability. Multiannual means display an annual cycle, with a maximum in June and a minimum in February–March, almost all over the territory.

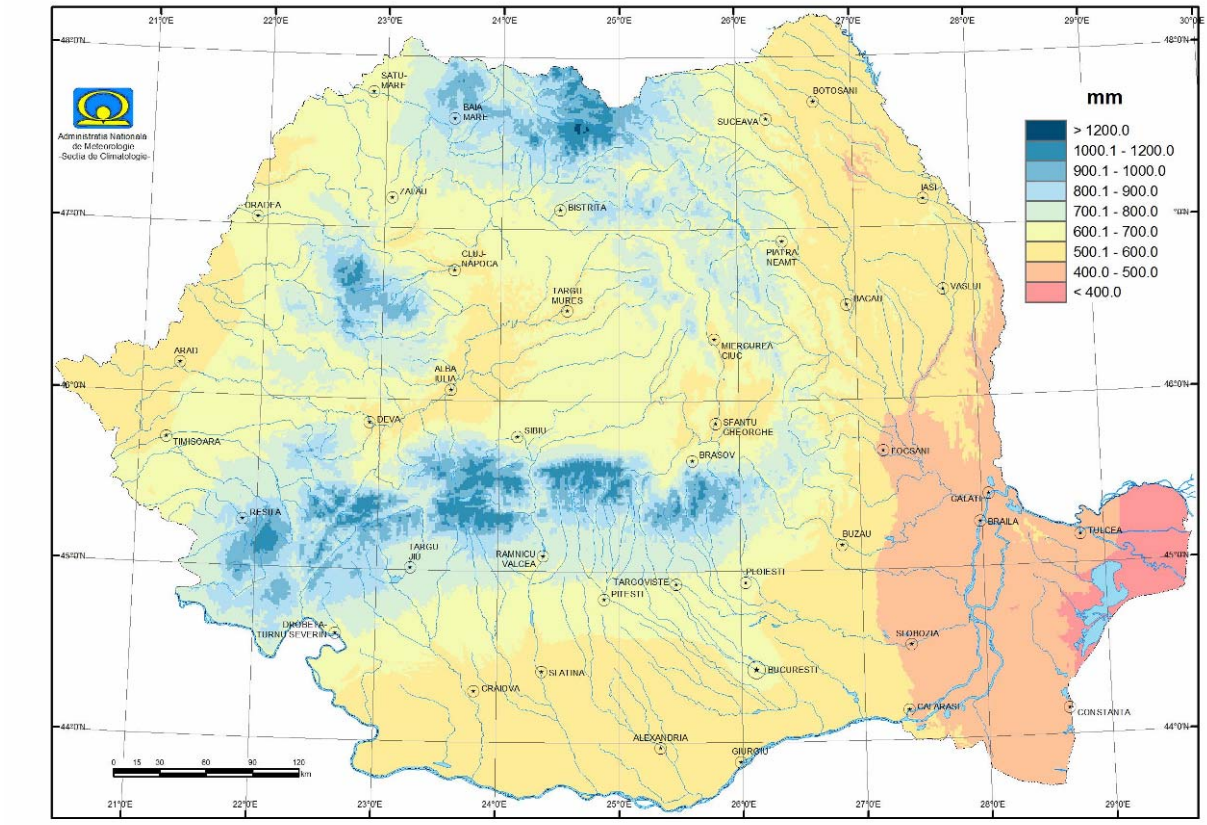

Figure 4.1. Mean annual precipitation; observation period from 1961 to 2005 from Romanian National Meteorological Administration.

The lowest annual precipitation amounts are recorded in the Dobrudja costal area and mostly in the east of the Danube Delta, where less than 400 mm fall on the average, whereas the most abundant precipitation exceed 1200 mm, localized in the mountain areas. Fig.4.1 and 4.2, provided by Romanian National Meteorological Administration, show mean annual and June precipitation, considering data from 1961 to 2005. In the summer period most of the precipitation is due to convective, intense and localized events [Ghioca, 2006].

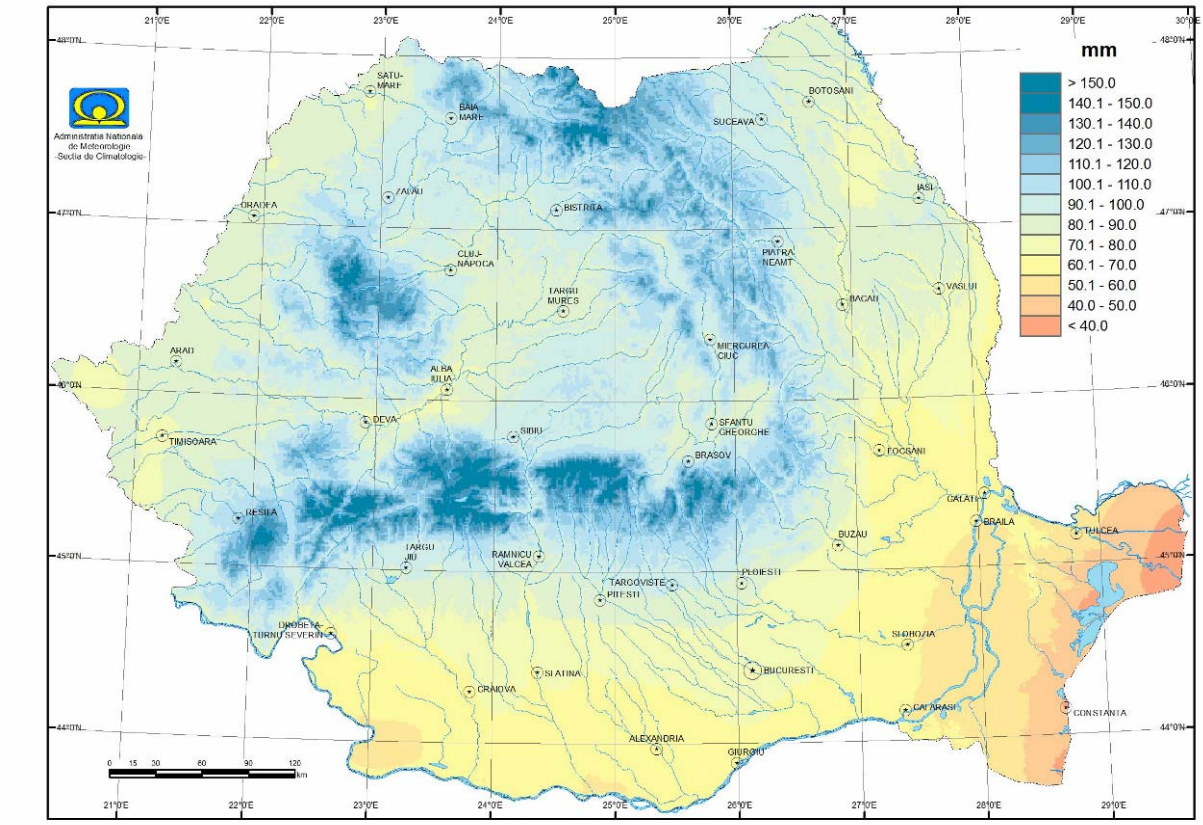

Figure 4.2. Mean June precipitation; observation period from 1961 to 2005 from Romanian National Meteorological Administration.

These meteorological characteristics lead to the fact that in Romania, as well as in many Central and Eastern European countries, flash floods are a phenomenon that takes place in small regions, characterized by limited spatial extent. Flash flood represents one of the most severe hazards in Romania, causing important damages and causalities. The Romanian flash floods are mainly due to massive and sudden rainstorms combined or not with a rapid snowmelt in the mountains.

Flash floods in Romania occur mostly during the warm season (June to August) and are related to high intensity rate: Mediterranean and Black Sea proximity provide a source of moisture for Romanian territory and S-shape of Carpathians Mountains creates typical conditions for orographic forcing. Flash floods are more frequent in mountain and watersheds with deep valleys, but they may occur everywhere in Romania.

At low levels the ways by which atmospheric parameters for heavy precipitation are brought together can vary substantially from case to case and in different parts of the country.

Heavy rainfall may or may not result in a flash flood, depending on the hydrological and geographical characteristics of the watershed where rainfall accumulates [Stancalie et al., 2008].

The national meteorological network includes 75 daily and 89 hourly raingauges. Considering that the Romanian surface is 237500km² wide this mean an average density of 1 raingauge over more than 2500km² for hourly data and 1 over 1450km² for daily precipitation. This density (average distance between gauges: 35 to 50km) is definitively too poor to describe spatial variability associated to convective events (needed spatial resolution would be at least 5 km).

Romanian meteorological service is also equipped with five S-band whether radars that cover, also considering a working range limited to 160km due to attenuation, most of the territory. In Fig4.3 raingauge network and three used radar working ranges are displayed together with the location of the five basins where flash flood analysis has been carried.

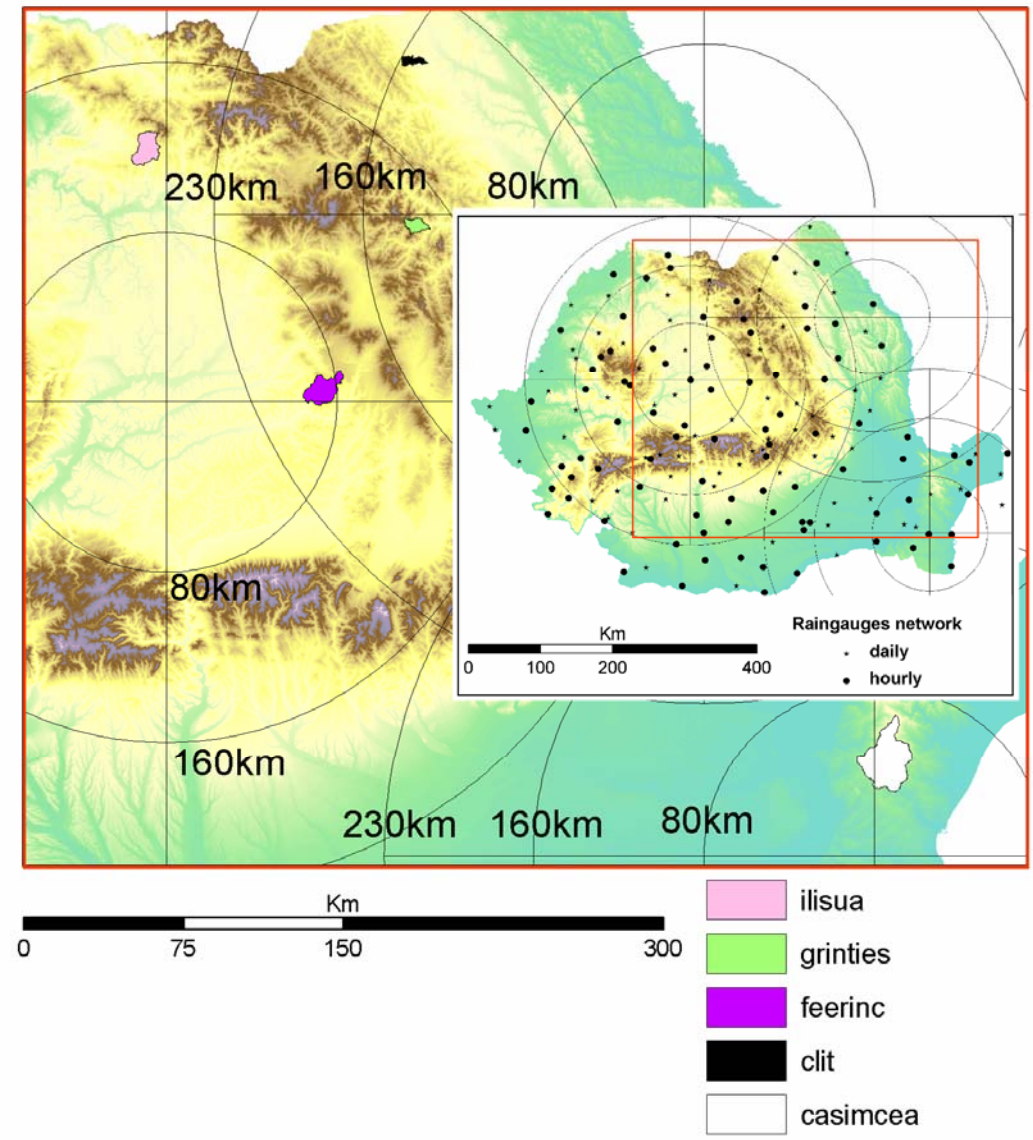

Figure 4.3. Location of the five studied basins in Romania with indication of radar coverage and raingauges position.

Larger stream (>1000 km²) are well gauged in Romanian, with time series up to several decades and frequent discharge measures to update rating curves; but at the scale at witch flash flood occurs, stream (few hundreds of km² or less) are often ungauged. Post event campaign is, in this situation, essential to have at least a minimal description of flood magnitude and dynamics.

Five documented flash floods have been analyzed with the collaboration of Romanian meteorological and hydrological national service involved un the *HYDRATE* European Project. The meteorological administration provided radar and raingauge data and its contribute has been fundamental for data correction and to have a final plausible spatial and temporal description of the storm case. The Hydrological Administration carried the post event surveys, with discharge peak value and timing estimation; it also provided the DTM at 20 m resolution for the hydrological model and information about basin land use; where present it collected additional rainfall data (outside the official meteorological network) and provided stream gauge data.

In the next paragraph the most documented case of Feernic River is described and analysed in detail. In the following one the result of a similar analysis carried in other four cases is reported.

4.1.2 Description of Ferrnic flash flood

Feernic River is a small stream in the Mures River catchment (27000 km²) that is a tributary of the Tibisco River. Feernic springs are located on the western slopes of Harghita Mountains (Eastern Carpathians), at 940m altitude. At the outlet located in Simonesti village the basin data are: surface 167km², mean altitude 637m, medium basin slope 23.5%, and medium slope of the river bed 16.0%. Geologically speaking, the upper part of the basin lies on the volcanic lava and pyroclastic rocks of Harghita Mountains, while the lower belongs to the flysch (marls and clays) of the Transylvanian Subcarpathians. Forests (about 20% of the basin surface) are composed by coniferous and beech on the mountain part of the basin; beech and chestnut oak on the hilly part. The percentage of arable soils is 20-25% and the rest of the land is used as pastures and meadows. Small villages are present in the valley along the river network. Climate of the catchment area is defined as moderately warm and mid-humid, with monthly temperature means from -4.5°C (January) to +18°C (July), and with annual mean precipitation total in the range 650 - 700mm. In the higher elevation of the catchment the climate is colder and more humid.

At the main bridge in Simonesti is present a stream gauge station, with level records and discharge estimations since 1961; this is the considered outlet for the entire basin. The highest recorded value before 2005 event is 131m³/s measured in 1975, while average discharge of 1.11 m³/s. During the studied event the station didn't work automatically, but

some manual record had been taken, including the maximum water level, from witch a 368 m^3/s discharge was estimated.

No raingauge is present inside the basin (the closest one is about 6 km SE of the divide), while the nearest observation radar is located about 75 km west of the catchment with no occlusion problems. Summer 2005 has been for the entire Romania and also for this region more rainy than usual: 170 mm were recorded in the nearest meteorological station from July 23 to August 22; two main event occurred: at the beginning of August, with cumulated precipitation in nearby raingauges between 45 and 100 mm in 4 days, and on August 17 and 18 with 20-80mm in 48 hours.

This antecedent brought the discharge to be slightly grater than usual (about 2 m^3/s) on the morning of August 23 when, above Transylvania region, occurred very instable air mass; high air humidity, high temperature of surface layer of atmosphere and orographic features crated the meteorological conditions for significant thunder activity: several isolated areas of torrential rain occurred over Transylvania. In the area of interest thunder activity had three isolated parts: on the hills of the Southerner divide; in the mid part of the basin, just upstream Lupeni village; and in the NE part of the basin.

The villages in the basin are relatively small as number of citizens and gathered in two township: Lupeni (4600 inhabitants) and Simonesti (3600) with rural settlement. Industry is absent, excepting the natural gas extracting, near Simonesti. Villages are mainly composed by one floor, rarely two, brick houses, and part of them are located in the inundation area. This part was mainly destroyed during the flash flood including some life losses. No water management tools, as dike, dam or artificial lake is situated on the stream, and inundation area starts to be develop closely upstream the villages where bed slope is milder.

On the territory of the analysed flash flood, after local information on precipitation in the area close to Lupeni was estimated to be about 100mm between from 11:30 to 12:45 UTC, and in area of Simonesti the duration was considered from 13:15 to 16:00. The flash flood affected the communities settled along the valley: Lupeni and Simonesti, and their constituent villages.

As soon as the access was possible, after water retired, the rescue teams arrived in the area for the first aid, and to save people isolated by water (about 2000 people). Flood damages consisted on:

- 11 people died in Lupeni and Simonesti, and 5 missing;
- 2 bridges and 8 footbridges broken;
- 1400 houses impaired (255 of them disrupted);
- in the main road the traffic was interrupted for one day, and kilometres of local roads were out of function;
- the electric network and methane gas pipelines were affected as long as sewerage systems;
- 1000 hectares of agrarian lands, pastures and meadows were flooded.

The following information and values were determined by the experts from National Institute of Hydrology and Water Management during a post-event survey the day after the flood. At Simonesti hydrometric station, on August 23, 2005 at 0600 UTC, the water of the river was 110cm, constant for many hours. At 1615 started a very dense drizzle and consequentially the level increased to 240cm at 1500. The thunderstorm intensity in the upper part of the basin increased and at 1600 water level reach at 300cm. At this time the technician of the water level gauging station left the hydrometric station, because the situation became dangerous: water level have already reached over the banks and over the bridge. Using long distance observation and from the day after survey (flood marks), the timing of the peak has been estimated to be at 1630 with a maximum values of 467 cm, that correspond to an estimated discharge of 368m³/s. At that moment the width of water sheet exceeded 400m. Many houses, farms and roads were flooded. A secondary peak discharge was observed at about 2300 UTC with water level around 280cm; this second peak is probably due to the fact that water and wooden debris stored behind an artificial barrier (a bridge located in the village few kilometres upstream Simonesti), collapsed; the destruction of the bridge caused the sudden water release and secondary flood wave.

No additional information was collect in other part of the watershed and none of the nearby raingauges registered any significant amount of rainfall. These facts brought to proceed with the meteorological and hydrological analysis just using radar data and hydrological modelling: the resulting analysis is for this reason quite uncertain, but this is a quite common situation for flash flood. Radar data, with a resolution of 1km grid, were processed with usual correction for ground clutter and attenuation; in the Z-R relation parameter a=300 and b=1.4 were used. These fist tentative precipitation patterns gave a non realistic rainfall distribution, with the most intense area located several kilometres outside the basin south of the divide; people involved the post event survey excluded intense rainfall in those area. In this case, from observation and Doppler radar analysis, no significant wind drift effect was considered possible. Speaking with radar technicians, it resulted that the only possible explanation of this incongruence is the wrong orientation of the radar reference. In this case the displacement has been corrected by rotating anticlockwise the raw data by 4 degrees (that means about 5.5 km). With this device, watching at the single time step rainfall distribution, the time and space distribution is more coherent when compared with the report based on eyewitness. In addition the statistics described in Eq.3.6 and 3.7 relative to the five closest raingauges reported in Tab.4.I shows an improvement due to the rotation; this comparison has some importance but final conclusions are limited by to the fact that none of those raingauges has experienced a significant amount of rainfall.

	Correlation	Bias	FSE	MAE
Rotated data	0.99	-0.17	0.52	0.29
No rotation	0.98	0.34	1.35	0.54

Table 4.I. Comparison of bias, fractional standard error and mean absolute error between the five closest raingauges and radar.

Area [km²]	Spec disch. [m³s⁻¹km⁻²]	Tot. Rain [mm]	Annual prec. [mm]	Monthly prec. [mm]	Previous 30day prec. [mm]
167	2.2	76	608	70	169

Table 4.II. Basin and event data for Simonesti flash flood.

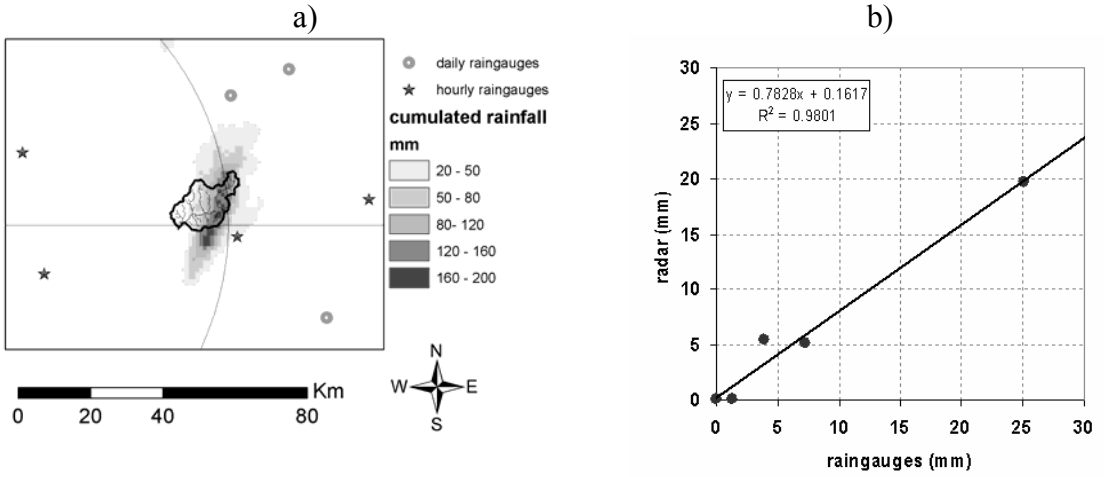

Figure 4.4. a) description of Feernic watershed with position of raingauge, distance from radar and estimated cumulated rainfall distribution basing on weather radar data; b) scatter plot between corrected radar data and the five closest raingauges for the cumulated rainfall at event scale.

The KLEM model has been routed with this precipitation input with a time step of 15 minutes using the synthetic network based on a 20 m DEM. A simple CN map is derived from land use data provided by Romanian Hydrological Service with values ranging from 40 for forested regions to 90 in for urbanized areas. Runoff generation and flood propagation parameters, reported in Tab5.III, were calibrated first to fit the observed peak discharge magnitude and timing secondarily than to match the flood wave shape.

S_0 (CN) [mm]	Ia/S	Recession [10^{-6} s^{-1}]	Threshold [ha]	Hillslope velocity [m s^{-1}]	Channel velocity [m s^{-1}]
305	0.15	15	0.6	0.05	2.5

Table 4.III. KLEM calibration parameters for Simonesti flash flood.

I Fig.4.5 the observed discharge values show an initial slow growth and then a sudden peak rising between 1600 and 1630 UTC, while the simulated hydrograph follow a milder curve. The impulsivity of the observed hydrograph could dependent from the blockage effect due to wood and solid material passing through narrow cross sections, while this dynamic is not considered by the model. At the scale of the entire basin (167km²) the mean areal precipitation results, after radar analysis, 76mm and an estimated runoff ratio value of 0.22 that is quite coherent with literature information, event description and terrain properties.

Since the only observed data concern the outlet near Simonesti, the model and the distributed precipitation data become powerful instruments to improve the knowledge about the dynamics along the river network. For this purpose further simulations have been carried, (using same parameterization) to investigate the simulated hydrograph in four subbasins

ranging from 4.6 to 60.8km². Cross section locations and specific simulate discharge hydrographs are described in Fig.4.3; different behaviour of the basin hydrological answer along the main river channel can be found:

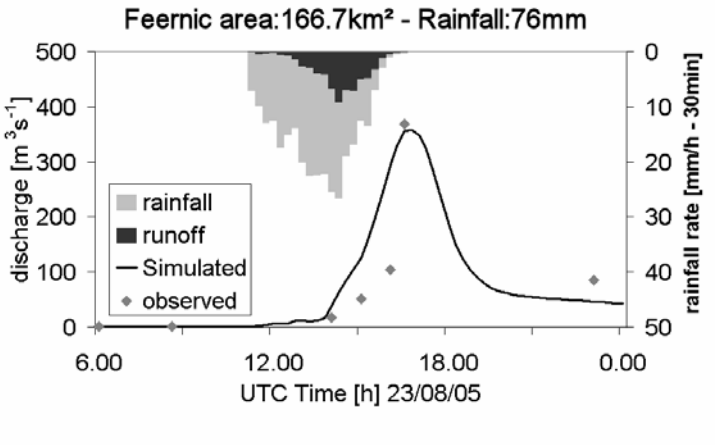

Figure 4.5. Simulated hydrograph compared with observed discharge.

- the upper part of the main river has experienced a relative medium amount of precipitation (127mm) with a specific contribution of about 4 m³/s/km²;
- the medium part has experienced the highest precipitation (up to 170mm during the entire event) and the short tributaries in this area have played a primary role on the flood generation, developing, with short timing offset, contribution up to 7-8 m³/s/km²;
- the lower part of the basin has a secondary importance on runoff generated volumes and the flood, along the main channel, propagated without any important contributes from its tributaries.

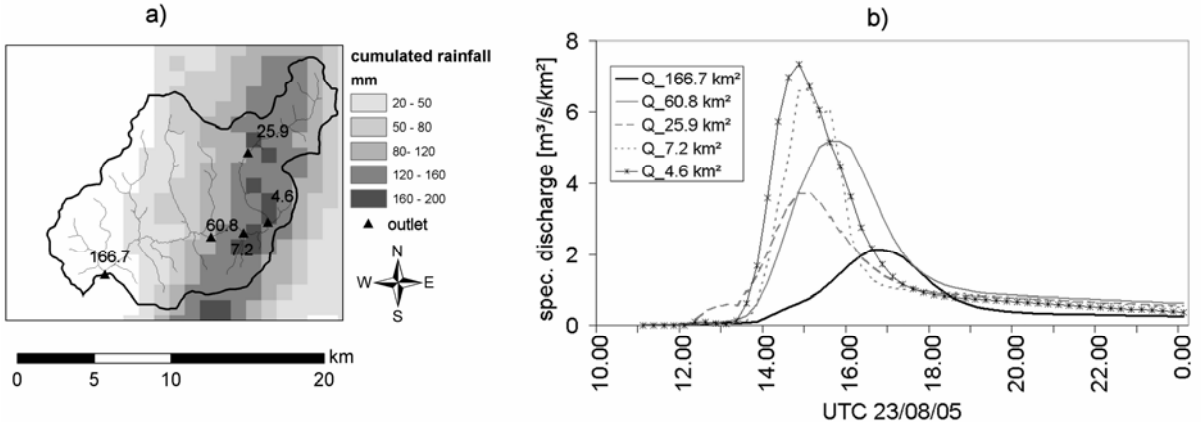

Figure 4.6. Hydrological analysis at subbasin scale: a) location of simulation outlets and picture of rainfall spatial variability; b) specific discharge.

Results of single simulated hydrographs, are here reported with the mean areal hyetograph for the four additional outlets:

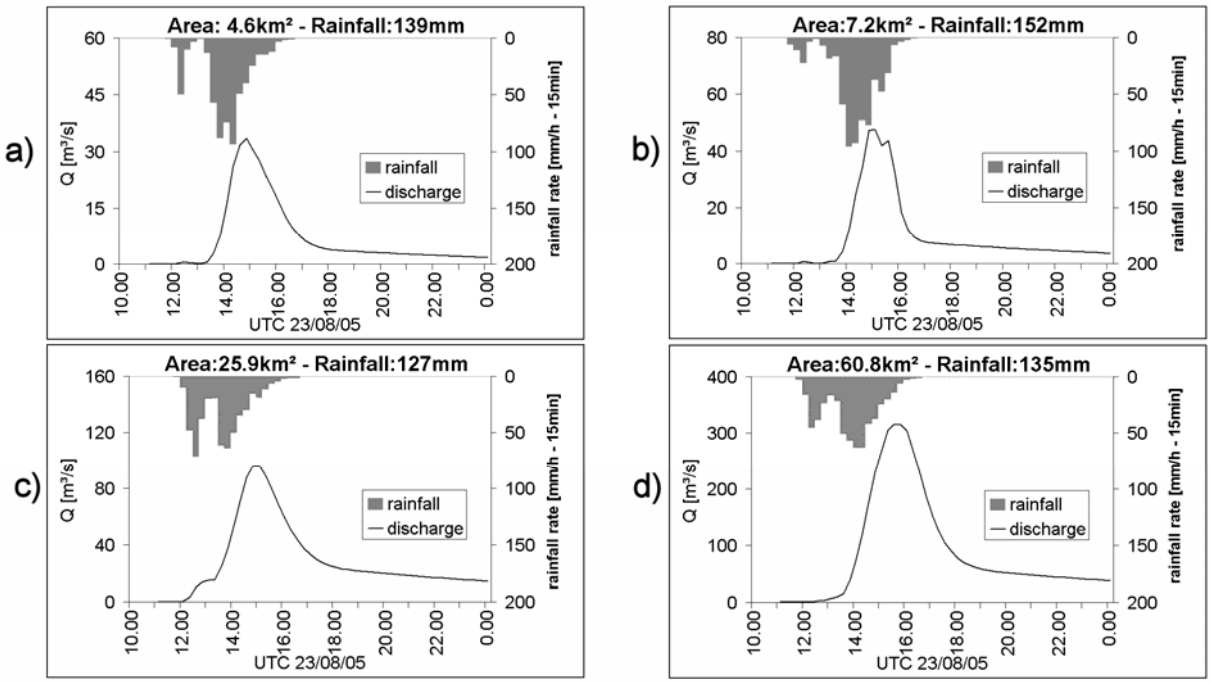

Figure 4.7. Hydrological analysis at subbasin scale.

4.1.3 Synthesis of other four Romanian flash flood analysis

Similar analysis has been carried in other four Romanian basins, selected from a larger dataset of catchments that experienced flash flood in the past years. Since the average information as event description are even poorer than the flood described in the previous paragraph, the selection of the four cases has been done according the availability and the quality of radar data: for the analysis the Z-R relation is here used with parameters a=300 and b=1.4. Elevation map and soil use is similar to ones for the Feernic flood. In some cases recorded reflectivity reached values up to 70dBZ: in these cases a maximum value of 60dBZ is considered to avoid overestimation due to hail presence.

Rainfall and discharge available data for the four events are resumed with the main information of each case.

- Casimcea basin (500km²), August 28, 2004. The flash flood event is part of a larger flooding that involved the Bleak Sea costal region. For both eastern Bulgaria and Romania, the meteorological situation resulted at the surface in wind field convergence (from North-West and North-East) and in a sustained, low-level, warm advection pattern, which transported abundant moisture, primarily from the Black Sea [Stancalie, 2008]. The entire event was characterized by two convective episodes. The first one, in the morning, generated over the Black Sea, in the vicinity of Romanian coasts, consisted in a supercell developed over Constanta city (with one hour precipitation up to 80mm). The second episode, in afternoon, was responsible for the flash-flood event at Casimcea. Like in the first episode, a bow-echo and a supercell where developed closed to the Casimcea watershed, and then moving toward West. The large extension of the event involved a considerable number of raingauges (see scatter plot in Fig.4.9b), that validate radar data. The flood destroyed 3 bridges and 8

footbridges, 53 houses were impaired (24 of them disrupted). The county road was affected in many places, being covered by waters and 1200 hectares of agrarian lands, pastures and meadows were flooded. Recorded hydrograph at the outlet show a fast discharge increasing few hours after the convective storm, with an estimated peak of 384 m³/s; since just a part of the entire basin was hit by intense precipitation, at the scale of 100km² the specific discharge probably reached a maximum values between 2 and 3 m³/s/km².

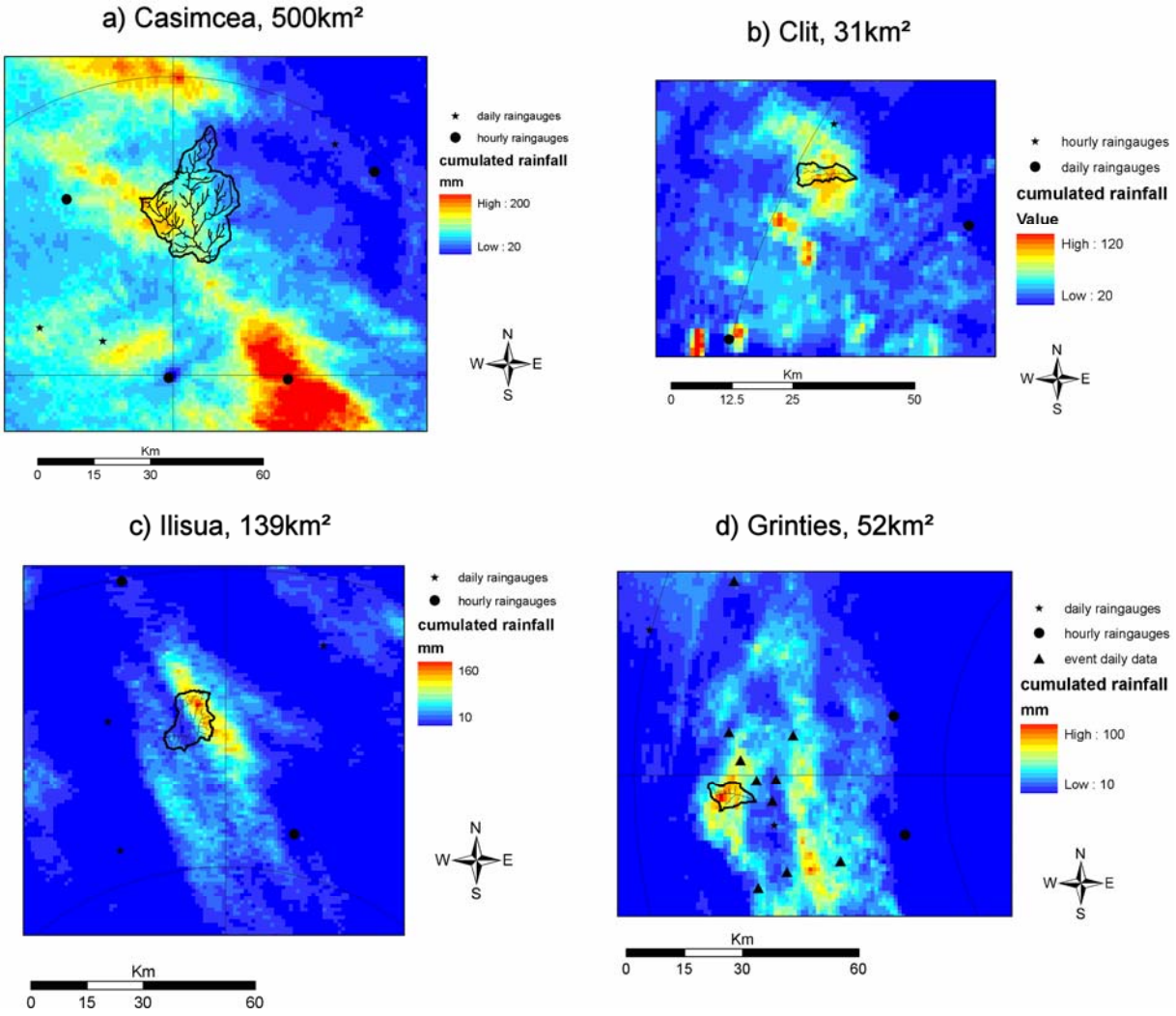

Figure 4.8. Cumulated precipitation spatial distribution in four flash flood events: a) Casimcea; b) Clit; c) Ilisua; d) Grinties.

- Clit basin (31km²), June 30, 2006. Meteorological situation in Europe consisted in Scandinavian high pressure area and in a smaller-scale disturbance affecting parts of Central and SE-Europe with the main focus for thunderstorm activity. The Mediterranean was dry and hot. High values of CAPE were registered in the Western parts where very instable Mediterranean air mass was present. The lower values for CAPE in the Eastern parts were also able to sustain the convective developments if the convection was initiated. The air mass that reached Romania had sufficient moisture in order to determine high precipitation, especially in Western parts. On 30 June 2006 air moisture, instability and lift acted together

in order to produce convection in this are of Romania. The North-Eastern parts were also characterizes by high values for vertical wind shear at low levels. After a 4° rotation the scatter plot regarding the four most heavily hit raingauges resulted quite coherent (Fig.4.9d). Clit stream was not gauged so the peak discharge at one outlet is obtained from post event estimation.

- Ilisua basin (139km²), June 20, 2006. No detailed meteorological situation is described and in this case radar information is the only quantitative description of the cumulated rainfall, since no raingauge experienced a significant amount of rainfall. Discharge at the outlet is estimated from post event survey.
- Grinties (52km²) August 04, 2007. Also in this case no much significant data about precipitation description from the official national raingauges network. In this case during the post event survey some information on rainfall amounts from unofficial raingauges have been collected. The following table is the result of comparison between radar estimation and unofficial records, with a good coherence of the two data.

Name	**Raingauge prec. [mm]**	**12:00- 19:00 Radar prec. [mm]**	**Dist from the basin [km]**
TASCA	47.2	41.9	25
SABASA	43	54.6	15
STRAJA	31.4	42.9	35
CEAHLAU	29.6	25.2	10
PLUTON	28.4	52.6	20
BICAZ CHEI	27	29.7	25
POIANA LARGULUI	23.2	16.3	10
BISTRICIOARA	21.5	17	10
FARCASA	66	55	10

Table 4.IV. Non-official cumulated precipitation data for Grinties event.

Here finally are described basin characteristic and parameterisation used to model the flood. The limit of this event approach is the sensibility of the model from initial condition parameters (S_0, Ia/S). This limit is acceptable when a good description of rainfall distribution and several cross section discharge information are available; the lack of these kind of information make the analysis weaker but this approach is still useful since in many situation no path can lead to more accurate reconstruction.

Basin name	**Area [km²]**	**Spec disch. [$m^3s^{-1}km^{-2}$]**	**Tot. Rain [mm]**	**Annual prec. [mm]**	**Monthly prec. [mm]**	**Previous 30day prec. [mm]**
Casimcea	500	0.6	62	419	45	94
Clit	31.2	5.4	81	619	95	192
Ilisua	139	1.39	64	797	110	335
Grinties	52	1.85	63	669	110	98

Table 4.V. Basin and event data for four flash flood cases.

Basin Name	S_0 (CN) [mm]	Ia/S	Recession [10^{-6} s^{-1}]	Threshold [ha]	Hillslope velocity [m s^{-1}]	Channel velocity [m s^{-1}]
Casimcea	406	0.15	15	2.0	0.05	3.0
Clit	127	0.1	15	0.6	0.1	3.0
Ilisua	165	0.15	15	0.6	0.1	3.0
Grinties	152	0.15	15	0.6	0.1	3.0

Table 4.VI. KLEM calibration parameters for four flash floods.

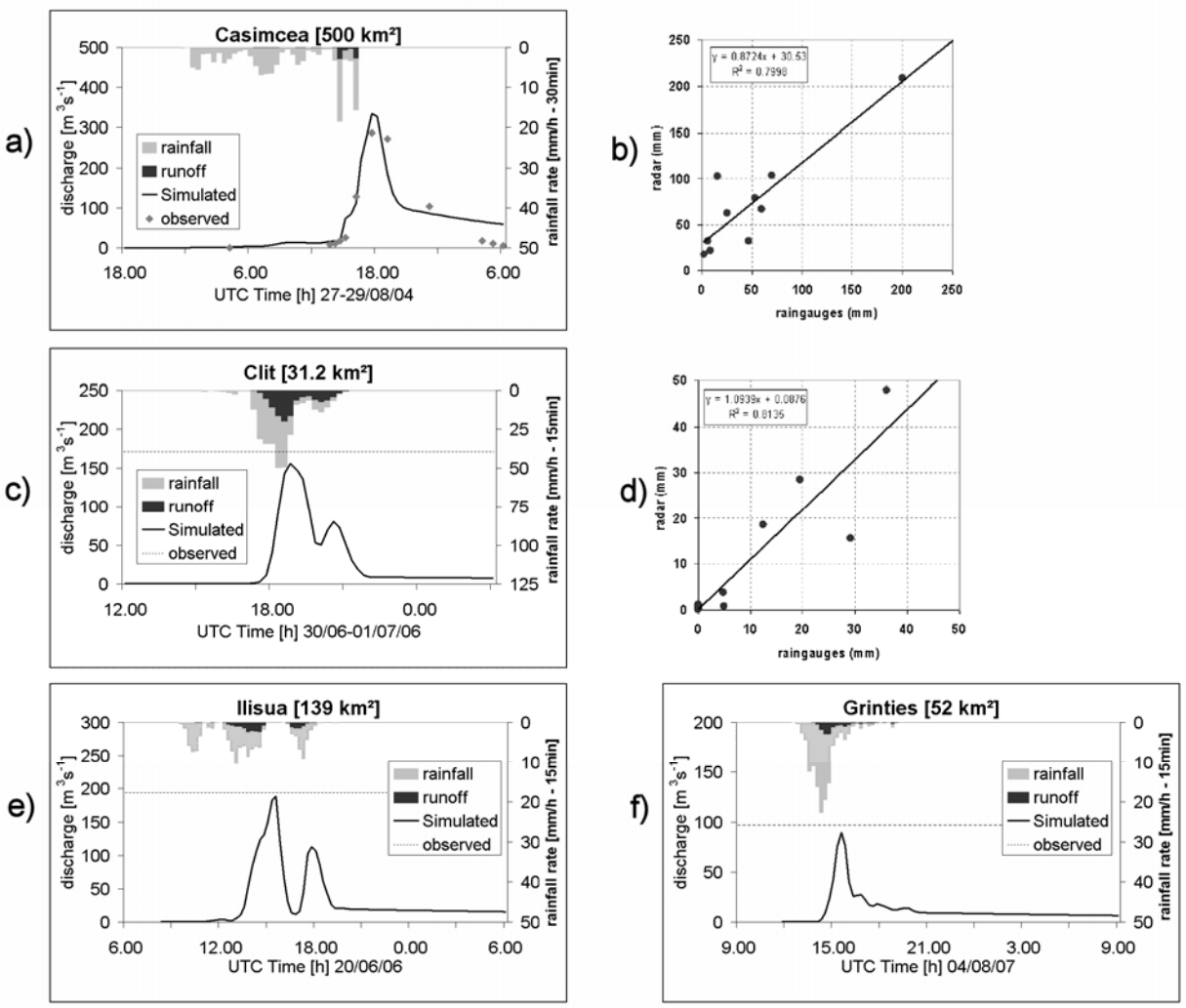

Figure 4.9. Simulated hydrograph compared with observed discharge for: a) Casimcea, c) Clit, e) Ilisua and f) Grinties; scatter plot are reported where a significant number of raingauges are avaliable: b) Casimcea and d) Clit.

4.2 Analysis of the September 2007 flash flood event in Western Slovenia

4.2.1 Hydro-meteorological features in Slovenia

Slovenia position in Central Europe, its pronounced orography, and presence of the Adriatic Sea contribute to form in the nation and it has three different climates: Middle-European, Alpine and Mediterranean. Slovenia varies in geological and tectonically aspects; 69% of its area are mountains and hills. Annual average intensity of rainfall varies a lot and average yearly intensity of rainfall is 1500 millimetres and average yearly runoff is about 1000 millimetres, but orography influences strongly spatial distribution of precipitation so annual average rainfall varies from 750 mm/year in the northeaster plain areas of Prekmurje to 3300 mm/year in the northwest in Julian Alps (climatologically the highest long-term precipitation amount in whole Alps [Reya, 1946; Frey and Schär, 1998; Vrhovec et al., 1998]). Frontal precipitations are enhanced by orographic influence; in case of strong events the combination of frontal precipitation with embedded orographically forced convection plays the most important role; finally during significant thunderstorms some parts of the region always get more rainfall precipitation then the others, [Brilly 1996]. The upper Soca river basin, and in general the area near the Triglav mountain is the region with highest precipitation in Slovenia and in whole Alps as well.

In Slovenia 16500 km² of territory drains into the river Danube, and 3750 km² into the Adriatic Sea. High precipitations rate and a considerable subsurface water storage amount produce a dense hydrographic network in some part of country, up to 2 km/km². Slovenia has a considerable number of small and steep headwater tributaries that flow with high velocity in the main river network. Floods in Slovenia occur mostly in spring (when snowmelt can play an important role) and autumn time (when processes are dominated by convective cell storms organized in mesoscale structures). Total inundated area under catastrophic condition (hundred years-return period of flood) is about 704 km² or 3.5% of total country surface: it is mainly bottom of narrow valleys. Even though agricultural employment has decreased from 50% in 1946 to 7.6% in 1991, still now almost 50% of inhabitants live out of heavy urbanised areas and about 25% of Slovenians live in households that engage in farming activities.

Landslides, torrential erosion and riverbank erosion are the most hazardous phenomena. Flash floods with heavy torrent erosion are yearly events in Slovenia and population is familiar with phenomena. The flood hazard zoning is incorporate in physical planning. Torrent control has more than hundred years of tradition in Slovenia: in the past few centuries a lot of structures for river bank protections, water diversion structures, small dams and bridges have been constructed, but the changing in economical and political organisation brings them to have poor maintenance and so they could be easily destroyed by flood flow causing aggravation of flow condition.

Slovenia meteorological network includes 290 rainfall stations with observation on 24 hours and 49 rain gauging station with continuous registration. For precipitation measurements there is, beside rain gauges, a source of information also the C band radar situated in the central part of the country on peak of mountain Lisca.

A systematic monitoring of flood level started in 1851, when the Drava River experienced an extraordinary flood; following are reported descriptions of last two major national floods, useful to describe the actual hydrological situation. The flood in 1990 interested the entire mountain territory in Slovenia and was caused by a storm that occurred at the end of October in high antecedent moisture condition, with cumulated values up to 140mm in 24 hours. The bad maintenance of control structures caused some dambreak effect due to the collapse of temporary blockage caused by landslide, as reported by Rajar and Zakrajšek [1993] for the Savica River. 520km² were interested by flood, with almost 100 destroyed bridges and 200 damaged; nine industrial facilities were destroyed and almost 400 were damaged; 190 homes were totally destroyed and 5080 were water damaged. Over 1200 landslides were triggered with the largest near Podvolovjek releasing 1.3 million cubic meters of earth. The total damage was estimated at more than 1100 million DM (about 560 million euro) [Blaz et al., 2008].

The autumn 1998 was a very active season, with three intense rainy periods in the north-west of the country: 5-10 October, 18-21 October and 4- 6 November. In beginning of October 150-350 mm of rainfall (in the Soca valley up to 520 mm) cause 20 years return period floods with landslides all over the country. In the second flood 100 to 200 mm of rainfall caused floods on rivers that mainly drainage karst region. Third period floods were the worst with 50 to 300 mm of rainfall. The floods exceed fifty years return period and on some places reach a hundred years return period flood. Hundreds of houses were flooded all over the country, landslides destroyed roads and railway and in some part of country were difficulties with power and water supply. International road connection between the Ljubljana and the Celje was closed for several hours. Some railway connections were also closed. Two people lost life by accidents related with flood, (Šipec 2000). The Savinja River overtops levees in the Celje. 950 km2 was inundated and 25 km2 of them was urbanised areas. Total damage was estimate on 350 mil of DM (about 180 million euro) [Dolinar, 2000].

4.2.2 Meteorological structures of 2007 event

On September 18, 2007, there was widespread flash flooding in Slovenia. One of the most severely affected areas was the Zelezniki municipality, where three people died and the flood damage to buildings and infrastructure was extensive. The Government of Slovenia declared the floods as a national disaster. In the entire nation there were seven human casualties and damage costs evaluated to 285 millions euro. More than 40 municipalities, i.e. about one third of the country, were concerned by this event. The city of Zelezniki (about 7000 inhabitants), located at about 50 km north-west of Ljubljana, was particularly affected by

the disaster (3 casualties, 100 millions euros of damages). The flood swept away cars, buses and severely damaged homes, a hospital and a water treatment plant [Bouilloud et al., 2009].

In North Europe a low pressure area developed during the pre-event days, acquiring great strength in the second half of September 17. A cold air front moved from Central Europe to Alpine area from NW direction; at the same time worm and moist air reached Ljubljana Valley from East Europe. [ARSO, 2007]. These conditions led to a constant NW moisture contribution and great atmospheric instability with strong wind up to 6km from terrain, and large convective system with peak of precipitation intensity insisting on the same area for several hours.

The first rain events started in early morning of September 18 between 03:00 and 05:00 UTC with a fast Eastward propagation. After a short break at 06:00 new convective storms took place in the Western mountain region with great intensity with a slower Eastern propagation. The most severe storms persisted several hours in the region between Idrica-Cerklje e Skofialoka, 40-70 km NE of Ljubljana until 12:00 and moved south toward Posocja, Tolmino, Radovlicja loosing intensity. Other rainfall structures developed during the afternoon in the Central-Northern part and in the evening in the South of the nation.

Data from raingauges and weather radar show that rainfall was distributed with a high variability, with consistent difference of cumulated values within few kilometre distance. A large area of the relief NE Ljubljana experienced cumulated rainfall that exceeded 200-300mm. The highest precipitation value from raingauge, 303mm, was recoded in Vogel, in the Trigav area, 15km east of the Seliska Sora Basin. The estimated return period time of this value, as long as for many other raingauges of the region, reached 20-50 years.

According to the Government of Slovenia (GOS) in Selscica Sora Basin, where damages were more considerable, flood caused more than Euro100 million in damage to Zelezniki Municipality alone (as much as in the remaining flooded areas). Here the flood swept away hundreds of cars, buses, and people, damaging homes, a medical clinic, and a local water treatment plant. On September 18, the GOS declared the floods a national disaster.

4.2.3 The flood in Selscica Sora Basin: rainfall distribution and IPEC results

Selscica Sora is the Northen of the two branches of Sora River, which is one on the main right tributary of the upper Sava River, where it flows few kilometres upstream Ljubljana (see Fig.4.10). The basin is almost completed forested in the upper part, with narrow valley with alluvional deposits and mainly grassland in the lower part; soils are well drained and varying in thickness over the bedrock. The geology is highly fractured and fissured with a variety of rock types including limestone, schist and shale. The permanent stream network (with contributing area greater than 1-2km²) is characterized by quite uniform slope of about 2-5%, while the ephemeral network is quite crowed, especially in steep hillslopes, and is characterized by high slopes. The upper valleys have generally a gravel road built few meter above the water level, and small villages consist on few houses along that road; single houses

are present also on hillslope where slopes are milder. Downstream Zelezniki a wide floodplain is present, with slower riverbed slope and several villages and cultivated field. In this valley the flood is well documented and known in the entire Slovenia, since for September 18 was scheduled the inauguration of a new car factory plant in Zelezniki: the national media were present due the prime minister presence: several videos are available on the web.

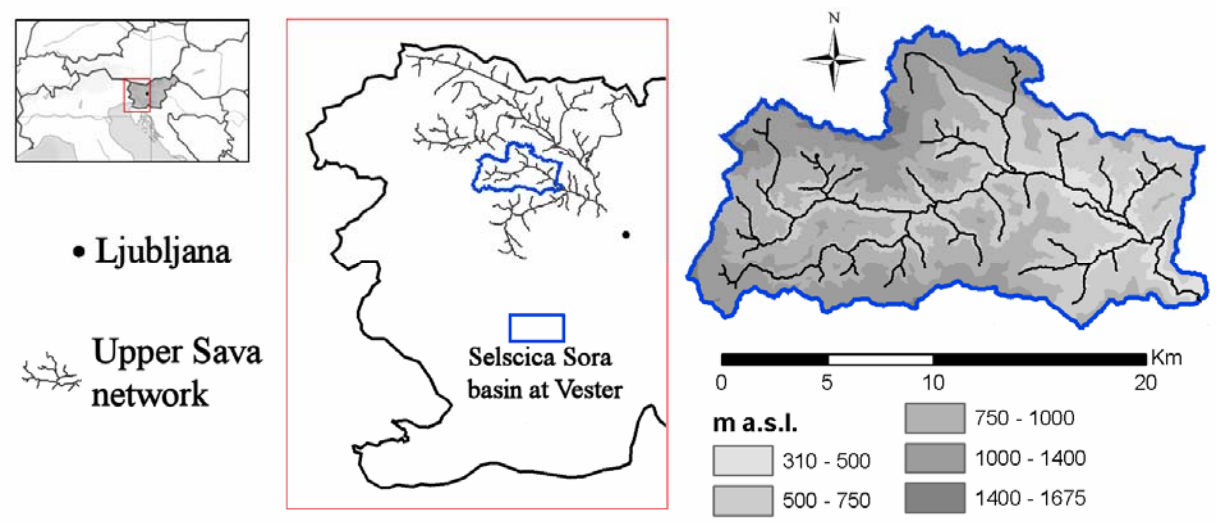

Figure 4.10. Selscica Sora catchment position in Slovenia with upper Sava river network.

In November 2007 about 20 European researchers carried on for the *HYDRATE* project an Intensive Post Event Campaign (IPEC). The survey aimed to rebuilt, trough standard procedures, flood dynamics and especially to improve the knowledge about the precipitation spatial and temporal distribution and about the discharge maximum values along the main and secondary river network. The study area, a 212km² basin considering as outlet the streamgauge in Vester, was divided in four regions, as shown in Fig.4.10, where radar distance and raingauge location are also reported: Davca, Upper Sora, Sora interbasin at Zelezniki and Sora interbasin at Vester.

The conventional data were quite poor: the only working streamgauge was located in Vester, 10-20 km downstream the area where major damages were observed: Davca subbasin and Zeleziniki; the streamgauge in Zeleniki went out of work at the beginning of the rising hydrograph. Just one raingauges is present in the basin, and few gauges nearby registered a consistent amount of rainfall; the unique raingauge within the watershed indicated a rain event mostly concentrated in 5 hours with a total amount of 220 mm. The main objective of the post event surveys was to understand rainfall spatial distribution and estimating discharge peak values and timing along the river network. Radar data and survey observations were carried separately and finally cross checked using hydrological modelling.

C-band weather radar located in Liscia was essential to understand precipitation spatial patterns. Data were corrected for ground clutter, screening effect and pre-processed with attenuation correction algorithms. Like in previous work [Delrieu et al. 1997; Serrar et al.

2000], three different drop size distribution (DSD) were assumed and the subsequent Z-R parameters. Since no DSD data were available for the Slovenian case, we actually considered a series of Z-R relationships calculated from various DSD models described in the literature and summarized in Delrieu et al. [2000]. This includes DSD models valid for widespread (a=242, b=1.43) and thunderstorm (a=533, b=1.36) rainfall and a Cévennes DSD model established in a French region prone to intense and long-lasting rain events resulting mostly from shallow convection triggered by the orography (a=362, b=1.40) [Bouilloud et al., 2009].

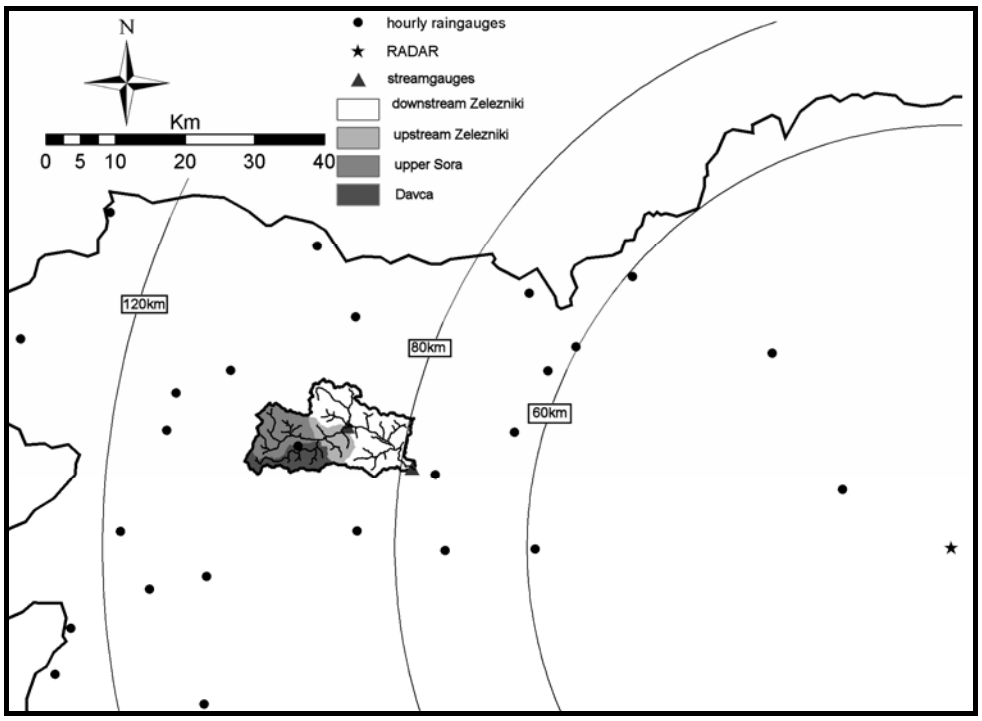

Figure 4.11. Study area of the IPEC with raingauge position and radar distance

Comparison of the results obtained with the three sets of relationships indicates that the widespread and Cévennes relationships lead to good and almost equivalent results while the thunderstorm relationship lead to worse results. Fig.4.12 shows the estimated rainfall distribution from radar observation after physical correction and a= 363 and b=1.40, while scatterplot between 31 gauges and radar extimation is reported in Fig.4.13. Radar analysis showed that precipitation moved in convective bands, 60-70 km in length and 8-12 km in width, from west to east over the country. The precipitation gradients in the directions orthogonal to the bands were significant, with differences in 1 hour precipitation totals of up to 50 mm within 7 km. The natural consequence of these precipitation patterns, which are relatively common in this climatic setting, is that neighbouring watersheds received different rainfall amounts and therefore exhibited contrasting responses to the event. The convective cells propagated quickly (60-70 km/h) through the convective band.

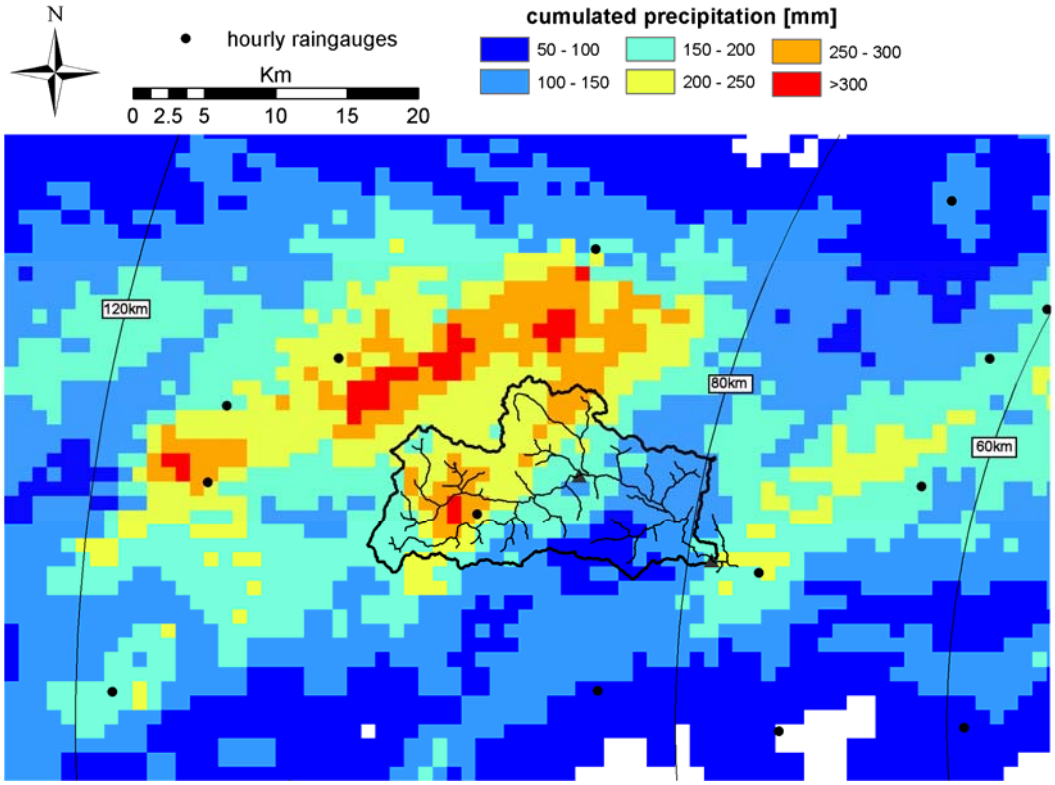

Figure 4.12. Cumulated precipitation from radar observation.

During the IPEC, river 24 cross section surveys (Tab.4.VII) were carried out in order to be able to calculate the peak discharge of the flood. The cross sections were surveyed using two methods; the most important reaches were surveyed with an electronic theodolite and additional cross sections were measured with a laser distance meter. Both types of survey measured the cross section, the river bed slope and levels of flood marks and recorded an estimate of the roughness coefficient of the channel and floodplain. Peak discharge is calculated at each cross section using the one-dimensional Manning-Strickler equation. Parameters were adjusted to take into account uncertainty and upper and lower bounds were given for each estimate.

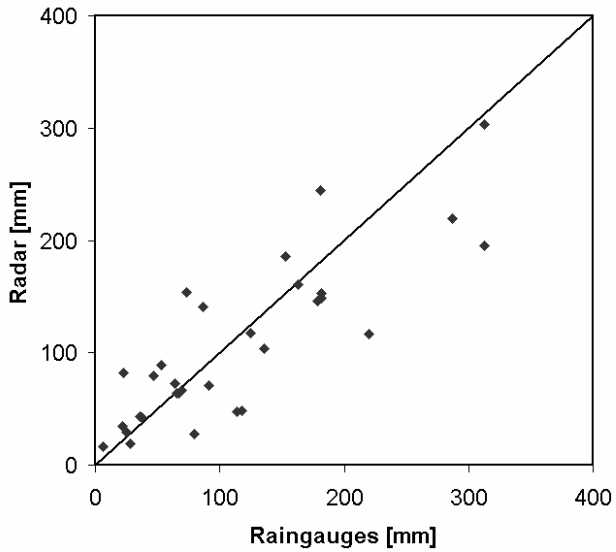

Figure 4.13. Scatter plot between radar estimation and 31 raingauge punctual measurements

Thirteen witness interviews were carried to add information to the analysis and in particular to improve the knowledge and time sequence of rainfall, discharge and other geomorphologic processes as solid and wood debris, landslide,... Each witness interview was carried out by one member of the *HYDRATE* team and one member of the ARSO (Agencija Republike Slovenije Okolje, Slovenia National Environmental Agency) and discussions were held with each witness individually. The witnesses were asked questions about what happened during the flood, the timing of the rain and the flooding and whether they knew of previous floods in to have happened in the area. Comparing different eyewitnesses report [Marchi and Bain, 2008] we can conclude with the following statements.

No.	Site	Upslope basin area (km^2)	Peak discharge (m^3s^{-1})	Peak timing [UTC]	Specific peak discharge ($m^3s^{-1}km^{-2}$)
1	S. Sora upstream Zadnja Smoleva	80.4	290-350		4.0
2	Zadnja Smoleva	7.5	16	11:00	2.1
3	Danjarska Grapa	9.2	80-120		10.8
4	Sranjnpoh	3.9	30-50		10.3
5	S. Sora downstream Danjarska Grapa	40.7	125-155		3.4
6	S. Sora between Zali Log and Davča	46.8	170-230		4.3
7	S. Sora upstream Zali Log	44.8	140-200		3.8
8	S. Sora at Dolenc, upstream Prednja Smoleva	95.5	330-430		4.0
9	S. Sora downstream Soriska	24.7	85-125		4.0
10	Globoka (tributary from Sorica)	11.0	10		0.9
11	S. Sora downstream Zadnja Sora	9.0	30-45		4.7
12	Zadnja Sora upstream Rovtarjev Grapa	2.3	7-12		4.4
13	Rovtarjev Grapa	2.6	10-15		4.6
14	Selscica Sora upstream Zadnja Sora	1.9	7		3.6
15	tributary between Globoka and Danjarska Gr.	0.2	5		25.0
16	Cesnjica in Zelezniki	25.8	35-50	14:00	1.5
17	S. Sora downstream of Zelezniki	147.2	260-320		2.0
18	Dasnjica in Zelezniki	10.8	25-40	14:00	2.8
19	Davca upstream confluence with Selscica Sora	31.8	80-120	11:15	3.8
20	Mustrova Grapa	4.2	8-15		3.1
21	Davca upstream Mustrova Grapa	21.4	140-170		7.0
22	Davca upstream reach, at the road to Pogorizar	9.8	50-60	11:00	5.6
23	Prednja Smoleva	5.7	9	10:30	1.6
24	Selscica Sora downstream Zadnja Smokva	88.0	180-195		2.1

Table 4.VII. IPEC results on 24 suveyed cross section

- In the upper Sora and the Davca valleys high intensity precipitations lasted form 7 to 11 UTC, river flow was characterized by high velocity, with level often more than 50cm above the road. Peak level was reached about at 11, and until the and on the day following the flood the water flow was consistently high.
- In Zelezniki the peak arrived at about 1200UTC where several houses were flooded with more than one meter of water for about two hours.

- Downstream Zelezniki the flow velocity was not very high, but most of the lower part of the valley, consisting in cultivated field, was flooded for several hours after the flood peak.

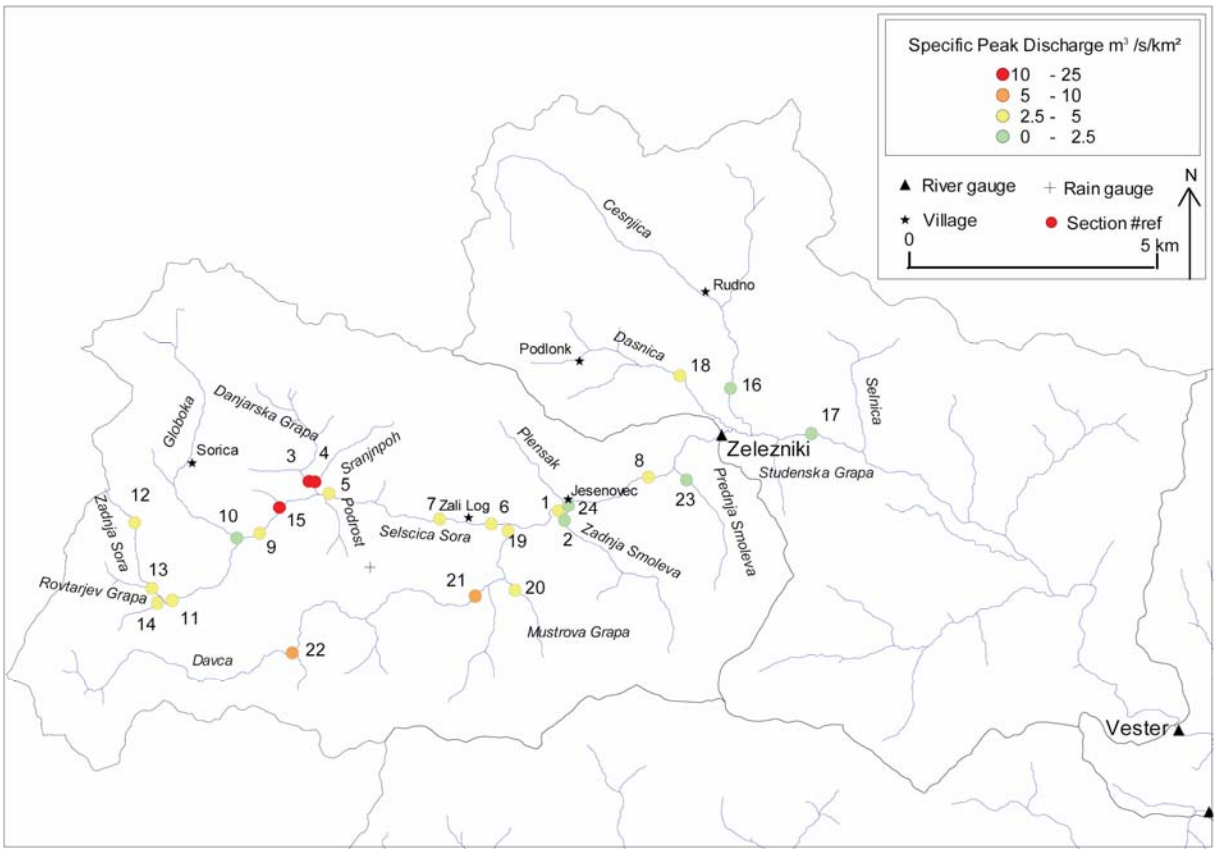

Figure 4.14. Geography of the study area with IPEC discharge estimation point locations.

Some historical information about Zelezniki area were also collected during the interviews. Until 1945, the town lived with water: a series of mill dams existed in the river bed upstream and in Zelezniki (about 30 mills in the valley). Before 1949, this part of the village was protected by a 3 meters high levee; on the other side of the levee a channel conducting water to the mills located downstream. There had been previous flood and debris flow events in the watershed in 2004, 1997, 1996, 1991, 1990, 1980, 1956 and 1926. It seems, however, that the majority of these incidents did not result in significant widespread flooding in the watershed and that, in contrast to the 2007 event, the consequences for the towns and villages were not severe.

A reconnaissance of the watershed found that there were widespread geomorphologic consequences of the event. There was erosion, transport and deposition throughout the main river channel and the tributaries; there were landslides on the valley sides and there were debris flows on many of the tributaries. The most severe debris flows were surveyed by measuring cross sections of the channel and measurements of alluvial fans to estimate the sediment volumes transported; the major one was surveyed in Zali Log. Here the eroded volume at several cross sections along the tributary is measured as well as the volume of

deposited sediment at the fan. There was some uncertainty in the estimates for this debris flow as there were several different sediment sources and several natural dams retaining sediment throughout the river course. Twenty four cross sections were surveyed, the slopes ranging from 20° to 10°, reducing in the deposition zone to 5º and there are some falls in the elevations due waterfalls. The difference in elevation from source to confluence is 250 meters. The estimation of the total volume of the fan is approximately 7000 m³. The field observations indicated that the origin of the debris was not a unique landslide source, but a general bed entrainment. There was a man-made structure (a wood store) in the central axis of the fan that survived the debris flow due to its orientation being longitudinal to the flow. It is possible that the structure contributed to blocking some sediments and slowing the debris flow at the base of the fan.

4.2.4 Focus on Davca tributary

The Davca Torrent is one of the tributaries of the Selscica Sora most severely hit by the flash flood. In the basin of Davca Torrent, field observations were carried out during the IPEC with the aim to depict the general characteristics of sediment and large wood transport. The Davca main channel is separated into different reaches in order to describe the processes related to sediment and to large wood (LW) transport which took place during the flood event. The reaches are marked on the longitudinal profile (Fig.4.15), which is derived from the DEM of the basin (12.5 m grid size), and therefore can be used for describing the channel bed at a large scale (i.e., > 100 m) only.

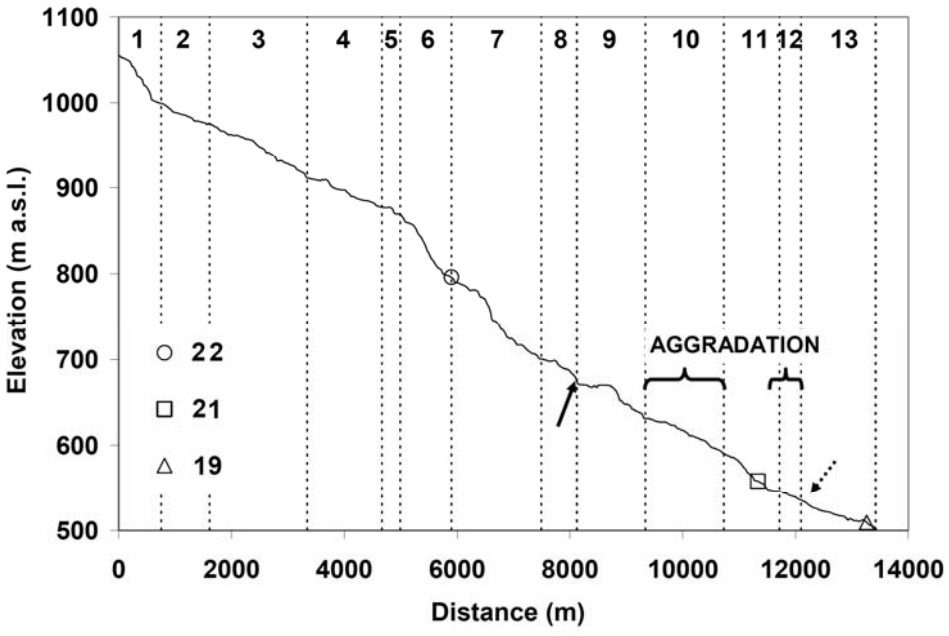

Figure 4.15. Longitudinal profile of the Davca Torrent. The solid row indicates the location of a major debris flow tributary, and the dotted line the confluence with the Mustrova Grapa. The void symbols (circle, square, and triangle) locate cross-sections where discharge was estimated.

Evidences of intense sediment transport were found at the headwaters (reach 1) below a 15-m high waterfall (downstream of the waterfall, abundant deposition of sediment, with

max size of about 30 cm was observed), and on a right tributary between the reaches 1 and 2 (hyper-concentrated flow with abundant LW recruited from the hillslopes). Overall, deposition of sediment and LW characterized the entire reach 2. Wood from upstream was trapped by the valley floor forest and by trees fallen into the channel as a consequence of bank erosion. The wide reach 2 ends at a road crossing where an eyewitness reported that the small bridge did not experience clogging during the flood, indicating how sediment and wood transport rates were not "excessive" here, despite a very high discharge (the flood marks are at an elevation 2.5-3 times the bankfull stage) was already present in this upper part of the basin. Also in the next downstream reaches (3 and 4), the event did not cause major instabilities in the channel. As a consequence, these two reaches lack significant wood and sediment sources adjacent to channel. Furthermore, several steep right-hand tributaries surely experienced high flow rates, but sediments and LW delivered to the main channel were of minor influence. Most of them underwent incision (up to 1 m) reaching the bedrock, with widespread bank erosion and associated recruitment of large trees, which were not transported to the Davca.

However, a road crossing (probably under-sized) between the reaches 4 and 5 likely caused backwater effects which led the channel to shift towards a forested floodplain just upstream of the bridge. Here many trees were recruited, further obstructing the bridge. In fact, there are evidences (lateral depositions, wood jams) that the main channel here spilled over the bridge. Downstream of it (reach 5), several huge LW jams (mostly composed of "fresh" trees) were trapped by standing trees on the floodplain and channel bends. These jams are up to 2m high, thus testifying a very high stage for a wide (15-20 m) cross-section. A possible flow surge issued from the bridge may be envisaged, but its effect must have been limited in length due to its small height and stored volume. Downstream of a check-dam (which separates reaches 5 and 6), the channel becomes steeper and then flows within a gorge over large boulders. Several large trees (beeches and spruces) fallen from the adjacent slopes are also present, but their transport was prevented by the narrow channel width. Between the reaches 6 and 7, the slope is lower, and the confinement of the channel on the right bank is less strict. Reach 7 is morphologically comparable to reach 6 and features a small debris flow on a right-hand tributary. In the reach 8, the main channel presents a milder slope and the valley floor widens considerably, with the presence of grassy floodplain. A probable hyper-concentrated flow on a left-hand tributary delivered some sediment to Davca. In contrast, the next channel reach (9), flowing in a gorge, features relatively abundant sediment sources from the right bank (debris flows, landslides). The reach ends at a bridge which was clogged by a probable combination of high water stage, intense coarse sediment transport, and floating LW supplied by nearby debris flows. Bridge clogging is indicated by upstream deposition of wood and sediment. The backwater effect led to channel aggradation, forcing the stream to flow on the road. The road embankment and the bridge obstruction finally breached, probably causing a flow surge downstream where high-elevation (>2m) marks were observed at channel banks. Reach 10 displays deposition of coarse sediment (up to 0.8-1m in diameter) and further

sediment inputs from the left slope (a small debris flow channel and several small landslides). Intense channel aggradation occurred where the valley widens, upstream of a bridge which collapsed and a huge LW jam was trapped upstream. The steeper, narrower reach downstream (11) was characterized by diffuse bank erosion and local bed incision.

Just upstream of the confluence with the Mustrova Grapa (reach 12), the Davca aggraded considerably, bridges were buried with sediments and wood and the flow invaded the road at left side. The bridge at the Mustrova-Davca confluence trapped some LW, but did not collapse because most of the flood water was flowing on the road. Part of the floating LW was then trapped by some trees at the road junction, while some accumulated against a building which resulted heavily damaged. Very coarse clasts (up to 0.8-1.0 m in diameter) were deposited upstream of the trees, and LW jams were up to 2 m high, both indicating very high stream power values. The total LW volume was estimated around 80 m^3, but much had been already carried away during restoration works. The longest wood elements (up to 8 m, roughly corresponding to channel width at the near upstream reaches) appeared to derive from riparian trees eroded by the flood, and the integrity of the bark cover hints to a brief transport distance, possibly just a reach length. In contrast, many shorter pieces showed clear signs of long residence time within the channel. Only a minor volume of LW elements likely reached the channel (Davca and Mustrova Grapa) and could be transported downstream (reach 13) towards the Selscica Sora. It is interesting to note that the peak discharge estimated for the Davca just upstream of the confluence with the Sora (section n.19) is less than at the cross-section number 21, located about 2 km upstream. Bearing in mind the large degree of uncertainty intrinsic in the estimates, possible interpretations of these results may include either flood attenuation at the confluence (due to valley widening, energy dissipation by obstacles), a dam-break flow surge related to the obstructed bridge between reaches 9-10, or their combination.

4.2.5 The flood modelling

The KLEM model has been preliminary routed in the four outlets of the basins shown in Fig.4.11 using the peak discharge values obtained during IPEC estimation to calibrate model parameters. CN values was obtained form land use map and a synthetic derange network was derived from a 12.5m resolution DEM: just four different land use classes were considered with curve number values ranging from 40 for dense forest to 90 for villages. 15 minutes rainfall fields from combined radar and raingauge observation were used for the flood simulation.

Model parameters were calibrated using the values in the three surveyed cross section and the data available from Vester streamgauge. As general approach runoff generation parameters were kept as uniform as possible in the entire basin, since there was no evidence of huge differences on local soil type and geology, geomorphology and cumulated precipitation value. In the entire basin Ia/S=0.2 and recession parameter 8 10^{-6} were set. During the campaign it

was noticed that soils are quite deep (more than one meter) in the floodplain and much thinner in steep hillslope (down to 10-20cm); this led us to calibrate S_0 parameter at subbasin scale according to subbasin average slope: DEM elaboration shows that upstream Davca and Sora confluence the average slope is much higher that downstream the same point. After a calibration procedure based on comparison with results in the four sections, S_0 was considered 305 mm for Davca and upper Sora basin, 380 for Zelezniki interrbasin and 405mm for Vester interrbasin. Field survey and interview collected velocity estimation; estimated values were very heterogeneous, but they clearly show that upstream the flood was characterized by much higher velocity than downstream. In the two headwater basin hillslope velocity is set to 0.2m/s and channel one to 4m/s, considering a 1 ha threshold. For Zelezniki interrbasin and steep tributary downstream Zelezniki chosen velocity parameters decreased to 0.1 and 3m/s, with 2.0ha threshold. In the remaining part of the basin 0.05 and 1.5m/s velocity were considered with 4.0ha threshold. This calibration shows coherence with peak timing estimation collected during the survey. Modelling results are shown in Fig4.16 for the four sections described above.

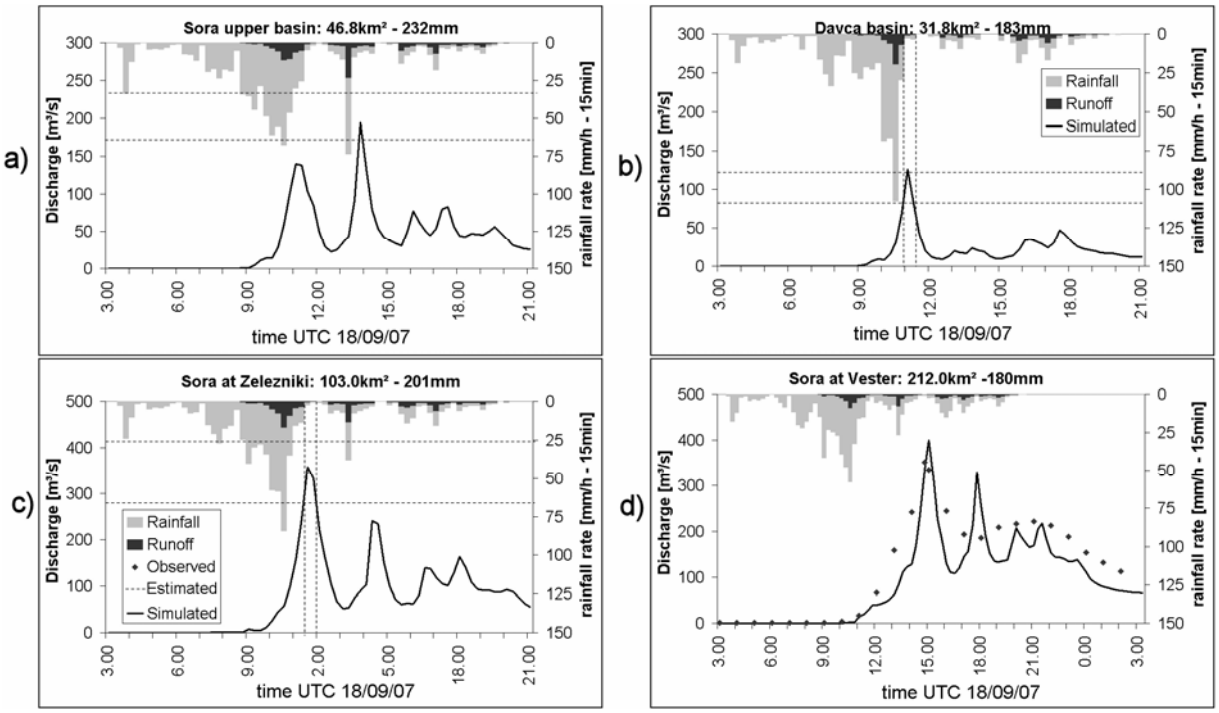

Figure 4.16. Comparison between IPEC data and KLEM model results for: a) Sora upper basin (section n. 6); Davca basin (section n.19); c) Selscica Sora at Zelezniki; d) Selscica Sora at Vester streamgauge.

Even though the kinematic wave model is not able to simulate behaviour as water storage in Zelezniki, results timing confirm observation from interviews about velocity propagation in the different part of the basin. It can be also noticed that in upper Sora catchment and in the downstream section a second peak three hours later of the first one appear in simulation. Analyzing the rainfall fields is possible to see at that time a strong convective cell approaching from north to upper Sora basin. None of the interviews report observations from that area, so it is not possible either to confirm or to exclude the modelled

features. As general guidance this observation suggests that after flood modelling a second survey can help to understand the reasons that lead to different results in modelling and IPEC comparison. The fact that no witness was easily found in the sparsely populated upper and Sora valley and the pre-assumption that there was no significant difference in timing with documented Davca catchment contributed that no specific IPEC valuation of peak timing in the first subcatchment was taken. Model results can't be validated or refused without a second survey, that was not possible inside this study.

For a better understanding of flood dynamic and modelling validation the simulation has been routed in nine additional surveyed sections, maintaining the same parameter set for the belonging basin. Fig4.17 shows that for most of the basins estimated and simulated peak discharges are compatible. A first suggestion to improve the knowledge on flood dynamics comes from the observation of results in section 2, 20 and 23, where relative low values of cumulated precipitation were found. The interpretation id open to two possibility: the first is that the three adjacent subcatchments have a particular geology; the second one is that the CN runoff generation model is not sharp enough to work, with the same calibration parameters, for basin that receive large different in precipitation contribution. A second observation come from section 10, where the simulated discharge is much higher than the estimated one; in this case in one interview is mentioned an indirectly account of relevant discharge in the considered tributary.

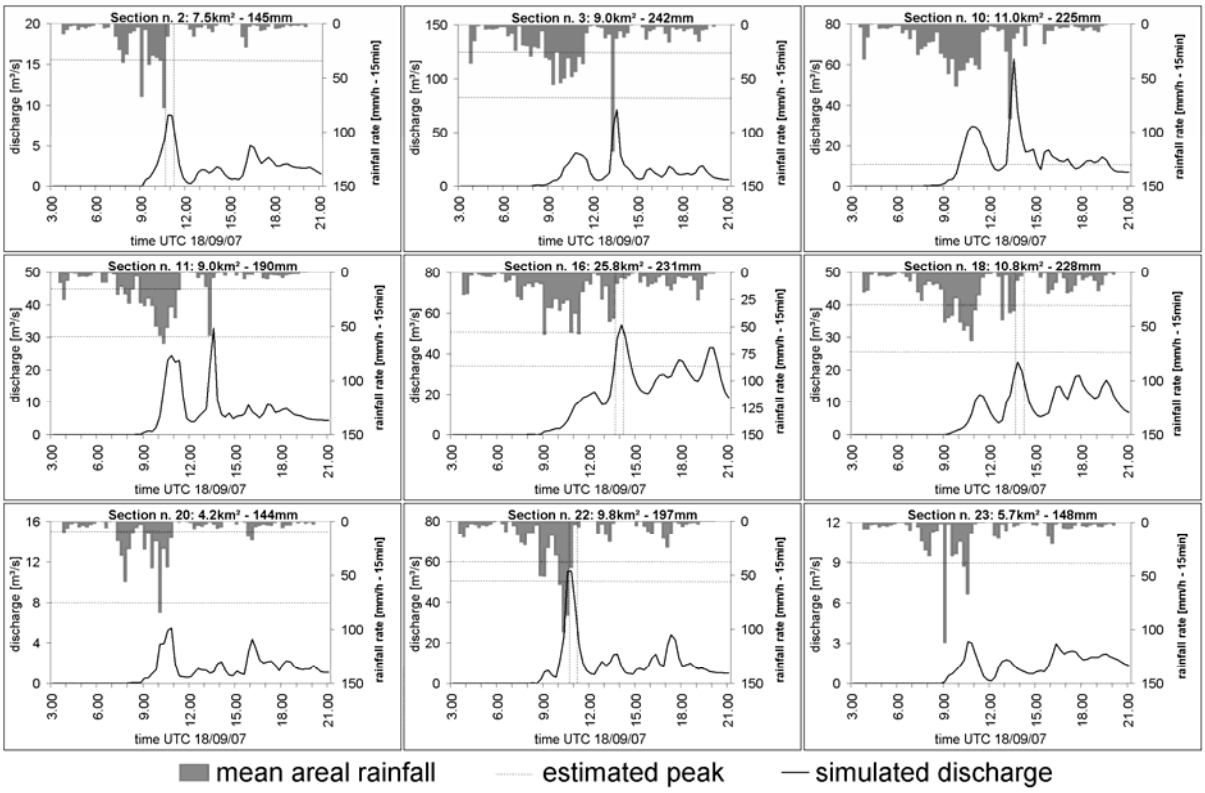

Figure 4.17. Comparison between IPEC estimations and KLEM model results in nine significant cross sections.

Considering that peak discharge estimation and flood modelling are processes in witch errors are quite frequent, results from a simplified models and a detail survey campaign show

quite consistent conclusions. Floods dynamic are comparable with other flash flood analysis (Borga et al., 2007) with upstream velocities greater that downstream ones and relative low runoff coefficient (0.15-0.25). Conflicting model results for this study show that a deep knowledge on flash flood dynamics can be obtained only after long time (several years). The fact that this event was surveyed little more than one year ago is a limitation on conclusive results; this study shows how detailed dynamics understanding is an iterative try and error process that need several alternate steps of field observation and flood modelling.

One example about how modelling results can be interpreted and guide a revision of IPEC collected data is the analysis of Mustrova Grapa, cross section n.20, where the estimated peak according to field observation was valuated between 8 and 15m³/s. Precipitation analysis shows that this basin was fed with a rainfall value significantly inferior to close upper Davca subcatchment (section n.22); hydrological modelling leads to a estimated peak value of 5.6m³/s. Similar precipitation and peak discharge values where found by an independent analysis carried by an *HYDRATE* French study group. This fact brought to additional inspection of the surveyed reach and suggested a discharge lower than that resulting from the reconstruction based on the flood marks: pictures taken during the campaign show that step-pools were not destroyed, there were not signs of erosion along the surveyed reach, and the vegetation along the banks was not severely affected by the flood. When reconsidering the estimation of peak discharge after model simulation, the operator could be "psychologically" induced to drive the reconstruction toward values close to those resulting from rainfall-runoff modelling. A second peak discharge estimation has been carried after a careful look at the survey data; specifically we consider that high values of the peak discharge were caused by a mistake in the identification of the water level in the surveyed cross-sections and so the energy slope was also modified: the new value adopted was obtained by excluding one (over five) unrealistic value of water level on the bank. The final peak discharge value is so considered 7.0m³/s.

4.3 Flash flood as triggers of debris flow: analysis of the 29 August 2003 event in the Cucco catchment

4.3.1 Introduction on debris flow

Debris flows in alpine basins play an important role in the evolution of headwaters, in the transfer of sediment from small drainage basins to main streams, and are a major source of risk for lives and property. Debris flows occur with different intensity, from minor events, which remain unperceived unless they encroach transportation routes or urban areas, to catastrophic events, which, in a very short time, cause major changes in the morphological settings of drainage basins and alluvial fans.

Large-magnitude debris flows in alpine basins are widely documented in the scientific and technical literature [Stiny, 1910; Montandon, 1933; Eisbacher and Clague, 1984, Rickenmann and Zimmermann, 1993; Mortara et al., 1995; Thouret et al., 1995]. Extreme debris flows often demonstrate unanticipated characteristics that point out limitations of predictive and risk management models. Documentation of these locally rare events may provide observations to advance understanding of the critical causative mechanisms and to improve predictive capabilities. Documentation of debris flows is mainly focused on mapping of the affected areas, estimation of the triggering rainfall, assessment of the volume magnitude and acquisition of field data for reconstructing flow variables like velocity and peak discharge [Marchi and Pasuto, 1999; Jakob et al., 2000; Gabet and Bookter, 2008].

Analysis of the triggering rainfall amount and intensity is usually based on raingauge networks. As such, it faces specific challenges due to the large space-time variability of the precipitation events and the sparseness of the measuring networks, particularly in the alpine terrain where debris flows are most common. Merging of raingauge measurements with observations from weather radar, characterised by high space-time coverage, is greatly expanding our ability to measure and monitor the rainfall distribution at the small space and time scales which characterise flash floods and debris flow events [Creutin and Borga, 2003].

Coupling fine scale rainfall estimates with spatially detailed surveys of the geomorphic response of the debris flow provide unique data to elucidate the hydrological and topographic controls of debris flows [David-Novak et al., 2004; Hicks et al., 2005]. Interviews with eyewitnesses provide information and anecdotal evidence on the time sequence and dynamics of the debris flows, and as such they add a time dimension to the spatial patterns of the geomorphic response [Borga et al., 2008]. In this study, the hydrological and hydrometeorological controls and the erosive response of an extreme debris flow event are examined. The debris flow (with a sediment volume of about 78000m^3) was triggered in the Rio Cucco basin (0.65 km^2) by a severe rainstorm occurred on August 29, 2003, on the Fella River basin (eastern Italian Alps). The storm lasted for about 12 hours from 1000 CET to 2200 CET (Central Europe Time), triggering shallow landslides on soil-mantled slopes, widespread debris flows in minor streams, and causing a flood with intense sediment transport in the main

stream (Fella River) and its major tributaries. Tropeano et al. [2004] provide a general description of debris flows and damages in the affected area.

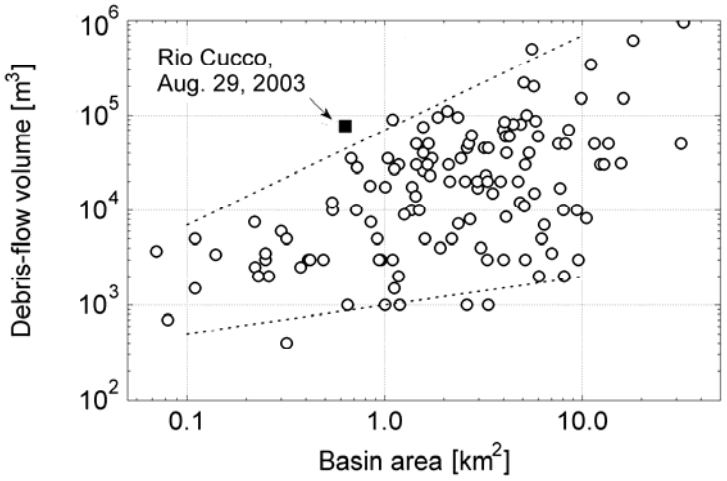

Figure 4.18. Scatterplot of debris-flow volumes versus drainage basin area in North-Eastern Italy (Rio Cucco data added in picture from Marchi and D'Agostino [2004]).

Fig.4.18 compares the magnitude of the August 29, 2003 event in the Rio Cucco with a sample of 127 debris flows observed since late XIX century in north-eastern Italy. The volume of the Rio Cucco debris flow lies above the upper envelope line drawn in the scatterplot of debris-flow volumes versus basin area, thus underlining the extreme intensity of the event. The analysis of the causative rainstorm is based on rainfall estimates from radar observations and data recorded by a raingauge networks. The 29 August 2003 debris flow is also of particular interest because it provides an end member in the spectrum of impacts of antecedent soil moisture on debris flow triggering. The event resulted indeed as a combination of two extreme events, since very high accumulations of rainfall over 3–6 hours occurred at the end of a climatic anomaly of prolonged drought and warm conditions in Europe and over the Mediterranean. These conditions led to very dry soil moisture status at the onset of the storm event.

The main objectives of this part of the study are to investigate the space-time structure of the triggering rainfall event, to analyse the hydrological processes that controlled the flood response and to document the debris-supply processes along the channel network and the sedimentary processes on the alluvial fan. These objectives are achieved by using and combining together fine-scale rainfall estimates obtained by merging weather radar observations with raingauge measurements, flood response simulations from a distributed hydrological model, post event field surveys of the erosive response and collection of eyewitnesses' accounts.

The Rio Cucco basin (0.65km²) is located on the right flank of the upper Fella River valley (see Fig.4.19). The catchment is made of two sub-basins, which merge in the central part of the alluvial fan (Fig.4.20a). For this reason, the hydrological analysis and the examination of the erosive response is reported here considering the two sub-basins

individually. Tab.4.VIII reports the main morphometric parameters of the two sub-basins. The geology consists of highly fractured Triassic dolomite and limestone. A spatially-limited outcrop of San Cassiano Formation (calcarenites intercalated with marls and pelites) is observed in the upper part of the basin.

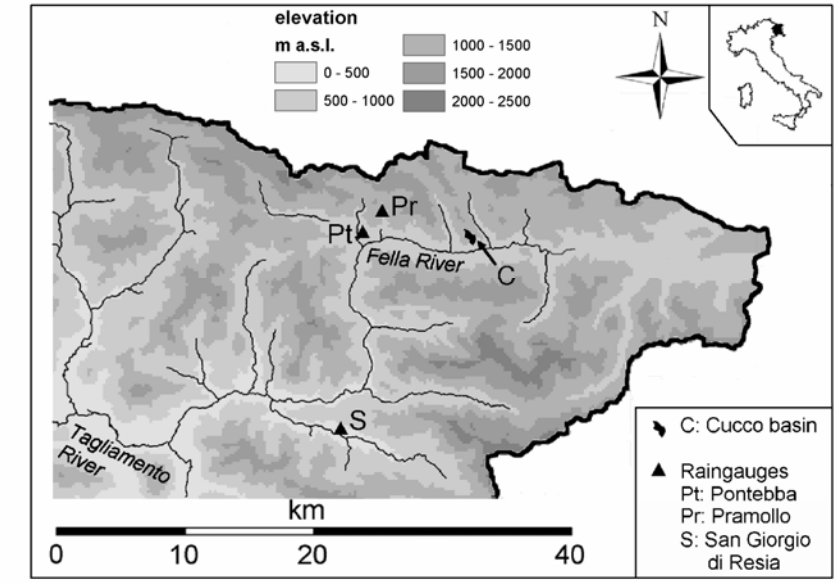

Figure 4.19. Location map of the upper Fella River basin showing the regional setting of the Rio Cucco basin.

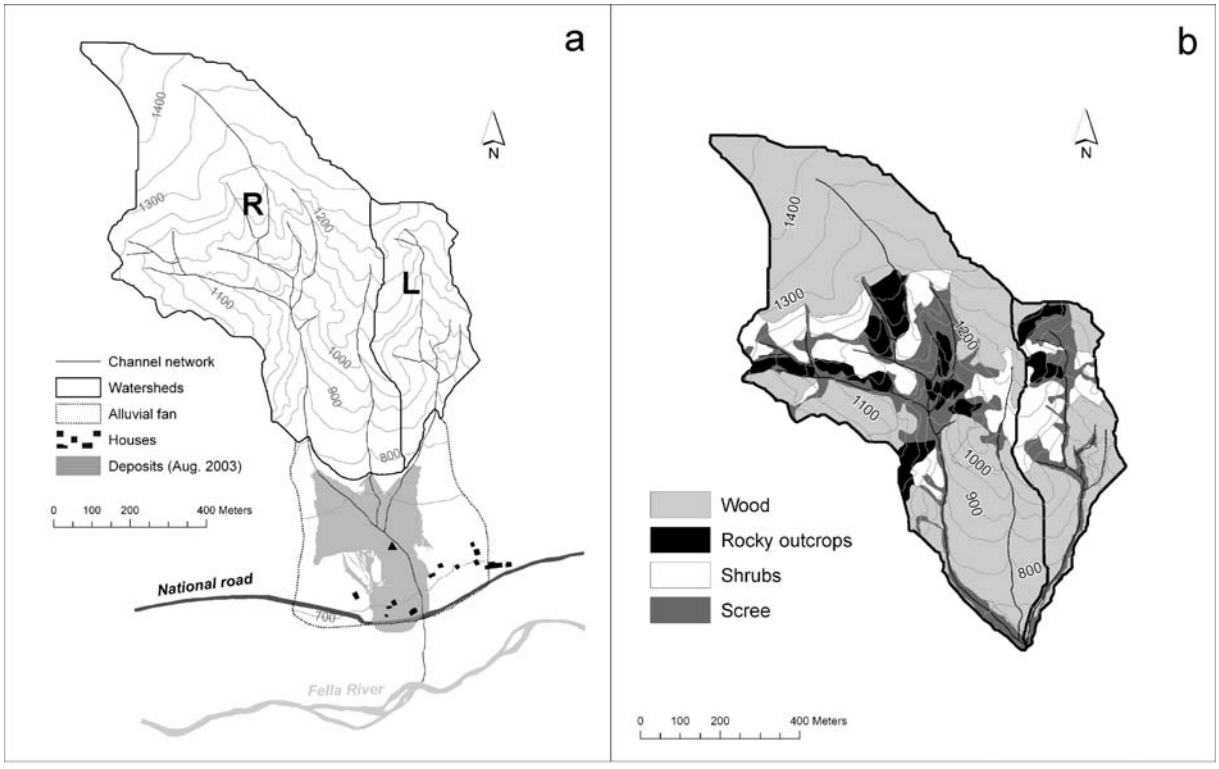

Figure 4.20. The Rio Cucco basin with: a) contours showing the topography of the basin, right (R) and left (L) subbasins, and the fan; b) land use distribution. Contour interval: 50 m.

Land use and land cover properties are reported in Fig.4.20b. The mean annual precipitation amounts to about 1600 mm with two maxima in June and autumn. High-intensity rainfall, which are responsible for debris-flow triggering have the highest frequency in July and August for 1 hour duration, in August and September for 3 hours duration and in October and November for longer durations (from 6 to 24 hours). Analysis of rainfall annual maxima at the regional scale [Norbiato et al., 2007] provided estimates of 100-year return period rainfall: these amount to 74.3 mm, 193.4 mm and 246.9 mm for 1, 6 and 12 hours, respectively.

	Left sub-basin	Right sub-basin
Area (km²)	0.125	0.524
Minimum elevation (m)	724	725
Mean elevation (m)	1020	1141
Maximum elevation (m)	1288	1481
Average basin slope (°)	46	40
Average channel slope (°)	25	25

Table 4.VIII. Main morphometric parameters of the Rio Cucco basin.

4.3.2 Field surveys procedure

Field observations aimed at assessing the debris volumes mobilisable by debris flows in the Rio Cucco basin were carried out during the weeks before the flood (July and August 2003). Active channel stretches were surveyed in order to determine the volume of debris mobilisable from channel beds and the potential for landsliding in the immediately adjacent slopes of the torrent. Topographic maps at the scale of 1:5000 were used in the surveys. Field observations were repeated immediately after the flood of August 29, 2003 to determine the contribution of individual sediment sources to the overall sediment budget and to characterise flow processes on the alluvial fan. This provided a unique opportunity to evaluate the geomorphic impact of this catastrophic debris flow. The channel network and the sediment sources on side slopes were surveyed to assess the eroded debris volumes. Field measurements were carried out using a GPS receiver, a laser range finder and measuring tapes. Erosion was assessed by comparing the topographies surveyed before and after the event of August 29, 2003. The geometric settings of each sediment sources (extent and depth) were used for computing eroded volumes. Erosion marks and fresh exposures of bedrock channels, previously filled with debris, made it possible a reliable assessment of erosion depths. Debris-flow deposits on the alluvial fan were also surveyed, paying attention to both the estimation of accumulated sediment volumes, and to morphological and sedimentological features. The boundaries of the deposits were mapped using a GPS; their thickness in the various parts of the alluvial fan was estimated from field observations carried out during the removal of accumulated debris.

A survey on soil hydraulic properties was carried out on the nearby Uqua basin [Borga et al., 2007], more accessible to hydrological field survey and similar to the Cucco as far as

soil properties are concerned. Two local residents were interviewed about the magnitude and timing of both rainfall and debris flow. Comments on rate of stream rise and timing of the debris flow start and peak, as well as about the type of the solid transport (bed load or debris flow), were noted. One of the two eyewitnesses was a retired forester, quite experienced in documenting and reporting natural disasters in mountainous areas.

4.3.3 Hydrometeorology

On August 29, 2003, at the end of a prolonged drought, a Mesoscale Convective System affected the study area, starting at 1000 CET and lasting for 12 hours. The storm affected a 1500 km² wide area, and caused loss of lives and substantial disruption of the local economy, with damages close to 1 billion Euro [Tropeano et al., 2004; Borga et al., 2007]. C-band OSMER radar station, located at Fossalon di Grado, 90 km from the Cucco basin in the south direction, and 15 raingauges were used to describe rainfall fields with 15 minutes time step and 1km spatial resolution.

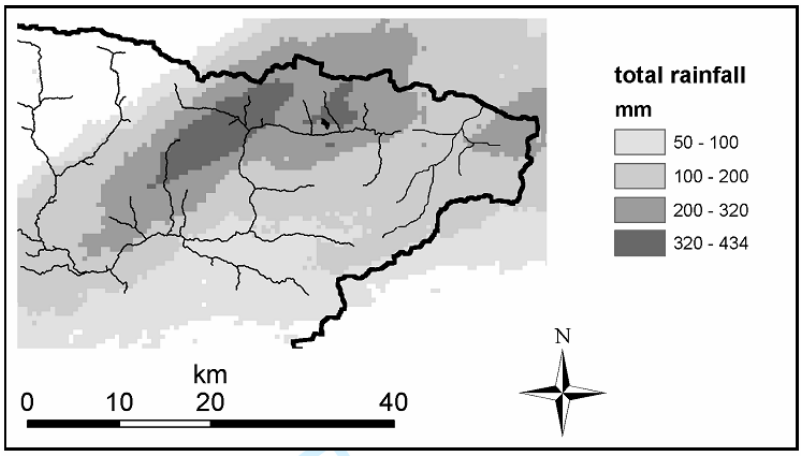

Figure 4.21. Storm total rainfall (mm) for the August 29, 2003 event.

The storm total precipitation (Fig.4.21) exhibits two local peaks of rainfall accumulations exceeding 320 mm. One of these includes the Cucco catchment. A striking characteristic of the event is its organization in four well-defined banded structure. Some of the bands persisted in the same locations for the duration of the event. New cells formed repeatedly over the foothills of the Alps and intensified while being lifted onto the orographic barrier; this caused the quasi-stationary and persistent banded pattern. The steadiness of these rainbands led to highly variable precipitation accumulations; the rain gauge at Pontebba recorded 389.6 mm of precipitation in 12 hours, while San Giorgio di Resia, located just 15 km to the south (Fig.4.19), but not directly under a band, recorded only 68.4 mm during the same period. Extreme spatial gradients in precipitation accumulations up to 80 mm/km can be recognised in Fig.4.21. The size of the storm measured at the Pontebba raingauge, located eight kilometres to west with respect to Rio Cucco, was 88.6, 233.4, 343.0, 389.6, and 396.2 mm for the 1-, 3-, 6-, 12- and 24-h maximum, respectively.

The rain rate time series (averaged over 15 minutes) over the Cucco basin (Fig.4.22) shows a sequence of four rainfall pulses with increasing peak rainfall intensity with cumulated values 331.5mm. The final one consisted on 125 mm h^{-1} intensity from 1745 and 1830 CET. The storm chronology derived from radar is consistent with an eyewitness account placing a high rainfall period around 1545 CET and another one around 1800 CET.

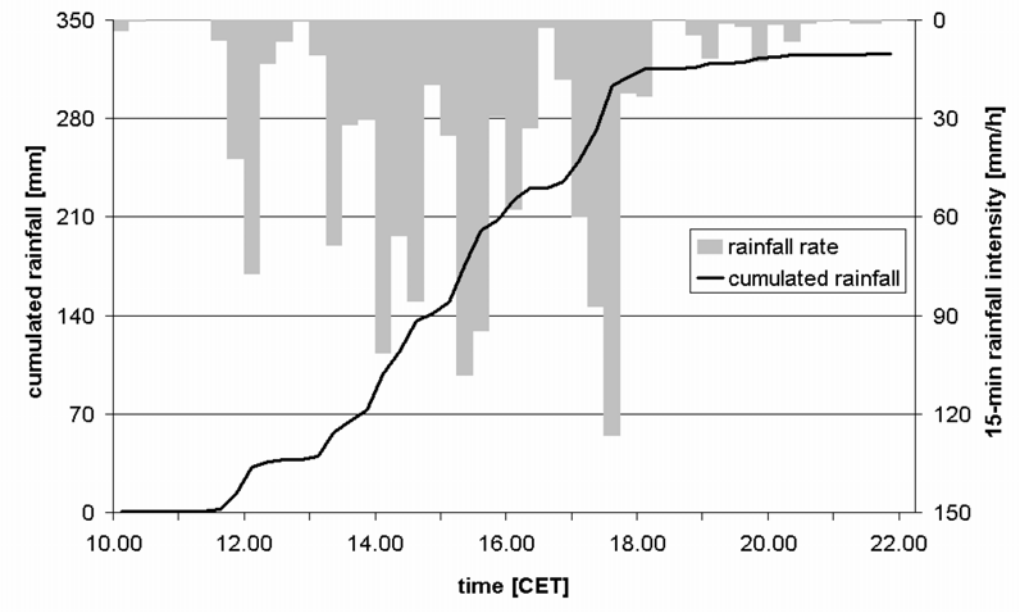

Figure 4.22. Time series of 15-min rainfall rates and cumulated rainfall over the Cucco basin.

4.3.4 Flood modelling and analysis

The application of GRISS-2D to the Rio Cucco basin is based on transposition of parameter values from the nearby Uqua basin (23.9 km²), similar in soil properties and geomorphology. For the Uqua basin, indirect liquid peak discharge estimates and time of the peak flow were available for the August 2003 flash flood [Borga et al., 2007], hence allowing adjustment of model parameters. The soil depths of the vegetated area have been considered variable with slope, as shown in Tab.4.IX, accordingly with field observations. The topography was represented through a raster-type DEM with cells size of 5 m; the model was applied at time intervals of 15 min.

Parameter	Value			
Roughness coefficient (G-S) – Hillslope [$m^{1/3}/s$]	0.1			
Roughness coefficient (G- S) – Channel [$m^{1/3}/s$]	10			
	Forest	Rocky outcrops	Shrubs	Gravel
Lateral saturated hydraulic conductivity [m/h]	0.5	0.0	0.5	1.0
Vertical saturated hydraulic conductivity [mm/h]	80	0	80	150
Suction Head [m]	0.3	0.0	0.3	0.0
Effective porosity [-]	0.4	0.0	0.4	0.4
Soil depth [m]		0.0		4.0
<30°	0.8		0.6	
30°-60°	0.4		0.3	
>60°	0.2		0.15	

Table 4.IX. GRISS-2D parameterisation: roughness coefficients and soil hydraulic properties.

The results of the application of GRISS-2D to the 2003 flood on the two sub-basins of Rio Cucco at their confluence are shown in Fig.4.23. Several features are worth analysing in this figure. First, the results point out the strong impact of the low initial soil moisture conditions on the flood response. This influence is not unexpected, due to the combination of the exceptionally dry summer 2003 and high soil moisture capacity characterising the study area [Borga et al., 2007]. Precipitation during the first two rainfall pulses (from the start of the event to 1400 CET) is almost completely infiltrated, with initial losses exceeding 80 mm. These results are confirmed by the eyewitnesses accounts, who reported liquid response only after 1400 CET. The third rainfall pulse generates a first significant runoff peak in both sub-basins, with a simulated peak discharge at the confluence around 8 m³/s. After a rainfall hiatus around 1700 CET, the last peak discharge is reached at 1745 CET, with a simulated liquid peak discharge of 11 m³/s, corresponding to a unit peak contribution of 17 m³/s/km².

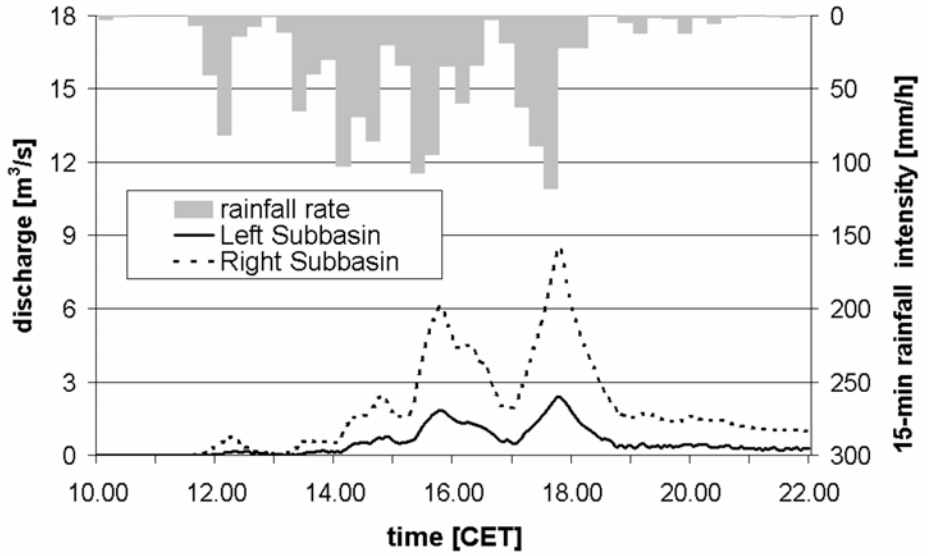

Figure 4.23. Results of GRISS-2D application for the two sub-basins of the Rio Cucco

These results confirm the findings from examination of scale-dependent flood response reported for this event by Borga et al. [2007] that founded similar estimates of unit peak discharges at basin scale of 1 km² in the portion of the Fella basin affected by the central convective band. Furthermore, the major controls of the flood response were both the exceptional cumulated rainfall amount, and the large rainfall intensities. The computed runoff ratio is around 0.5, pointing out the impact of the dry antecedent soil moisture conditions on runoff generation.

A major geomorphic impact of the flood was the enlargement of the active channel network and the generalised channel and bank erosion observed along the river network. In the wider sections, river banks collapsed and retreated, thus injecting a large volume of sediment into the active channel. In the narrower sections, bank undercutting triggered sideslope failures, to the detriment of colluvial or weathered bedrock slopes. The total

estimated eroded volume amounts to 78000m³, with an estimation standard deviation around 8000 m³. This leads to a confidence interval ranging from 70000 to 85000m³. In spite of its smaller area, the left subbasin provided the largest contribution to the total erosion, with a volume of about 45000m³). About 20% of the total eroded volume estimated in the field derived from newly formed erosion areas. Sediment supply mostly came from channel bed and banks, whereas the contribution of shallow landslides was limited to the slopes adjacent to the channel network, which are characterised by thick debris, steep slopes, and where flow concentration occurred. The limited occurrence of landslides on most basin area can be ascribed to the low gradient of the lower part of the basin, as well as to thin soil cover on most slopes in the middle and upper part of the basin. Debris volume deposited on the alluvial fan, estimated though surveys carried out just after the event, amounts to about 85000- 100000 m³.

The chronology and the flow characteristics of the debris-flow response have been established based on interviews to the two eyewitnesses. Accordingly with the witnesses' reports, the event was divided into three phases, corresponding to different flow processes. During phase1 a remarkable solid transport was reported, mainly as bed and suspended load. Phase2, from 1700 to 1800 CET, corresponds to the largest rainfall pulse and is the most intense phase of the event, with a prevailing contribution of the left sub-basin; this phase was described by one witness with typical features of a debris flow. Phase3 is characterised by lower solid concentration with further accumulation of sediment on the alluvial fan. The relatively high runoff rate during the receding phase of the flood points out the role of subsurface flow activated by the large amount of infiltrated water. Erosion mostly occurred along streams and on unvegetated slopes close to the channels, whereas the extent of failures on forest-covered slopes was spatially limited: as support of this hypothesis no important presence of woody debris was reported by eyewitness. These evidences and the results obtained by the hydrological model were used to evaluate the consistency between the runoff volumes and the sediment volumes generated during the three phases. To this purpose, the water-sediment balance during the various phases was analysed by assessing the sediment concentration by volume (C_v), given by:

$$C_v = V_s / (V_s + V_w) \quad (4.1)$$

where V_s is the solid volume and V_w is the water volume. The water volume is given by the combination of the runoff volume and of the soil water stored in the eroded volumes. Both values were computed by means of the hydrological model. The overall solid volume was computed based on the observed sediment volume by using a soil porosity value of 0.4, yielding an overall value of solid volume equal to 47000 m³. On the basis of the accounts of the eyewitnesses, a value of C_v=0.1, typical of intense waterlaid sediment transport, was used to compute the solid volume in the first and third phases of the event. The corresponding cumulated volumes were then subtracted to the overall observed solid volume, thus obtaining the solid volume and the sediment concentration in the second phase. Cumulated surface water and storage in the soil on eroded areas from GRISS-2D modelling (4500 m³ for the left branch

and 6000 for the right one) made considered the water volume computation for phase2. Tab.4.X shows that the sediment concentration for phase2 amounts to 0.36 and to 0.72, for the right and the left tributary, respectively. One should note that these estimates represent average values over a 60 min time interval which encompasses the whole debris flow. It is likely that the peak values are characterised by higher concentration. Wile the values of C_v computed for the right sub-basin are in agreement with the values usually reported for debris flow [Costa, 1988; Coussot and Meunier, 1996], the one reported for the left sub-basin appears very high. Obviously, several factors influence the estimation of the concentration values for phase2, including uncertainties in the evaluation of runoff volumes and the choice of concentration values during the rest of the event. Large values of concentration for the left tributary are not inconsistent with the observations reported by witnesses. The formation of temporary channel blockages can be inferred from the report of one eyewitness, who observed low discharge immediately before the main surge. Together with documented collapses of channel banks, these observations could indicate a temporary obstruction of the channel due to landsliding of the channel sideslopes. These phenomena were likely to cause the entrainment, at discrete pulses, of partly unsaturated material from the sideslopes, resulting in the increase of the solid concentration of the debris flow.

	Left Subbasin			**Right Subbasin**		
Time [CET]	V_w [m^3]	C_v [-]	V_s [m^3]	V_w [m^3]	C_v [-]	V_s [m^3]
15:30-17:00	4 460	0.10	500	14 320	0.10	1 590
17:00-18:00	10 280	0.72	26 010	28 300	0.36	16 230
18:00-20:00	4 400	0.10	490	19 650	0.10	2 180
Total	19 140		27 000	62 270		20 000

Table 4.X. Water-sediment balance during the various flood phases. V_w: water volume; V_s: solid volume; C_v: sediment concentration by volume

4.3.5 Conclusions

August 29, 2003 marks one of the most intense Mesoscale Convective Systems over the eastern Italian Alps. The storm produced record rainfall on the 0.65 km² Rio Cucco basin, with 331 mm of rainfall in 9 hours. Radar observations, corrected by using raingauge measurements, were used to examine the rainfall evolution over the basin. The rain rate time series consisted of several pulses of increasing intensity, which started at 1130 CET and ended around 1830 CET.

The hydrologic response was simulated using a spatially-distributed, process-based hydrological model. The low initial soil moisture conditions had a remarkable impact of flood formation, causing initial losses exceeding 80 mm. The huge cumulated runoff amounts, together with high rainfall intensities on the time scale of up to one hour, resulted in a flood peak reaching almost 20 m³/s/km². The major controls of the flood response were the

exceptional cumulated rainfall amount, required to exceed the large initial abstractions, and the large rainfall intensities required to generate high flood response.

Geomorphic impacts of the event within the drainage basin consisted in intense erosion along the channel network and, locally, in the failure of adjacent slopes. The comparison of the topography of the eroded areas, carried out before and after the event, afforded estimation of the volume of sediments, which estimated amounts from 70000 to 85000 m³. In spite of its small size, the left sub-basin supplied most of the sediment.

The accounts of two eyewitnesses about timing and flow type during the event confirmed the results of field observations and were used to establish a budget between simulated water runoff volumes and solid volumes eroded from the watershed. This was carried out by computing the sediment concentration during the various phases of the event. A particularly high value of sediment concentration was estimated for the left sub-basin. This could be referred to particular dynamics of sediment mobilisation in this sub-basin, in which the failure of temporary channel obstructions and the collapse of the outer channel banks in curves increased the solid concentration of the debris flow.

Chapter 5 - SPATIAL VARIABILITY IN FLASH FLOOD EVENTS

5.1 Introduction: rainfall and soil properties resolution in flood response modelling

A key question in hydrology is how spatial variability in rainfall and soil properties can be represented and aggregated in hydrological models of flood response. This can be expected to depend on complex interactions between the rainfall space-time variability, the variability of the catchment soil and landscape properties, and the spatial scale (e.g. catchment area) of the problem. This question has important practical implications concerning the accuracy of flood predictions from catchment runoff models. Such flood predictions may underpin flood warning procedures in real-time and form a key role in the design and planning of flood risk management measures. However, although the literature on the relationship between spatial rainfall and runoff response is extensive, results have been contrasting and sometimes contradictory [Segond et al., 2007; Nicotina et al., 2008]. This illustrates the complexity of the problem, which is compounded by the fact that the effects of rainfall spatial variability are usually assessed indirectly, via a watershed model. Only a few studies have considered this problem in the context of extreme flash flood analysis [Le Lay and Saulnier, 2007], probably due to difficulties in the documentation of this type of flood events [Creutin and Borga, 2003; Borga et al., 2008]. However, hydrological analysis of extreme flash floods, usually associated to large space-time rainfall variability, is expected to be most sensitive to the spatial aggregation of rainfall and soil properties.

Given the lack of guidance, this part of the study explores the importance of spatial rainfall and soil properties aggregation for distributed rainfall–runoff modelling as a function of rainfall type and catchment scale, with emphasis on extreme flash floods in humid temperate regions in general, and the alpine region in particular.

Among the major effects of varying the aggregation length on the sampling of a generic spatially-continuous field (such as rainfall), are the effects on the spatial variance and on the integral scale of the variable of interest. The spatial variance is a measure of how different the variables are in space. The integral scale is a measure of the average distance over which a variable is correlated in space.

Theoretical and empirical evidence indicates that the measured (apparent) variability of the spatially-continuous fields decreases with increasing the aggregation length, and that this depends on two terms: extent and support [Journel and Huijbregts, 1978; Blöschl and Sivapalan, 1995; Skøien and Blöschl, 2006]. ‘Extent’ refers to the overall coverage of the data (the watershed scale, given here by L_w, root square of the watershed area); ‘support’ refers to

the resolution area (the aggregation length, L_r). The apparent spatial variability of the rainfall field decreases with decreasing the 'extent' and with increasing the aggregation length. The first effect is a logical consequence of the existence of spatial correlations: for a given aggregation length, the smaller L_w, the closer the data and, thus, the closer their values. The second effect arises because dispersion within a fixed domain L_w decreases as the support L_r increases: the rainfall values at 8-km resolution are less dispersed than the rainfall values at 1-km resolution, for a fixed domain.

In the case of rainfall, increasing the aggregation length leads not only to a reduction of the apparent spatial variability. It has been found [Ogden and Julien, 1994; Winchell et al., 1998; Segond et al., 2007] that the uncertainty in the location of precipitation over the catchment boundary leads to an error in basin-averaged rainfall depth estimation, which becomes significant when the ratio L_r/L_w exceeds a certain threshold. This error occurs because there are regions of heavier or lighter precipitation outside the immediate boundaries of a catchment. When the aggregation length is increased, rainfall values pertaining to areas just outside the catchment may enter the computation of the average rainfall over the basin, hence leading to a rainfall volume error.

The sensitivity of runoff modelling to both attenuated spatial variability and rainfall volume error introduced by increasing the rainfall aggregation length depends strongly on the smoothing effect of catchment characteristics [Winchell et al., 1998; Bell and Moore, 2000; Segond et al., 2007; Moulin et al., 2008]. When there is not enough variability in rainfall to overcome the damping and filtering effect of the catchment, detailed knowledge of rainfall spatial variability is not required to model the catchment response, and an accurate estimate of the basin-averaged rainfall may suffice for runoff modelling [Beven and Hornberger, 1982; Naden, 1992; Pessoa et al., 1993; Obled et al., 1994; Woods and Sivapalan, 1999; Andreassian et al., 2001; Smith et al., 2004]. In the last decade, several studies have identified that the damping effect of the catchment may depend on the dominant runoff generation processes, with the infiltration-excess runoff generation more sensitive than saturation-excess runoff generation to space rainfall resolution [Winchell et al., 1998; Segond et al., 2007; Nicotina et al., 2008]. However, there is not an agreed approach to quantify the damping effect of a given catchment and the conclusions drawn from the different studies depend heavily on the runoff model, the characteristics of the rainfall forcing and the type of catchment examined.

Focusing the analysis on flash flood events allows one to isolate specific runoff generation mechanisms and catchment properties which are perceived as dominant with this type of events. More specifically, the substantial role exerted by Hortonian runoff generation with high intensity rainfall events emphasise the role of surface runoff and of the river network geometry in the averaging of space-time rainfall [Norbiato et al., 2008]. The concept of flow distance, e.g. the distance along the runoff flow path from a given point to the outlet, may provide a useful metric to examine the influence of rainfall resolution on runoff modelling when rain exhibits significant spatial variability and linear routing through

branched channel networks plays a significant role [Woods and Sivapalan, 1999]. The damping effect arises here because the excess rainfall generated at points placed at equal flow distance will be averaged out in the runoff propagation process, in spite of their inherent spatial variability. On the other hand, a short distance in (x, y) space, reflecting a relatively low rainfall variability, can correspond to a large difference in flow distance to the catchment outlet. The averaging of space-time rainfall fields across locations with equal flow distance coordinates may be sensitive to the spatial resolution of the rainfall representation and as such it may explain, at least partially, the pattern of runoff model sensitivity to rainfall resolution. Moreover, use of the flow distance metric may allow to isolate the effect of increasing rainfall aggregation length on the shape of the response and on the peak timing, a feature of runoff response which has received relatively scarce attention so far in the literature.

The effects of the spatial representation of soil properties on runoff modelling have been less investigated than those induced by rainfall sampling. However, this question has important implications in the applications of distributed runoff models. Indeed, one of the main advantages that this model possess with respect to their lumped-parameters counterpart is the possibility to account for the spatial variability of the local runoff production, by means of the specification of the soil-related parameters. However, the determination of the actual spatial variability of the soil parameters is often limited by the large amount of data required, which are generally quite difficult to obtain. A pragmatic solution for reducing the data requirements of distributed models is to increase the aggregation length in the spatial representation of the soil properties.

Among the studies focused on the impact of representation of the spatial variability of soil parameters on hydrologic response, many have dealt with the Hortonian runoff generating mechanism. Several investigations have shown that runoff is strongly influenced by the spatial variability in soil hydraulic properties, and more specifically in the soil hydraulic conductivity [Woolhiser et al., 1996; Merz and Plate, 1997]. The impact of soil properties spatial variability on runoff response depends largely on the duration and on the magnitude of the rainfall event. Ogden and Julien [1994] and Saghafian and Julien [1995] found that the influence of spatial variability in soil hydraulic properties diminishes as the watershed approaches equilibrium runoff conditions. Merz and Plate [1997] and Merz and Bardossy [1998] found that the impact of soil hydraulic properties is large for medium flood events and relatively small for both very small and for large runoff events. These researchers observed that for events with low rainfall intensity, mainly the impervious areas contribute and the effects of spatial variability are small. Increasing the rainfall intensity leads to a sensitive range with a small difference between rainfall intensity and soil hydraulic conductivity. Under these conditions, runoff is very sensitive to the spatial pattern of infiltration, and hence to its spatial representation. A further increase of the rainfall intensity leads to an expansion of the source areas for overland flow generation and to a smaller influence of the spatial pattern of infiltration.

5.2 Analysis of space variability

To characterize the influence of temporal and spatial variability of rainfall on flood response, we utilized 30-min, 1-km and 16-km radar rainfall fields to compute the following quantities:

1) the mean rainfall rate over the catchment at time t during the storm, $M(t)$;
2) the normalized time-distance of rainfall from the basin outlet, $D(t)$; and
3) the normalised dispersion of rainfall, S_{NOR}(t).

The statistics normalised time-distance and normalized dispersion are introduced here to provide information on the spatial distribution of rainfall relative to the basin network structure. The drainage network, as represented by the routing time $\tau(u)$, provides a natural metric for analyzing the spatial distribution of rainfall, as shown previously by Woods and Sivapalan [1999], Zhang et al. [2001], Smith et al. [2005] and Borga et al. [2007]. The routing time incorporates both geometric and kinematic properties in its determination.

The normalized time-distance at time t, $D(t)$, is a function of the rainfall field $R(t, x,y)$ and the routing time $\tau(u)$. It is defined as the ratio of the rainfall-weighted centroid routing time $D_1(t)$ and the mean routing time d_{mean},

$$D(t) = \frac{D_1(t)}{D_{mean}} \tag{5.1}$$

In Eq. (5.1) the time-distance $D_1(t)$ is given by

$$D_1(t) = |A|^{-1} \int_A w(t,u)\tau(u)du \tag{5.2}$$

where A is the spatial domain of the drainage basin and the weight function $w(t,x, y)$ is given by

$$w(t,x,y) = \frac{R(t,x,y)}{|A|^{-1} \int_A R(t,x,y)dxdy} \tag{5.3}$$

The value d_{mean} is defined as

$$D_{mean} = |A|^{-1} \int_A \tau(u)du \tag{5.4}$$

Values of $D(t)$ close to 1 reflect a rainfall distribution either concentrated close to the mean time-distance or homogeneous, with values less than one indicating that rainfall is distributed near the basin outlet, and values greater than one indicating that rainfall is distributed towards the periphery of the drainage basin.

The rainfall-weighted flow time-distance dispersion is given by:

$$S(t) = \left\{ \int_A w(t,u)[\tau(u) - D_1(t)]^2 du \right\}^{0.5} \tag{5.5}$$

The dispersion for uniform rainfall is defined by:

$$S_1 = \left\{ \int_A [\tau(u) - d_{mean}]^2 du \right\}^{0.5} \tag{5.6}$$

and the normalised dispersion is given by

$$S_{NOR}(t) = \frac{S(t)}{S_1} \tag{5.7}$$

Values of $S_{NOR}(t)$ close to 1 reflect a uniform-like rainfall distribution, with values less than 1 indicating that rainfall is characterised by a unimodal peak, and values greater than 1 indicating cases of multimodal rainfall peaks close and far from the basin outlet.

Effects of rainfall and soil properties spatial aggregation on flood response modelling are examined here with reference to three length scales: the aggregation length of the rainfall data, L_R; the characteristic length of the watershed, L_W, taken as the square root of the watershed area; and the aggregation length of the soil properties (represented here by the CN parameter), L_G. To elucidate the controls of input aggregation on model error, the KLEM model was applied over the different subbasins with four different input (rainfall and soil properties) resolutions were considered, corresponding to 1-, 4-, 8- and 16-km aggregation lengths.

As shown above, varying the spatial rainfall resolution induces i) rainfall volume errors, ii) a reduction of the rainfall apparent spatial variability and iii) a distortion of the rainfall geometry with respect to the flow distance metric. In order to separately address the effects of rainfall spatial variability alone, we performed numerical experiments in which rainfall depths are rescaled and forced to be exactly preserved at each time step over the range of rainfall resolutions and catchment scales examined. This allows also to isolate the effects of rainfall volume errors with respect to the 'total' error induced by increasing rainfall aggregation length. Moreover, in order to clarify the relative roles of transport paths and of heterogeneity in the runoff generation processes, we performed numerical experiments in which the infiltration is 'turned off', by assuming that the soil is perfectly impermeable.

The error analysis was carried out for rainfall and runoff volumes and for peak discharges, by comparing results obtained by using a given input resolution with those obtained from 1-km grid size, considered here as the reference resolution. The error statistics 'normalised rainfall volume error' ε_r , 'normalised runoff volume error' ε_v and 'normalised peak discharge error' ε_q were computed for rainfall volume, runoff volume and peak discharge, respectively, as follows:

$$\begin{aligned} \varepsilon_r &= \frac{|P_{Lr} - P_1|}{P_1}, \\ \varepsilon_v &= \frac{|V_{Lr} - V_1|}{V_1}, \\ \varepsilon_q &= \frac{|Q_{Lr} - Q_1|}{Q_1}, \end{aligned} \tag{5.8}$$

where P_{Lr} and P_1, V_{Lr} and V_1, and Qp_{Lr} and Qp_1, represent the rainfall volume, the runoff volume and the peak discharge resulting from aggregation over L_r- and *1*- km length, respectively.

Runoff modelling at increased aggregation length was carried out by using the same parameter values obtained by calibration at 1-km aggregation length. It is well known that re-calibration of model parameters after changing rainfall aggregation length may adjust and compensate for the biases in rainfall volume and spatial distribution [Borga et al., 2006]. However, the focus of this study is on the examination of the influence of sampling input characteristics on runoff modelling alone, without accounting for the role of calibration and re-calibration.

Precipitation analysis and final results of this chapter are divided in two different sections: section 5.3 focuses on three flood events characterized by different rainfall spatial variability in Cervo River (Piomente region, North West Italy), and analysis is applied on four subcatchments (from 75 to 983km²); section 5.4 regards a major flash flood event in Fella Basin (in Friuli Venezia Giulia region), where ten subcatchments from 10.5 and 623km² are chosen for the analysis. Each study includes a fist detailed analysis on rainfall spatial variability within selected subcatchments at different scales, then a simplified KLEM model is used to investigate spatial aggregation effects on mean areal rainfall and peak discharge value at subcatchment scale.

5.3 Influence of rainfall and soil properties spatial aggregation on extreme flash flood response modelling: an evaluation based on the Sesia river basin, North Western Italy

5.3.1 Sesia basin and Cervo study area

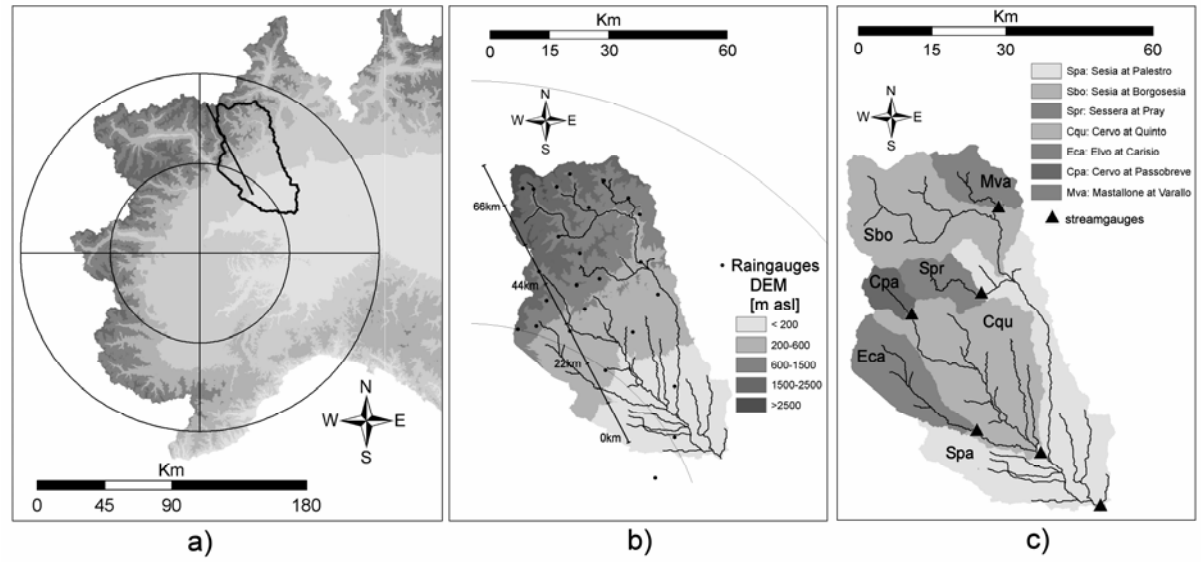

Figure 5.1: Study area with: a) location of the Bric della Croce weather radar and of the Sesia river basin in northwestern Italy; b) digital terrain model (DTM) of the Sesia river basin with raingauge locations; c) sub-basins of the Sesia river basin. The straight line in figures (a,b) marks the location of the cross-sections in Fig.3. See text for further details.

The Sesia river basin (North Western Italy, see Fig.5.1) is a left-hand tributary of the Po river, with a drainage area of 2587 km^2 at Palestro and elevation ranging from 108 m a.s.l. to 4555 m a.s.l. (Punta Gnifetti). The area is included within the Piemonte region and is characterised by three distinct pluviometric regimes: (i) the plain area, with mean annual precipitation ranging from 900 to 1100 mm; (ii) the Alpine foreland area, where mean annual precipitation locally increases up to 2000 mm (upper Cervo river basin); (iii) the inner Alpine area, where precipitation decreases to 1400-1600 mm, due to rain shadow effect of the southern ridges. Four subbasins of the Sesia river basin at Palestro are considered in the study, ranging in size from 75 to 983 km^2 (Table 5.I).

River	Stage gauge	Area	Catchment elevation			Channel length
		[km^2]		[m asl]		[km]
			Min	Max	Average	
Cervo	Passobreve	75	593	2536	1492	14
Sessera	Pray	126	400	2556	1155	27
Mastallone	Varallo	146	473	2460	1319	23
Elvo	Carisio	261	177	2533	621	38
Cervo	Quinto	983	132	2536	507	59
Sesia	Palestro	2586	108	4555	737	115

Table 5.I: Main morphological characteristics of the six study basins.

The Sesia River basin has a wide range of land use and land cover properties, resulting in a heterogeneous mix of hydrologic response properties. The mountainous fraction of the basin, which amounts to 45%, is characterised by steep and rocky slopes with generally thin soil layers. A widespread forest and grass coverage is present. Human activities are mainly concentrated on the lower part of the main valleys. Population density is quite low with the exception of Biella town and its industrial area along the Cervo River. The plain portion of the basin is characterised by a very low gradient. The area is almost completely exploited for rice cultivation. Population density is low with the exception the town of Vercelli along the Sesia River. This portion of the catchment provides a relatively low contribution to the floods generated in the upper mountainous area and the hydraulic propagation phenomena produce strong lamination effects.

Very intense storm events are often observed on the upper part of Cervo catchment and of the Sesia valley due to the orographic effect on south humid flows from the western Mediterranean. Growth of precipitation with altitude has been thoroughly documented and quantitatively examined in this section of the Alps during the MAP experiment (Houze et al., 2001). The catchments are characterised by very quick responding tributaries and present short lag-times. As such, the Sesia river basin has been a workshop for hydrologists and geomorphologists to study extreme floods. The basin includes the 1.2 km^2 Rio della Gallina experimental catchment, which provides documentation of extreme floods at small scales, as exemplified by the event of September 24 1981, with 17.9 $m^3/(s\ km^2)$ specific peak discharge [Caroni et al., 1986]. Extreme flooding occurred in the upper Sesia River basin on November 2-3 1968, with specific peak discharges exceeding 20 $m^3/(s\ km^2)$ at spatial scales up to 40 km^2. This catastrophic flood was characterised by widespread triggering of shallow landslides and debris flows, and caused 72 casualties. Post event analyses of this flood prompted the first quantitative attempt in Italy to provide a spatial description of hillslope and torrent failures and to relate these failures to the generating hydro-meteorological and hydraulic processes [Carraro et al., 1969].

5.3.2 Meteorological description of the three studied events

The 5 June 2002 and 2 August 2005 flash flood events in the Sesia river basin provide the principal targets of opportunity for study of runoff model sensitivity to rainfall and soil properties resolution. Analyses of the flood event of 15 September 2006 are used to further examine response properties to a storm event characterised by smaller space-time variability. The regional flood response of the Sesia river basin is examined in terms of space–time rainfall variability and heterogeneous land surface properties. The objectives of this study are therefore to document the hydrometeorological processes that control extreme flash flood response in the Sesia river basin and to examine the characteristics of runoff model sensitivity to varying radar rainfall and soil properties aggregation lengths. To elucidate the controls of

input spatial aggregation on model error, the KLEM distributed hydrologic model is applied over four different sub basins ranging from 75 km^2 to 983 km^2 and by using four different rainfall resolutions: 1-, 4-, 8- and 16-km. The range of spatial resolution covers the aggregation scales often encountered in flood and flash flood forecasting.

Basin	Tot.rain [mm]	Tot.runoff [mm]	Peak dis. [m^3s^{-1}]	Spec. peak dis. [$m^3s^{-1}km^{-2}$]	Runoff ratio	Lag time [h]
Event 2002						
C. at Passobreve	301	123	359	4.8	0.41	3.5
S. at Pray	217	86	582	4.6	0.40	3.0
M. at Varallo	249	110	462	3.2	0.44	3.0
E. at Carisio	138	59	663	2.5	0.43	6.0
C. at Quinto	97	41	1304	1.3	0.42	10.0
S. at Palestro	113	51	3944	1.5	0.45	11.5
Event 2005						
C. at Passobreve	184	44	304	4.1	0.24	1.5
S. at Pray	63	8	45	0.4	0.12	6.5
M. at Varallo	117	22	72	0.5	0.19	25.0
E. at Carisio	-	-	-	-	-	-
C. at Quinto	41	4	331	0.3	0.10	4.5
S. at Palestro	54	9	765	0.3	0.16	12.5
Event 2006						
C. at Passobreve	264	125	340	4.5	0.47	11.5
S. at Pray	242	82	276	2.2	0.34	7.0
M. at Varallo	197	59	163	1.1	0.30	9.5
E. at Carisio	168	41	313	1.2	0.25	14.0
C. at Quinto	145	44	991	1.0	0.31	16.5
S. at Palestro	157	44	2632	1.0	0.28	19.0

Table 5.II: Rainfall and runoff over the study basins for the 2002, 2005 and 2006 flood events.

The analyses reported in this study are based on radar rainfall fields, a dense raingauge network and 30-min discharge observations from the six stream gauging stations, for three flood events. These three events were chosen because, in spite of the different space-time rainfall patterns, they generated fairly similar and large specific peak discharges over the 75 km² wide Cervo basin at Passobreve (ranging from 4.1 m³/(s km²) for the August 2005 event to 4.8 m³/(s km²) for the June 2002 event) (Tab.5.II). The June 2002 flash flood event produced record flood peaks and extensive shallow landsliding in the upper Cervo river basin and its tributaries, with peak event rainfall up to 400 mm over 22 hours and hourly intensities exceeding 80mm/hr. The August 2005 event had similar duration, but was characterized by two short convective storm episodes with duration of 6-8 hours each and a much less spatial extent. The event cumulated peak rainfall was around 230 mm, with hourly rainfall intensities up to 50 mm/hr. The September 2006 flood event was much longer and lasted almost 30 hours. It was characterized by mainly stratiform rainfall including small convective cells, giving cumulated rainfall event up to 430 mm and intensities up to 40 mm/hr.

Space-time variability of rainfall is examined through analysis of rainfall fields at 1-km spatial resolution and 10-min timescale derived from volume scans of the the Bric della Croce (ARPA Piemonte, Italy) Doppler weather radar. 10 min rainfall data from 25 raingauge

stations in the Sesia river basin (with a spatial density of around 1 station per 100 km^2) were used in the elaboration.

A number of procedures were applied to the reflectivity data to correct for the following error sources: ground clutter, partial beam occlusion, path attenuation and vertical profile of reflectivity correction. There were no reports about hail during the events, so no correction was implemented to remove hail contamination. A summary of the correction procedures is provided below.

An algorithm based on Doppler velocity and clear air echo statistics was used to flag clutter contaminated data in the polar volumes. Correction for beam occlusion is based on off-line computation of the percentage of beam power intercepted by the orography by using a model of beam propagation and a digital description of the orography [Borga et al., 2000; Pellarin et al., 2000]. Path attenuation due to precipitation (which can generate large errors at C- band at high rainfall rates [Faure et al., 2005]) is corrected by using a variational method with gauge accumulations as external constraints and the Hitschfeld-Bordan [1954] equation as model [Berenguer et al., 2002].

The algorithm by Andrieu and Creutin [1995] was used for adjustment for the vertical profile of radar reflectivity. The parameters required in the various adjustment procedures were fitted to provide minimal bias and good reconstruction of the event rainfall, as measured by the raingauges [Borga et al., 2002].

Event	FSE	MRE	Correlation
2002	1.09	0.01	0.75
2005	1.03	0.01	0.87
2006	0.62	0.02	0.80

Table 5.III: Comparison between raingauge measurements and radar rainfall estimates at hourly time step over the 25 raingauges (for FSE and MRE definition see section 3.1).

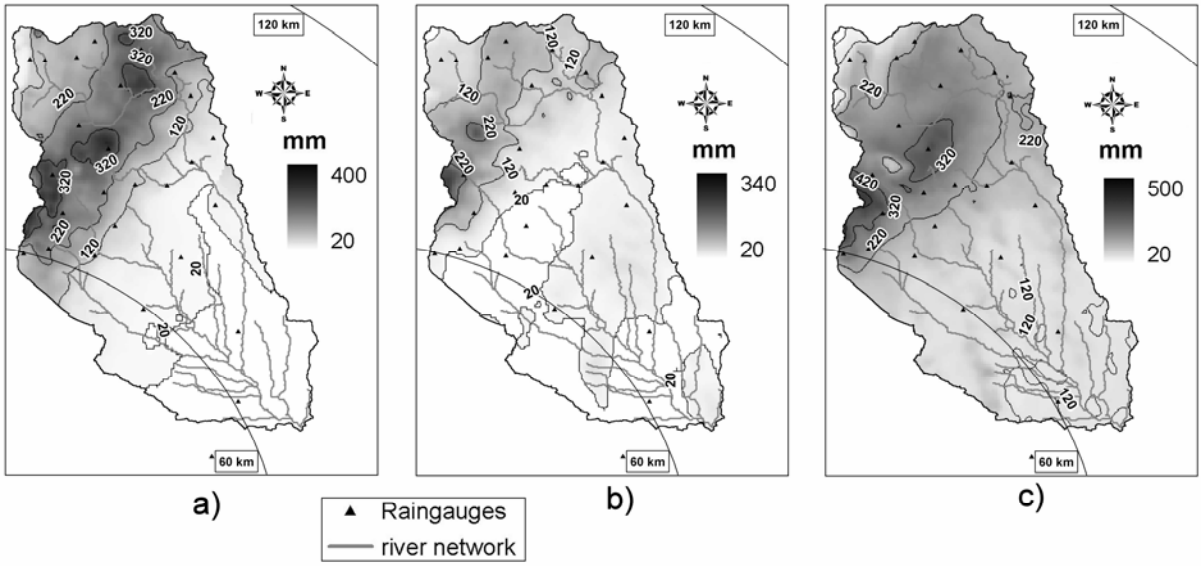

Figure 5.2: Storm accumulated rainfall (mm) for: a) 2002, b) 2005 and c) 2006 flood events. Triangles represent raingauges position and different grey scales are used in the three events to display rainfall spatial distribution.

Rainfall estimation was based on the lowest adjusted polar cell with occlusion less than 60%. After correction, the reflectivity factor Z was converted to rainfall rate R through an empirical Z-R power function using a=300 and b=1.5 for R in mmh^{-1} and Z in mm^6m^{-3} (see Eq 3.5).

The quality of final radar rainfall estimates are evaluated by comparison between hourly rainfall estimates obtained from radar observations and from raingauges, and are summarised in Tab.5.III for the three events. Inspection of this table shows that the performance of the radar estimation algorithm is rather good, with negligible mean relative error, correlation ranging from 0.75 to 0.87 and fractional standard error ranging from 0.62 to 1.09. As expected, the accuracy of the estimation is best for the more stratiform event of September 2006, for which attenuation is a less important error source and variability of the reflectivity to rainrate relationship parameter is speculatively less important. Precipitation was analysed by using animations of both the instantaneous rain rates at the 10 min time steps and the cumulated rain amounts over a given period. A synthesis of this information is provided by Fig.5.2, which gives the storm total precipitation for the three events.

The storm total precipitation pattern for the three events reflects the influence of the orography, with local peak of accumulations extended over a band crossing the Cervo at Passobreve, the Sessera at Pray, the central portion of Sesia at BorgoSesia and the Mastallone at Varallo. Areas in the plain portion of the basins, as well as areas in the inner alpine region received comparatively less rainfall. This rainfall pattern resembles that of the average annual precipitation. The orographic enhancement is emphasised for the 2002 and 2005 storm event, and less for the 2006 event (at least over the catchments considered here). Peak accumulations exceed 350 mm for the 2002 event, are around 220 mm for the 2005 storm event and exceed 420 mm for the 2006 event.

Some insight into the physical processes producing the small-scale precipitation patterns can be seen by examining the space-time radar reflectivity with a Hovmüller diagram (Fig.5.3). We choose a south-east to north-west reference line 77 km long (Fig.5.1), whose direction is almost parallel to the major drainage line in the Sesia, but also minimise radar beam blocking by orography. The local minima of reflectivity at x=57 km and x=62 km, mainly visible for the events of 2005 and 2006, are artefacts due to the terrain screening of the radar. These artefacts are clearly emphasised when the precipitation is mainly stratiform, as in the 2006 event. The striking feature of this diagram is the drifting of reflective features that develop upwind, particularly for the 2002 and 2005 storm events. For these two events, the maximum over the mountains at x=50 km is due to the amplification of these drifting features. For the 2002 event, orographic precipitation locked to the terrain dominates from 0900 to 1900 UTC. For the 2005 event, this feature can be well recognise from 0000 to 0400 UTC and from 1000 to 1600 UTC. The orographic enhancement is much less significant for the 2006 event.

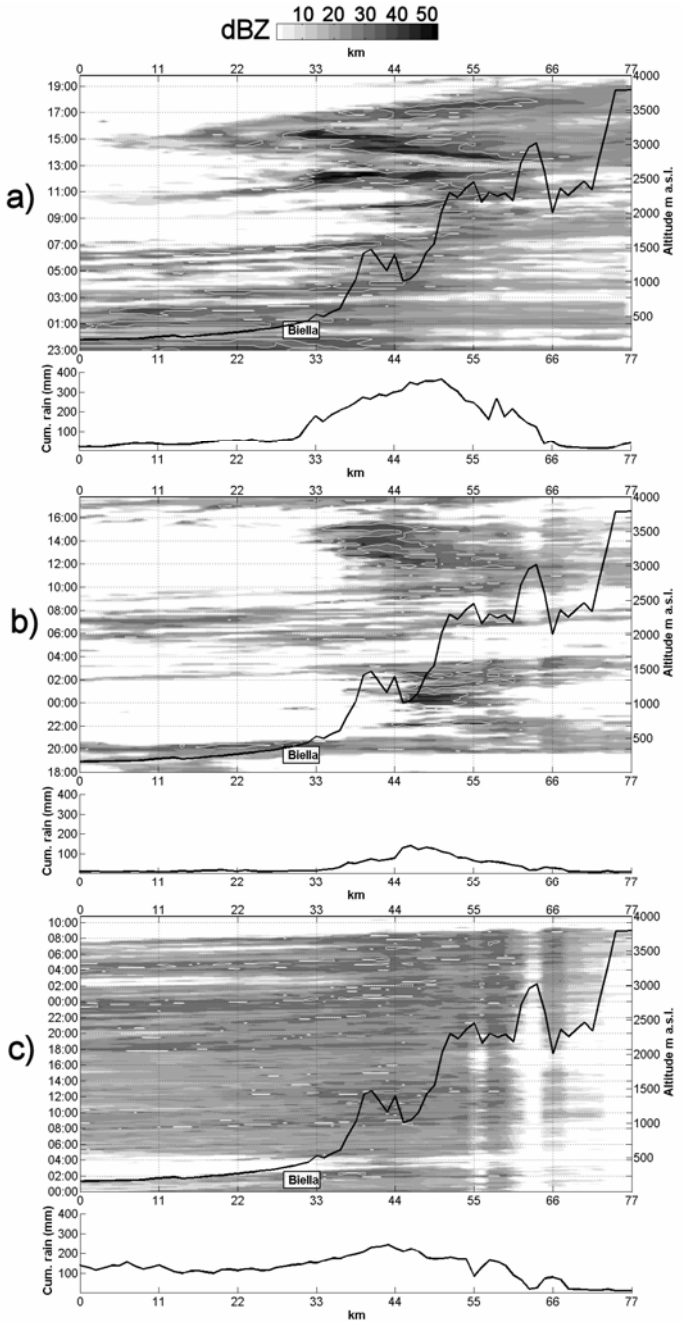

Figure 5.3: Time [UTC] versus distance diagram for 1.5° Bric della Croce radar reflectivity along the line marked in Fig.5.1 for the three storm events: (a) 2002, (b) 2005 and (c) 2006. Terrain (solid line in the upper part of each plot) and storm cumulated precipitation (lower part) are also shown.

Figure 5.3 allows one to evaluate the spatial and temporal scales of the patterns of enhanced precipitation. For the 2002 event, the spatial scale along the reference line at 30 min accumulation is around 8 km, whereas it is around 4 km for the 2005 event. This is associated to the spatial variability of the rainfall fields, which is higher for the 2005 event with respect to the 2002 storm event.

The structure of the rainfall spatial variability has been examined by using the climatological variogram [Berne et al., 2004]. The domain used for this analysis is a 64 km by 128 km region centred on the Sesia River basin, with a time accumulation of 30 min. With the approach based on the climatological variogram, one may take into account information from

all the realizations (e.g. rainfall field for successive time steps) assuming the fields to have similar statistical characteristics except for a constant factor. The variogram can therefore be normalised by the respective variance of each field considered and then averaged over all the realizations. Assuming the structure functions have the same shape, the mean normalised variogram obtained, also called climatological variogram, is representative of all the realizations. In particular, we have used here a two-parameter exponential models, which led to estimates of the integral scale of 8 km, 6 km and 20 km for the 2002, 2005 and 2006 storm events, respectively. This is consistent with previous findings about the different space-time variability of the three events.

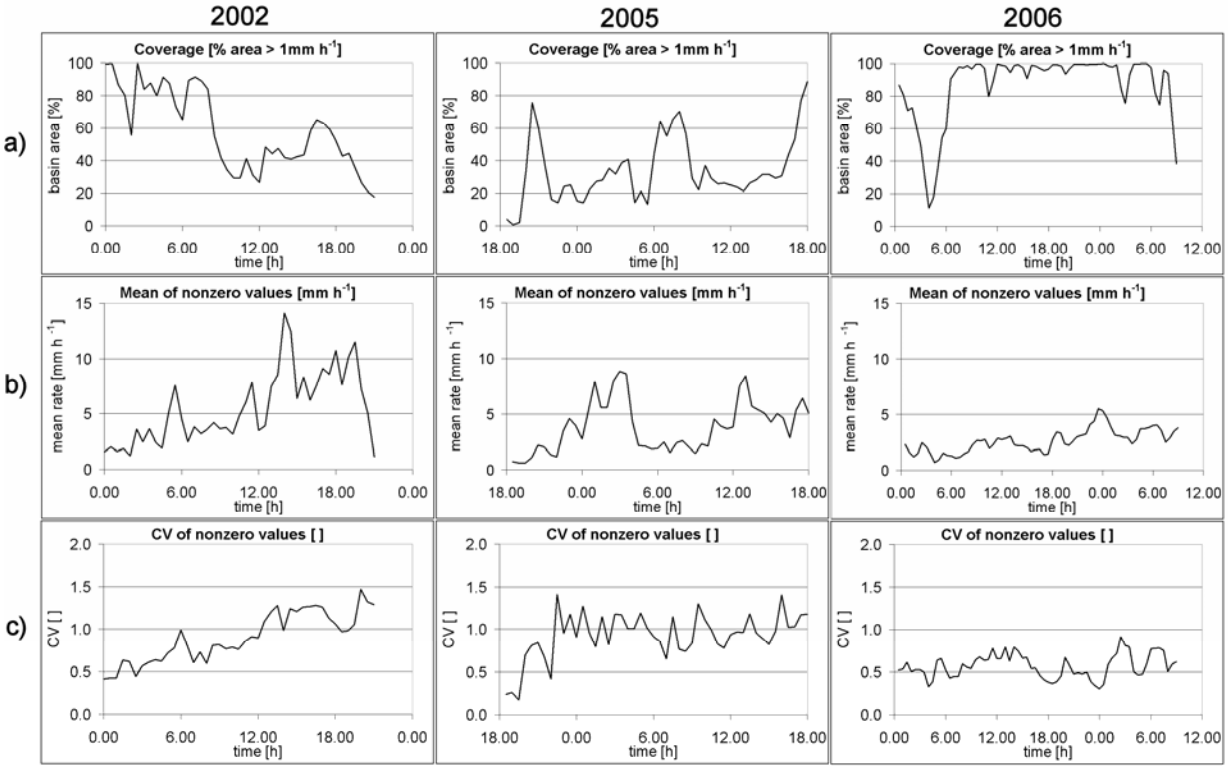

Figure 5.4: Precipitation analysis on Sesia basin at Palestro. Time series of: a) fractional coverage (threshold 1 mm h^{-1}); b) mean rain rate of non zero bins [mm h^{-1}]; c) coefficient of variation of nonzero rain rates.

The contrasting temporal evolution and spatial structure of the three storms are illustrated in Fig.5.4 a-c, where the values of the fractional coverage, mean rainfall (for positive bins), and coefficient of variation (standard deviation divided by the mean) of rainfall rate (for positive bins) are reported for the Sesia basin at Palestro at 30 min time step. A rainfall threshold of 1 mm/hr was used to distinguish rain-no rain areas. These analyses highlight the contrasting temporal evolution of the three storms. For the June 2002 event there was a sharp decrease in fractional rain area with evolution of the MCS. Fractional coverage was exceeding 80% until 0800 UTC and decreased sharply between 0800 and 1000 UTC to 30%, ranging then from 30 to 65%. This corresponds to the increase of the mean rain rate over non-zero bins, which was up to 8 mm/hr until 1200 UTC and then increases up to 13 mm/hr during the second part of the storm. The rain rate variability increased in a parallel way,

reaching values of 1.4 during the second part of the storm. A similar variability in storm properties with time is observed for the August 2005 event, whereas the September 2006 event, by contrast, exhibited relatively minor changes. Fractional coverage of rainfall ranged between 60% and 80% and coefficient of variation ranged between 0.3 and 0.9 for the 2006 event.

5.3.3 Analyses of flood response

In this section we examine flood response properties of the Sesia river basin, with particular emphasis on effects of the different spatial and temporal rainfall forcing. A summary of the data is reported in Tab.5.II to permit water balance and response time analysis. Data reported in Tab.2 show that there are systematic differences among the events and, for each event, among the surveyed basins. The cumulated rainfall data reported for the largest basin (Sesia at Palestro) is highest for the September 2006 event (157 mm) and lowest for the August 2005 event (54 mm), with the June 2002 event characterised by an intermediate value (113 mm). However, runoff depth is highest for the June 2002 event (51 mm), whereas the September 2006 event ranks second (44 mm). This clearly depends on the very high rainrate intensities which characterised the June 2002 event with respect to the less intense September 2006 event. Moreover, initial conditions were likely wetter for the June 2002 event (up to 805 mm rainfall recorded in the 30 days before the flood) than for the September 2006 event (up to 420 mm rainfall recorded in the 30 days before the flood). Initial conditions were comparatively less humid for the August 2005 event, with up to 100 mm rainfall recorded in the 30 days before the event.

The impact of the orography on basin average rainfall depths is very important for the June 2002 and August 2005, as illustrated by the ratio between the basin-averaged depth over the Cervo river basin at Passobreve and over Cervo at Quinto. This amounts to 3.1 and to 4.5 for the 2002 and 2005 events, respectively. The ratio is much lower for the 2006 event, with a value of 1.8.

The model was implemented at 30-min time step and using a 50-m grid size cell for the description of landscape morphology. Soil properties were described by means of the CN parameter by using a 1 km-grid size, as computed by the Regional Agency for Environmental Protection. CN values at the 50-m grid size scale were obtained by projecting the values at 1-km grid size over the 50-m grid size. CN values range from 35 to 50 in the upper Sesia and Cervo catchments, and increase up to 70 in the plain portion of the catchments, reflecting agricultural and urban land use.

The KLEM model parameters were estimated simultaneously over multiple catchments by means of a combination of manual and automatic calibration to minimise an integrated normalised integrated root mean square error over the flood hydrograph. Parameter estimation was carried out by using 1-km rainfall estimates and by considering separately the catchments in the upland portion of the Sesia River and those in the plain portion. This is consistent with

the differences in runoff generation and runoff propagation mechanisms between the different basin portions. The I_a parameter was estimated by considering separately the different events (which were characterised by different values of initial soil wetness) and uniformly over the various catchments. After calibration, hillslope velocity ranges between 0.05 and 0.1 m s^{-1}, whereas channel velocity ranges between 1.5 and 3.5 m s^{-1}. In both cases, the higher values were associated to the upland catchments. Hillslope-channel threshold area ranges between 0.02 and 0.05 km^2. These values are consistent with earlier results obtained by Borga et al. [2007] and Sangati and Borga [2008] for other flash flood events simulated by using the same runoff model.

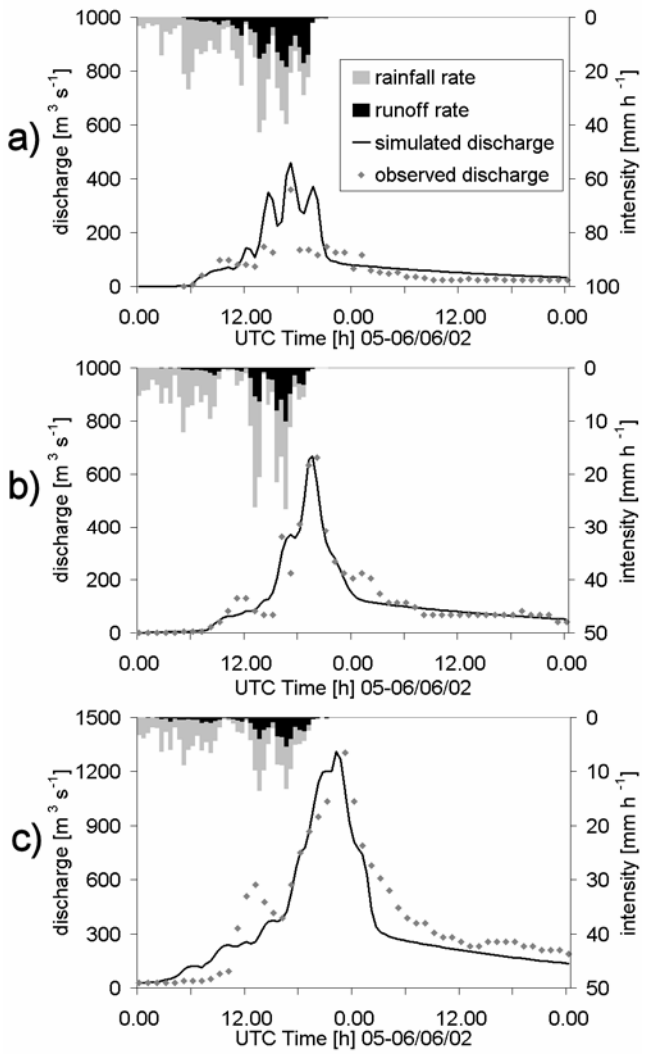

Figure 5.5: Results of KLEM application for the three Sesia basins for the 2002 event:
a) Cervo at Passobreve [75km^2];
b) Elvo at Carisio [261 km^2];
c) Cervo at Quinto [983km^2].

Results for the 2002 flood event at three streamgauge sections (Cervo at Passobreve, Elvo at Carisio and Cervo at Quinto) are reported in Fig.5.5. These results show that the model reproduces the volume of the main peak and the time of peak discharge reasonably well. The model capability to capture the recession characteristics of the flood varies across

the catchments, being relatively good for the Elvo at Carisio and less good for the Cervo at Quinto. This depends mainly on the simplifying assumptions made in the representation of the subsurface flow. For Cervo at Passobreve, the model generates a multipeaked response which is not observed in the measured streamflows. Whereas the first peak is likely due to modelled overestimation of the initial soil moisture conditions, the third peak probably depends on errors in the radar estimation of rainfall over this relatively small basin.

5.3.4 Results spatial variability analysis

Results are reported in Fig.5.6, 5.7 and 5.8 for four nested catchments along the Cervo river and for the events of 2002, 2005 and 2006, respectively. The four nested Cervo catchments are closed at Passobreve (75 km²), at two intermediate river sections (with drainage area of 249 and 501 km^2, respectively) and at Quinto (983 km^2). Rainfall fields aggregated over length scales of 1 and 16 km are used in the analyses. Inspection of the mean rainfall intensity highlights the effects of the rainfall volume error related to uncertainty of rainfall location with respect to the watershed boundary. Examination of the mean rainrate in Fig.5.6 to 5.8 shows that aggregation at 16-km scale has significant smoothing effects over the smallest basin (Cervo at Passobreve) and that these effects reduce with increasing the basin size. The effects are comparatively more significant for the 2002 and 2005 events, characterised by more marked spatial variability and shorter integral scale.

A similar pattern can be recognised for the normalised dispersion, with precipitation at 1-km exhibiting a more unimodal peak (towards the upper portion of the basin) with increasing the basin size, and a more uniform distribution for the smallest basin. The effect of increasing the aggregation length on the normalised dispersion is again to reduce its deviation with respect to 1.0, which implies a more uniform distribution.

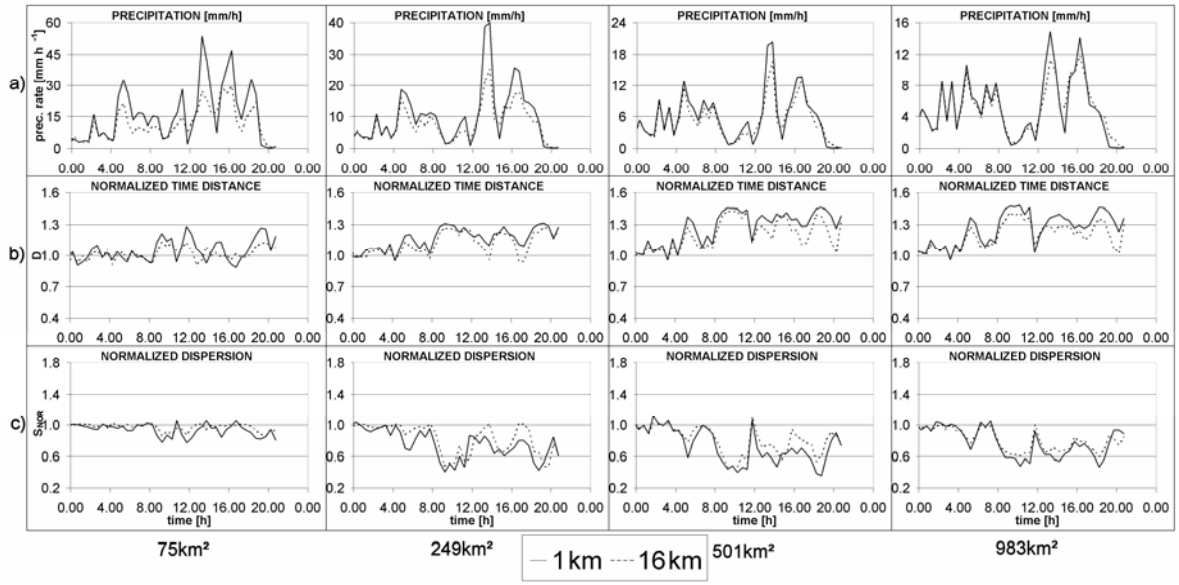

Figure 5.6: Precipitation analyses for the 2002 event for four nested catchments with two different rainfall grid resolution (1 and 16 km): a) mean rainfall intensity [mm h^{-1}]; b) normalized time distance; c) normalized time dispersion.

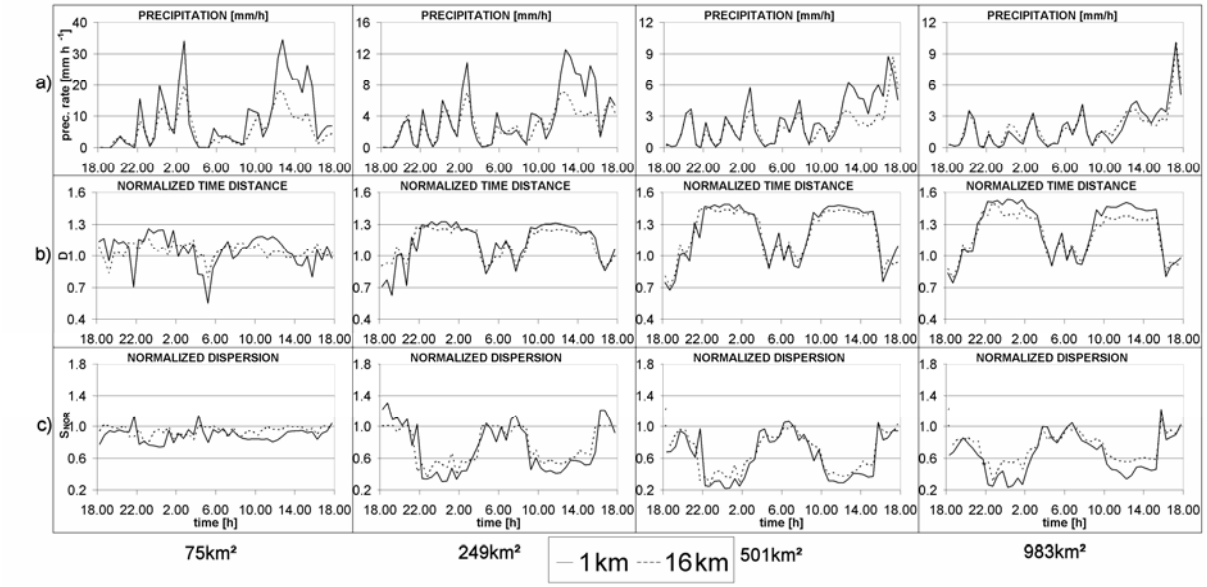

Figure 5.7: Precipitation analyses for the 2005 event for four nested catchments with two different rainfall grid resolution (1 and 16 km): a) mean rainfall intensity [mm h^{-1}]; b) normalized time distance; c) normalized time dispersion.

Patterns of normalised distance highlight the effect of orography on precipitation, particularly for the 2002 and 2005 events. The effect is obviously more significant as the basin size increases and extends downslope. For these events and for a basin size exceeding 500 km^2, the normalised distance is close to 1.5, particularly during periods of intense precipitation. On the contrary, normalised distance is close to one for the small catchment (e.g., systematic rainfall variability at this scale is negligible when measured with respect to river network), and aggregation has very limited effects on it.

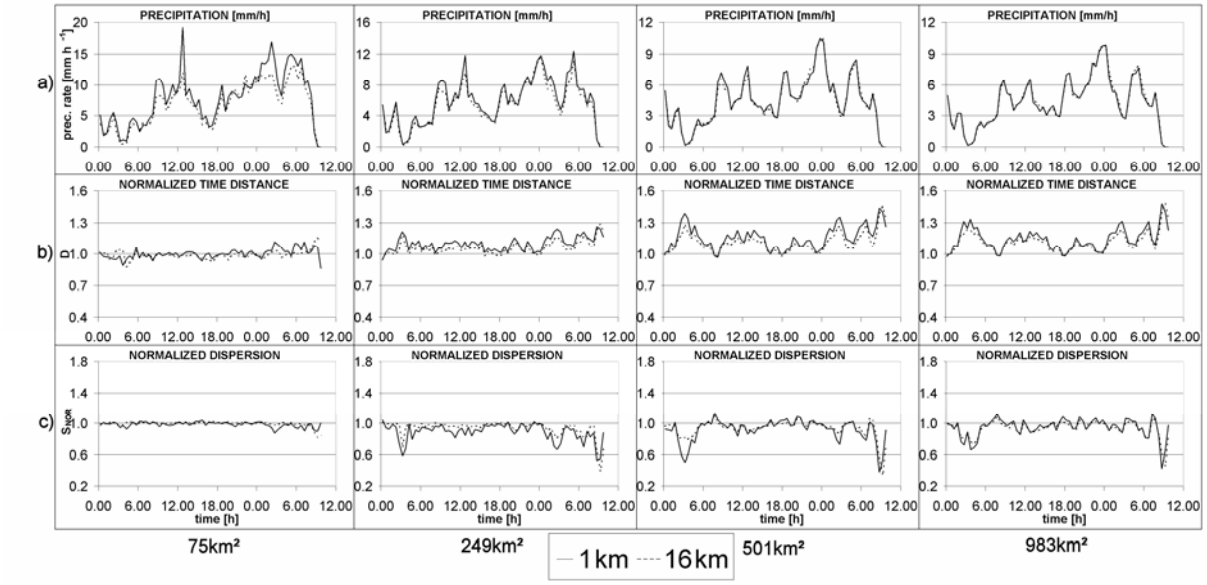

Figure 5.8: Precipitation analyses for the 2006 event for four nested catchments with two different rainfall grid resolution (1 and 16 km): a) mean rainfall intensity [mm h^{-1}]; b) normalized time distance; c) normalized time dispersion.

The effect of increasing the spatial aggregation length on the normalised distance is in general to systematically reduce its deviation with respect to the central value of 1.0. This is expected, since for a spatially uniform rainfall pattern the value of the normalised distance would be equal to 1.0. The difference in normalised distance between 1-km and 16-km aggregation lengths has been examined quantitatively by computing the mean error between the two time series, as follows:

$$Bias_D = \frac{1}{n}\sum_{i=1}^{n}\left(D_{i,16} - D_{i,1}\right) \tag{5.9}$$

where $D_{i,Lr}$ represents the normalised time distance at time i and at L_r rainfall aggregation length, and n is the number of time steps. The values of the statistics $Bias_D$ have been reported in Tab.5.IV for the four basins and the three events.

Event	75 km^2	249 km^2	501 km^2	983 km^2
2002	2.9	6.4	7.1	5.7
2005	1.0	2.9	3.6	4.7
2006	1.6	3.4	3.5	2.1

Table 5.IV: Mean difference (in percent) between normalized time distance computed at 1-km and at 16-km rainfall resolution ($Bias_D$) for the 2002, 2005 and 2006 events over the four study basins.

It should be noted that the structured rainfall variability imposed by orography shows, for the study basins, a significant overlap with the structure of the flow distance. This is due to the morphology of the drainage basins, which are elongated in the direction parallel to the orographic grow of the precipitation. When heavy rainfall lies on a sufficiently narrow range of isochrones, as it occurs for 2002, the smoothing effect due to increasing the aggregation length may result in a significant distorsion of the rainfall field geometry with respect to the river network. To elucidate the controls of input spatial aggregation on distributed hydrological model error, KLEM model is applied over the four different subbasins described above and by using four different rainfall resolutions: 1-, 4-, 8- and 16-km. The range of spatial resolution covers the aggregation scales often encountered in flood and flash flood forecasting.

5.3.5 The rainfall volume error

The normalised rainfall volume error versus the ratio L_r/L_w is reported for the three events in Figure 5.9. The figure shows that the sensitivity of rainfall volume error to L_r/L_w is large for the 2005 event, relatively small for the 2006 event and intermediate for the 2002 event. There is a close correspondence of sensitivity to the size of the integral scale for each event. This is expected, because the effect of the uncertain location of variable rainfall with respect to the catchment boundary should increase with the relative spatial variability, e.g. with decreasing the rainfall integral scale. The figure shows that there is a L_r/L_w threshold of enhanced sensitivity, which is around 0.5 for 2002 and 2005, and around 1.0 for 2006. The figure also shows that there may be a range of errors for a given value of L_r/L_w , which indicates that the ratio is not able to capture completely the variability of the error. Among other factors, this may depend on the choice of the watershed area square root as the

characteristic watershed length. Given that the rainfall volume error is controlled mainly by the interplay between the rainfall spatial variability and the watershed boundary shape, and since for a given watershed area there may be a range of watershed boundary shapes [Rinaldo et al., 1995], it follows that the basin area may not describe completely the error. Investigations are on going to identify a better geometry descriptor capable to characterise more completely the effect of increasing the rainfall aggregation length on the rainfall volume error.

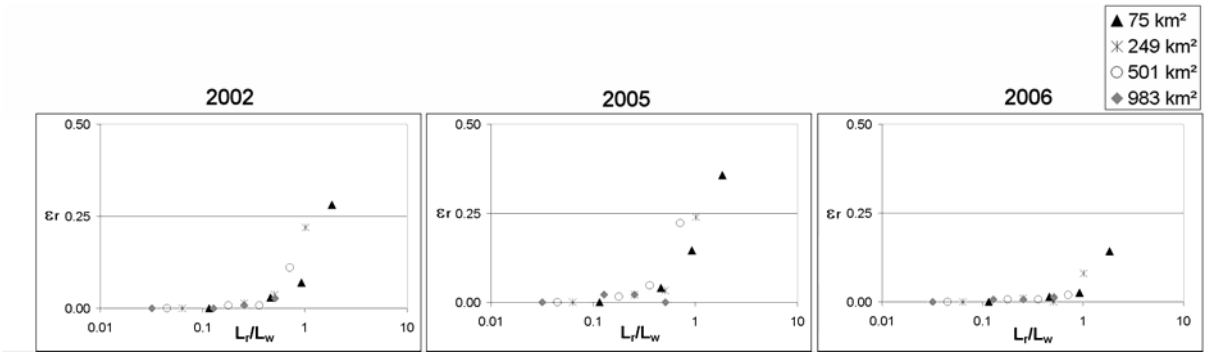

Figure 5.9: Normalized rainfall errors versus L_r/L_w ratio for the 2002, 2005 and 2006 storm events.

Results shown in Fig.5.9 generalise those reported at the previous section for the four nested Cervo basins, and examined by using 1-km and 16-km grid resolutions. Relatively large errors were found for grid size equal to 16 km for the Cervo basin at Passobreve. This corresponds to L_r/L_w equal to 1.93, for which the normalised rainfall volume error range between 15% (2006 event) and 32% (2005 event). On the contrary, almost negligible errors were found for the Cervo basin at Quinto, for which L_r/L_w is equal to 0.51. Indeed, Fig.5.9 shows that for this value of L_r/L_w the normalised rainfall volume error is always less than 5%.

5.3.6 Role of runoff transport processes

To clarify the role of runoff transport processes alone on the sensitivity of runoff model to rainfall aggregation length, we carried out a set of experiments by 'switching off' the runoff generation model. We assume in this way that the soil is everywhere completely impervious. Results for the peak discharge error are reported in Fig.5.10a, whereas Fig.10b displays the results after rescaling of rainfall input to be exactly preserved at each time step over the range of rainfall resolutions and catchment scales examined. This was obtained by multiplying the rainfall field at each time step by a constant that force the rainfall volume to be equal to that estimated at 1-km aggregation. We termed 'conservative' these results, and 'non conservative' the original results obtained before rescaling the rainfall input. Fig.5.10c reports the difference between the non conservative and the conservative error statistics, and as such it reflects the effects of the rainfall volume errors. Runoff volume error statistics are not reported for this case, since they are exactly equivalent to those already reported in Fig.5.9 for the rainfall volume errors.

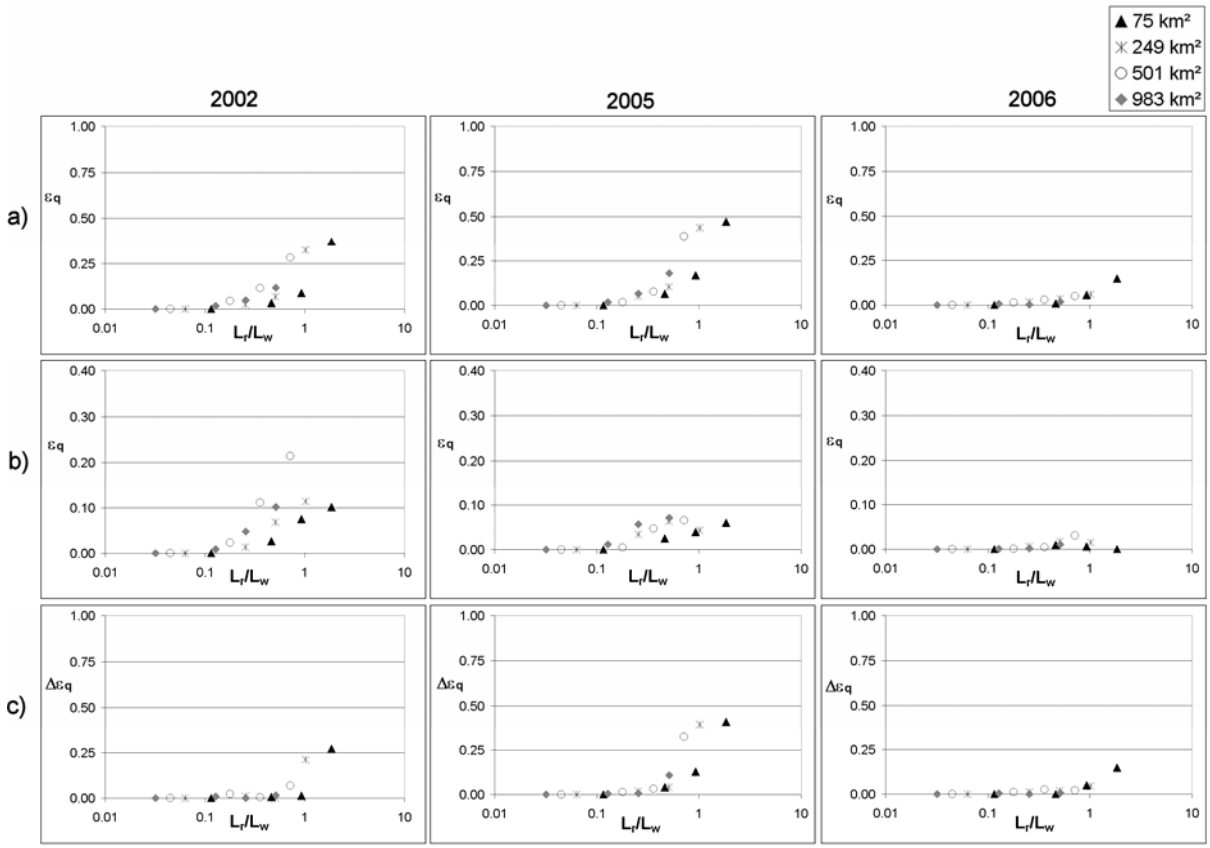

Figure 5.10: Normalized peak discharge errors versus L_r/L_w ratio for the 2002, 2005 and 2006 flood events, with hypothesis of impermeable soil (CN=100): a) before rainfall volume rescaling (non conservative results); b) after rainfall volume rescaling (conservative results); c) difference between non conservative and conservative results.

The relationship between peak errors and L_r/L_w reported in Fig.5.10a shows that the peak error reaches a value of almost 50% for the 2005 event at L_r/L_w equal to 1. The corresponding error amounts to 35% for the 2002 event and is almost negligible for the 2006 event. Fig.5.10b reports the peak errors induced by the combination of attenuated rainfall spatial variability and distorted geometry with respect to the river network. Here, the pattern of the error should increase up to L_r/L_w around one, and then stabilise around this value, which indicates the error arising when considering the runoff model with input from a spatially uniform rainfall distribution over the catchment. This value is expected to increase with increasing the catchment size, which explains why we should expect that in this figure the experimental results will group according to catchment size. This effect can be recognised in Fig.10b. It is interesting to note that the figure highlights the effects of the biased spatial rainfall distribution with respect to the river network outlined at Section 5.1.4, as expected. Peak discharge errors for the event 2002 (2006) are the most (least) sensitive to increasing the ratio L_r/L_w, following the patterns of deviation of normalised time distance at the various aggregation lengths with respect to 1-km reported in Table 5.IV.

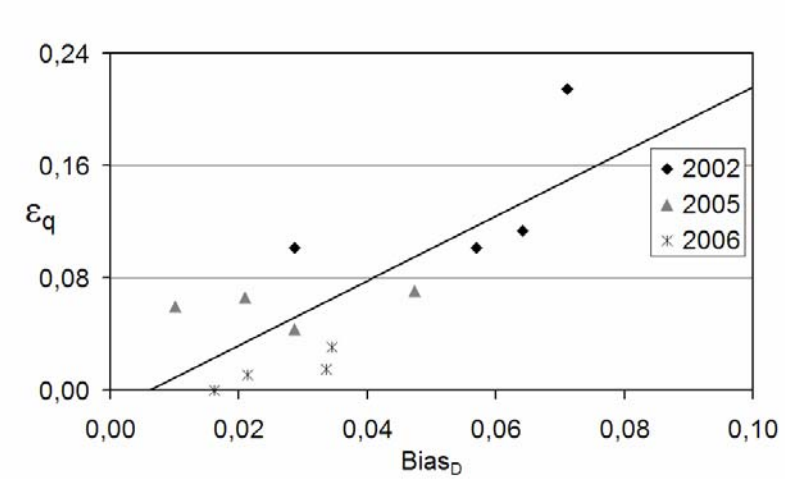

Figure 5.11: Normalized peak discharge errors versus mean difference between normalized time distance computed at 1-km and at 16-km rainfall resolution ($Bias_D$), with hypothesis of impermeable soil (CN=100). The figure shows also the best fit line. Linear correlation coefficient amounts to 0.76.

Examination of the simulated hydrographs (not reported here) shows that flood peak time errors arise for the 2002 event alone, with the 16-km –derived flood peak anticipated by 30 min with respect to the reference peak for all the catchments but the smallest. Errors in the flood peak timing correspond also to a deformation of the flood response, and then to flood peak errors. We examined quantitatively the relationship between the simulated flood peak errors and the deviations in the normalised time distance, as summarised by the statistic $Bias_D$ (Eq.5.9). The relationship between the $Bias_D$ and the normalised peak discharge error after rescaling is reported in Fig.5.11, which shows a significant correlation between the two variables (the linear correlation coefficient is equal to 0.76, which is significant at 5%). This means that the distortion of spatial rainfall geometry with respect to the river network is an important control on peak discharge error for the 2002 event, which is characterised by a persistent and significant pattern of increasing precipitation with orography overlapping with the isochrone pattern. More precisely, the effect of aggregation is to smooth out the rainfall concentration, which at 1-km resolution is placed towards the far periphery of the basin, and then to reduce the response time, as shown by the anticipated peak timing.

Figure 5.10c highlights the role of rainfall volume errors on the peak discharge error. The error patterns follow closely those of the rainfall volume errors, as expected, with the 2005 event showing a peak of sensitivity. It is possible to identify a L_r/L_w threshold of enhanced sensitivity, which is around 0.5 for 2002 and 2005 - the same as for the rainfall volume errors. The percentage of error due to rainfall volume error on the total error varies greatly with catchment and event. For example, when considering the value of L_r/L_w equal to 1, the impact of rainfall volume error on total error is almost zero for 2002 at 75 km^2, and almost 90% for 2005 at 249 km^2.

5.3.7 Role of runoff generation and transport processes

In this section we examine the effects of both runoff generation and transport processes, by considering the actual distribution of CN values. Results are reported in Fig.5.12 and 5.13 for the volume and peak errors, respectively, by displaying 'non conservative', 'conservative' and 'difference' statistics.

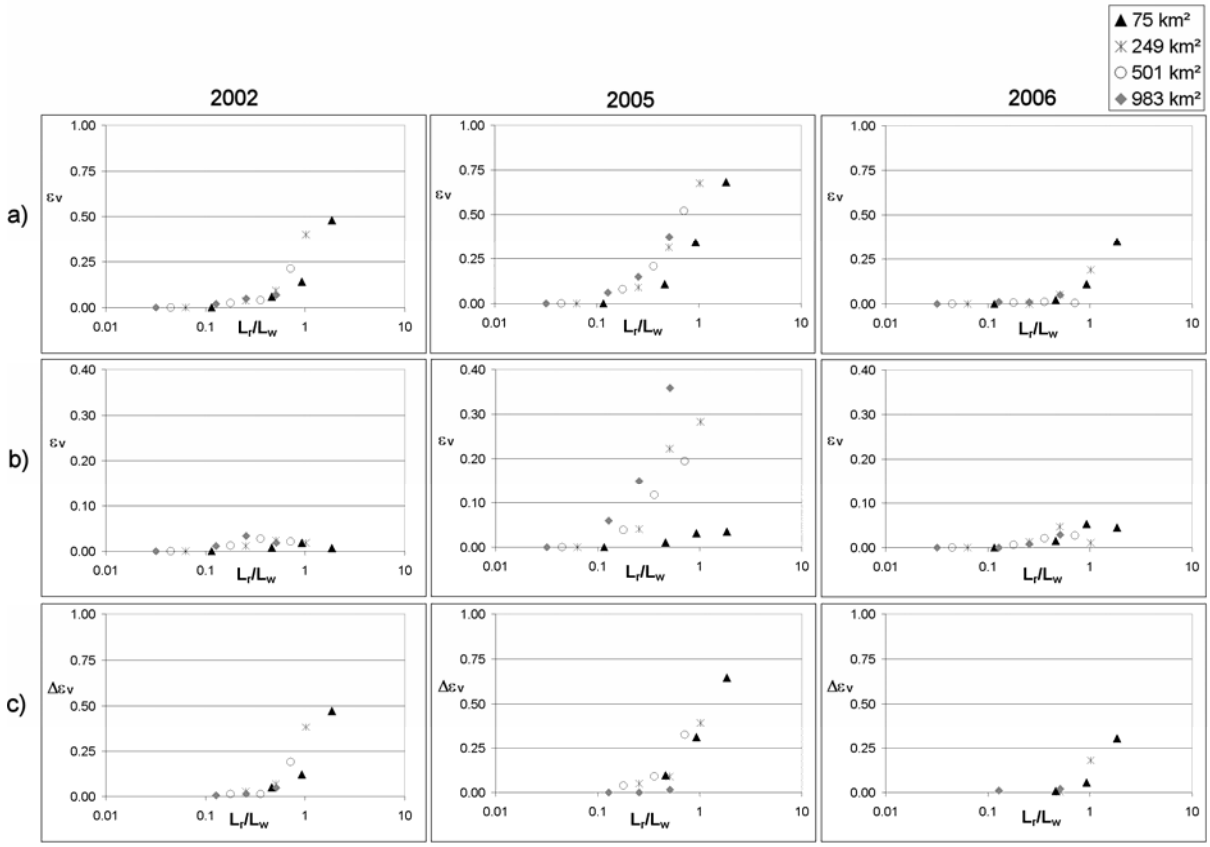

Figure 5.12: Normalized runoff volume errors versus L_r/L_w ratio for the 2002, 2005 and 2006 flood events, for the actual CN distribution: a) before rainfall volume rescaling (non conservative results); b) after rainfall volume rescaling (conservative results); c) difference between non conservative and conservative results.

Large runoff volume errors are shown in Fig.5.12a, particularly for the 2005 event, which is characterised by values around 0.75 for a value of L_r/L_w equal to one. The impact of reduced rainfall variability alone on runoff volume errors (Fig.5.12b) is also very large for the 2005 event, due probably to the combination of the low runoff coefficient, large intermittency and large rainfall spatial variability. Figure 5.12b shows for the 2005 event a sharp differentiation between the smallest basin, where the event reached the highest specific peak discharge, and the group of the other three basins, characterised by high rainfall intermittency and very low runoff coefficients. The impact of rainfall variability is much less effective for the 2002 and 2006 events, characterised by higher runoff coefficients and with most of the runoff generated from very wet areas. The impact of the rainfall volume error on the runoff volume error is described in Fig.5.12c, which indicates that the general pattern of rainfall volume errors is transmitted to the volume errors, with the 2005 event showing highest

sensitivity and the 2006 event showing lowest sensitivity. The figure shows also that the rainfall volume errors generally magnify through the rainfall-runoff modelling, as it is expected after examining the structure of the SCS-CN runoff model.

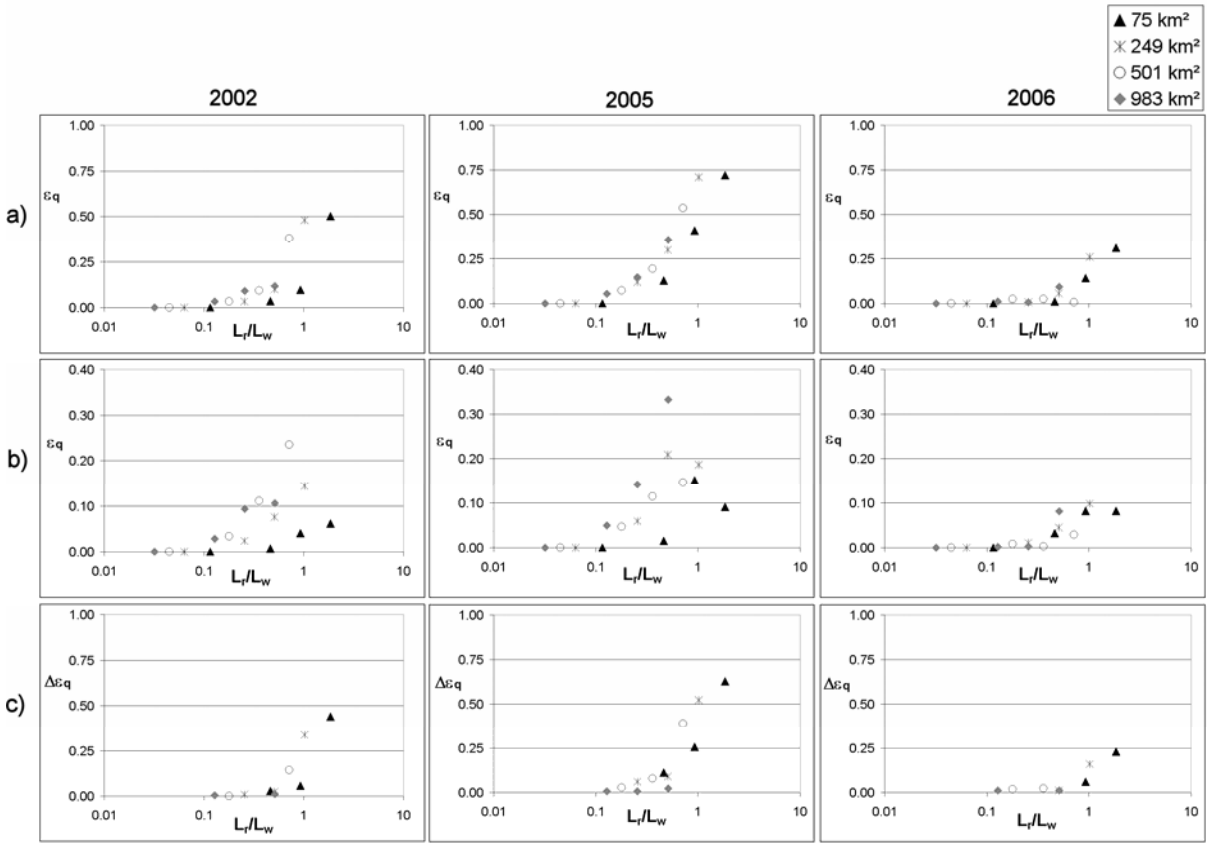

Figure 5.13: Normalized peak discharge errors versus L_r/L_w ratio for the 2002, 2005 and 2006 flood events, for the actual CN distribution: a) before rainfall volume rescaling (non conservative results); b) after rainfall volume rescaling (conservative results); c) difference between non conservative and conservative results.

The values of peak discharge errors reported in Fig.5.13a,b,c show that the errors are always larger than in the impervious case reported in Fig.5.10a,b,c. This is expected, since the infiltration process injects further spatial variability, both random and structured, into the rainfall-runoff process. The effects of reduced and distorted rainfall spatial variability on peak discharge is particularly severe for the 2002 and 2005 events, with peak errors exceeding 20% and 30%, respectively, at catchment scales down to 249 km^2. These results confirm that the correct estimate of rainfall volume is not enough for the accurate reproduction of flash flood events characterised by large rainfall spatial variability, but may suffice for less spatially variable flood events, like the 2006 event (which shows anyway errors up to 10%).

Interestingly, for the 2002 event the peak discharge errors are almost independent from runoff volume errors, which show that increasing the rainfall aggregation length induces for this event mainly a deformation of the flood shape. Indeed, the peak timing error is particularly severe for this event, with the 16-km rainfall resolution flood peak anticipated by 0.5 hr, 1.5 hr and 1.0 hr at 249 km^2, 501 km^2 and 983 km^2 catchment scale, respectively, with

reference to the 1-km rainfall resolution flood peak. The patterns of peak discharge errors due to rainfall volume errors closely portray those reported for the impervious case, but with a magnification which almost double their values (as an obvious outcome of the magnification of the rainfall errors through the hydrological model used here when the non-linearities in the infiltration processes are accounted for).

5.3.8 Role of soil properties spatial aggregation

The analysis of the impact of aggregation of soil properties was carried out by aggregating the value of the S parameter (corresponding to the CN parameter through Eq.3.52) over the same resolutions used for rainfall aggregation analysis, and by using 1-km rainfall resolution. Results are reported in Fig.5.14a,b and show the ratio L_G/L_w versus the normalised runoff volume error and the normalised peak discharge error, respectively. The resulting pattern of sensitivity of runoff volume and peak discharge to increasing the soil properties aggregation length is in agreement with findings from earlier studies, which reported higher sensitivity for events with relatively low runoff ratio [Merz and Plate,1997; Merz and Bardossy, 1998]. Accordingly, the event 2005 is characterised by large errors both on runoff volumes and peak discharges, particularly for the larger catchments which are characterised by high rainfall intermittency for this storm.

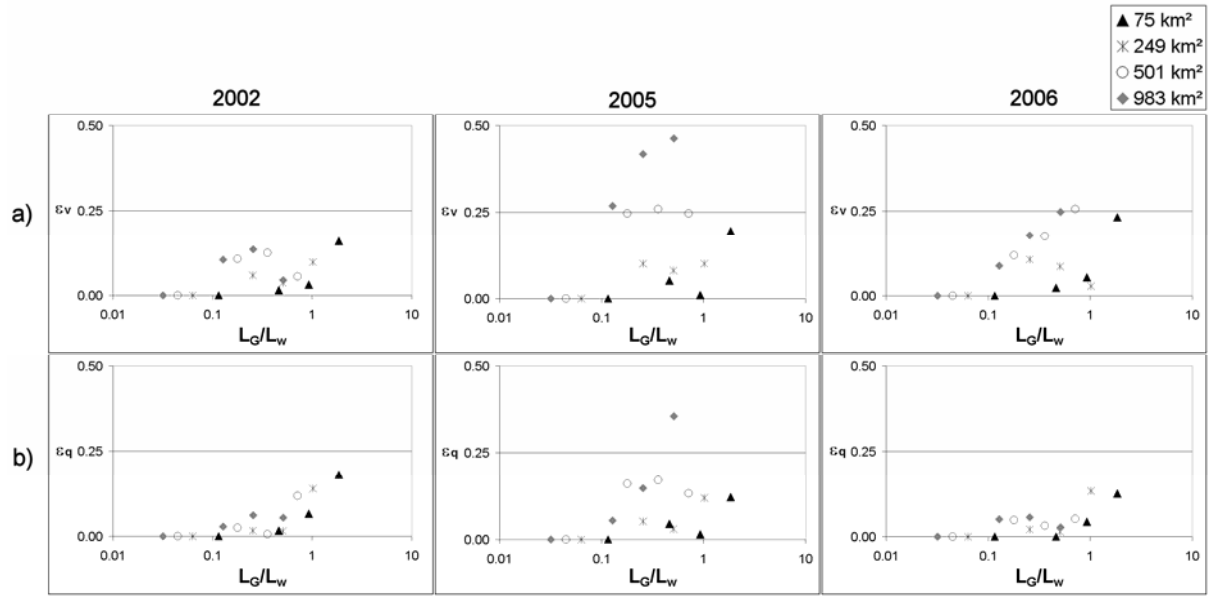

Figure 14: Normalised runoff volume errors (a) and normalized peak discharge errors (b) versus L_G/L_w ratio for the 2002, 2005 and 2006 flood events, due to soil propriety aggregation.

Results in Fig.5.14a,b can be compared with their counterpart obtained by increasing the rainfall aggregation length and after rescaling to preserve the rainfall volume (Fig.5.13b and 5.14b, respectively). Comparing the results reported for the peak discharge errors indicates that the magnitude of the error is similar for the two cases. Conversely, large differences can be noted for the runoff volume errors, particularly for the 2002 and 2006 events. This suggests that the effect of increasing the soil properties aggregation length is first

on the runoff volume, and it is then transmitted to peak discharges. As a result, the shape of the flood wave is only slightly influenced by modifying the detail of the soil property spatial representation. Indeed, no peak timing errors were reported for this case. On the contrary, rainfall aggregation may have a limited influence on runoff volumes, and may exert in spite of this a remarkable impact on the peak discharge, mainly through a different spatial organisation of the runoff volumes. This is nicely described by our findings for the 2002 event. These considerations suggest that re-parameterization of the runoff model may easily adjust for aggregation of soil properties, whereas this may be a more complex task for the case of rainfall spatial aggregation. However, the limitations of our study should be borne in mind when considering possible generalisations of these findings. As far as the influence of soil properties aggregation is of concern, the main limitations arise from the lack of sharp differences in the soil properties spatial distribution, and the stringent assumptions made in the runoff model used for this study. Examination of cases with a more even representation of urban and rural land uses may lead to different results. Analogously, different sensitivity patterns may emerge with the use of more complex runoff models accounting for a range of runoff generation processes.

5.3.9 Summary and conclusions

The literature on the significance of aggregation of rainfall and soil properties for runoff estimation is complex and sometimes contradictory. Effects can be expected to vary depending on the nature of the rainfall, the nature of the catchment, and the spatial scale of the catchment and rainfall. For temperate regions, the review highlighted the trade-off in terms of catchment response between the impact of spatial variability of rainfall, its aggregation and the smoothing effect due to the heterogeneity of the catchment. The mountainous region on the northern border of the Piemonte region in Italy produces some of largest unit discharge peaks in the northern Mediterranean basin and is monitored with a dense network of weather radar and raingauge stations. This offered an opportunity to examine the impact of spatial aggregation of rainfall and soil properties on extreme flood modelling.

Flood response to three extreme storm events, occurred on the Sesia River basin, at four catchment scales ranging from 75 km^2 to 983 km^2, are reproduced by using high resolution radar rainfall estimates from the Bric della Croce weather radar and a distributed hydrologic model, based on a Hortonian infiltration model and a network-based representation of hillslope and channel flow. Four input spatial resolutions are considered, with grid size equal to 1-, 4-, 8- and 16- km, for rainfall and soil properties representation. Two dimensionless parameters given by the ratio between input length aggregation and the square root of the watershed area (L_r/L_w and L_G/L_w for rainfall and soil properties, respectively) are used to describe the sensitivity of the runoff model. Orographic enhancement of the precipitation, storm structure and motion play an important role in determining timing and rainfall contributions to the sub-basins, which in turn shape the flood response. Given the

focus on Hortonian runoff generation mechanism and surface runoff propagation through hillslopes and branched channel networks, we examine the role of runoff transport geometry in the coarsening of spatial rainfall representation and on simulated runoff volumes and peak discharges.

The rainfall spatial variability plays an important role when rainfall fields are systematically structured across locations with equal flow distance coordinates, as it occurs in the case of orographic effect and when catchments are elongated in the direction perpendicular to the mountainous range. When heavy rainfall lies on a sufficiently narrow range of isochrones, the smoothing effect due to increasing the rainfall aggregation length may result in a significant distortion of the rainfall field geometry with respect to the river network. In these cases, the increase of the spatial rainfall aggregation length leads to a significant deformation of the flood shape, with an anticipation of the simulated flood peak when the precipitation is concentrated towards the periphery of the catchment, and a delay of the simulated flood peak when the precipitation is concentrated towards the outlet of the catchment. These effects are negligible at the small catchment scale and become significant with increasing the catchment size.

When infiltration is 'switched off' in the runoff model and all the variability arises due to runoff transport processes, the distortion of the rainfall field geometry with respect to river network may be an important control on peak discharge error, even at catchment scales less than 500 km^2. Obviously, this distortion has no impact on the runoff volume error, which is in this case completely determined by the rainfall volume error. This volume error arises when rainfall values pertaining to areas just outside the catchment enter the computation of the average rainfall over the basin by increasing the aggregation length. The rainfall volume error is controlled mainly by the ratio L_r/L_w and by the rainfall integral scale; it exerts a dominant impact on peak discharges at small catchment scales (75 km^2), and becomes less significant by increasing the catchment dimension.

Errors on both runoff volumes and peak discharges increase when infiltration is taken into account in the runoff model. This is expected, since the infiltration process injects further spatial variability, both random and structured, into the rainfall-runoff process. The effects of reduced and distorted rainfall spatial variability on peak discharge have been found particularly severe for the flash flood events, with peak errors up to 35% for values of the ratio L_r/L_w around 0.5 and a catchment scale of 983 km^2. Effects are particularly remarkable when significant structured rainfall variability combines with relatively important infiltration rates due to dry initial conditions, as this emphasises the non linear character of the rainfall-runoff transformation. In general, these results confirm that the correct estimate of rainfall volume is not enough for the accurate reproduction of flash flood events characterised by large and structured rainfall spatial variability, even at catchment scales around 250 km^2. However, accurate rainfall volume estimation may suffice for less spatially variable flood events. The

results show also that the rainfall volume errors generally magnify through the rainfall-runoff modelling, at least for the runoff model considered here.

Increasing the soil properties aggregation length exerts similar effects on peak discharge errors as increasing the rainfall aggregation length, for the cases considered here and after rescaling to preserve the rainfall volume. Moreover, peak discharge errors are roughly proportional to runoff volume errors, which indicate that the shape of the flood wave is influenced in a limited way by modifying the detail of the soil property spatial representation. Conversely, rainfall aggregation may exert a pronounced influence on the discharge peak by reshaping the spatial organisation of the runoff volumes and without a comparable impact on the runoff volumes. Even with increasing the soil properties aggregation length, effects are particularly remarkable in those cases characterised by low runoff values and low values of runoff coefficients.

The present investigation has documented how input variability, as filtered by using different spatial aggregation lengths, feeds through to variability in modelled runoff response at the catchment scale. More extensive investigations would strengthen this understanding and provide additional guidance on the design of radar/raingauge networks for flow forecasting and the spatial resolution requirements for rainfall and soil properties at different catchment scales. Further work might determine whether the results obtained in this investigation apply to other model formulations and may be generalised to other hydroclimatic environments. In this framework, future investigations should focus on the sensitivity of the averaging of space-time rainfall fields across locations with equal flow distance coordinates to the rainfall aggregation length and to river network geometry. As shown here, this is a significant and relatively unexplored feature of catchments where rain exhibits significant spatial variability and linear routing through branched channel networks plays a significant role.

5.4 Role of spatial rainfall aggregation on flash flood modelling: analysis of the Fella 29 August 2003 case study

5.4.1 The Fella 2003 flash flood

The flash flood of the Fella catchment on 29 August 2003 (Fig.5.15) occurred at the end of a climatic anomaly of a dry and hot summer and was one of the most devastating flash flood events in North-eastern Italy since starting of systematic observations. The rainfall event started at 10:00 CET (Central European Time) and lasted for 10 hours, focusing on the 705 km^2-wide Fella basin (Fig. 2), which is a major left-hand tributary of the Tagliamento river system. The Fella basin has a mean altitude of 1140 m a.s.l., with an average annual precipitation of 1920 mm. Ten subbasins of the Fella river system are examined in this study, ranging from 10.5 km^2 to 623 km^2.

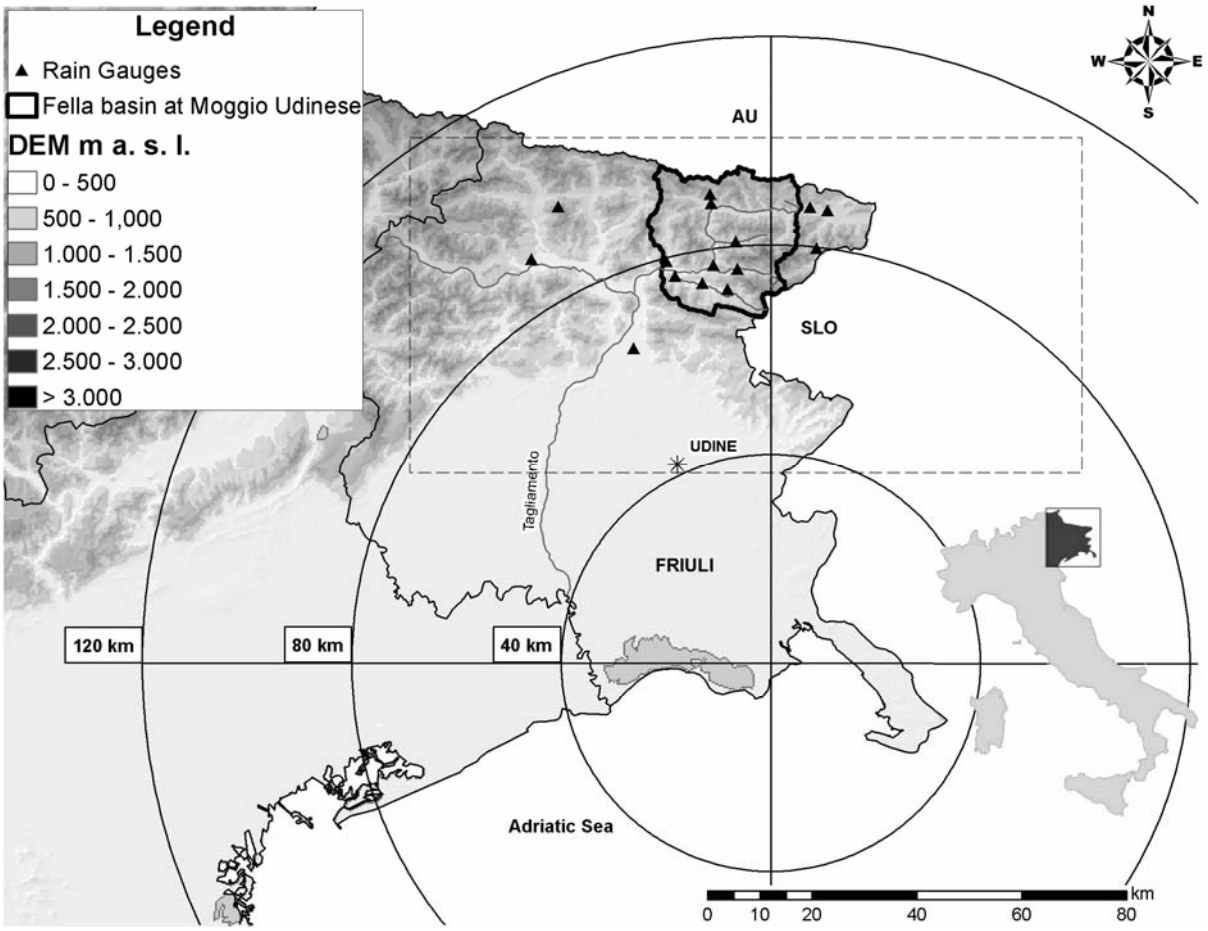

Figure 5.15: Location of the OSMER radar and the Fella river basin at Moggio Udinese with DTM of North-Eastern Italy. The locations of the raingauge stations used in the study are also reported. The dotted line rectangle represents the area used for the analyses of rainfall spatial variability reported in Fig. 5.17.

Extreme rainfall from the August 2003 storm was produced by quasi-stationary convective banded structures. Some of the bands persisted in the same locations for the duration of the event. The steadiness of these rainbands led to highly variable precipitation

accumulations and runoff [Borga et al., 2007]. The storm total precipitation (Fig.5.16) is characterised by a band of rainfall accumulation exceeding 300 mm localised on the right-hand tributaries of the Fella River. The storm total rainfall distribution reflects south west - north east motion of the storm elements and west-east shift of the tracks of the storms. Rainfall intensity up to 100 mm hr^{-1} over 15-minutes time step was recorded during the explosive growth phase of the storm (between 15:00 and 18:00 CET) [Norbiato et al., 2007]. Rainfall produced by the August 2003 storm resulted in severe flooding throughout the Fella river basin. The storm produced catastrophic flooding at drainage areas up to 80-90 km^2.

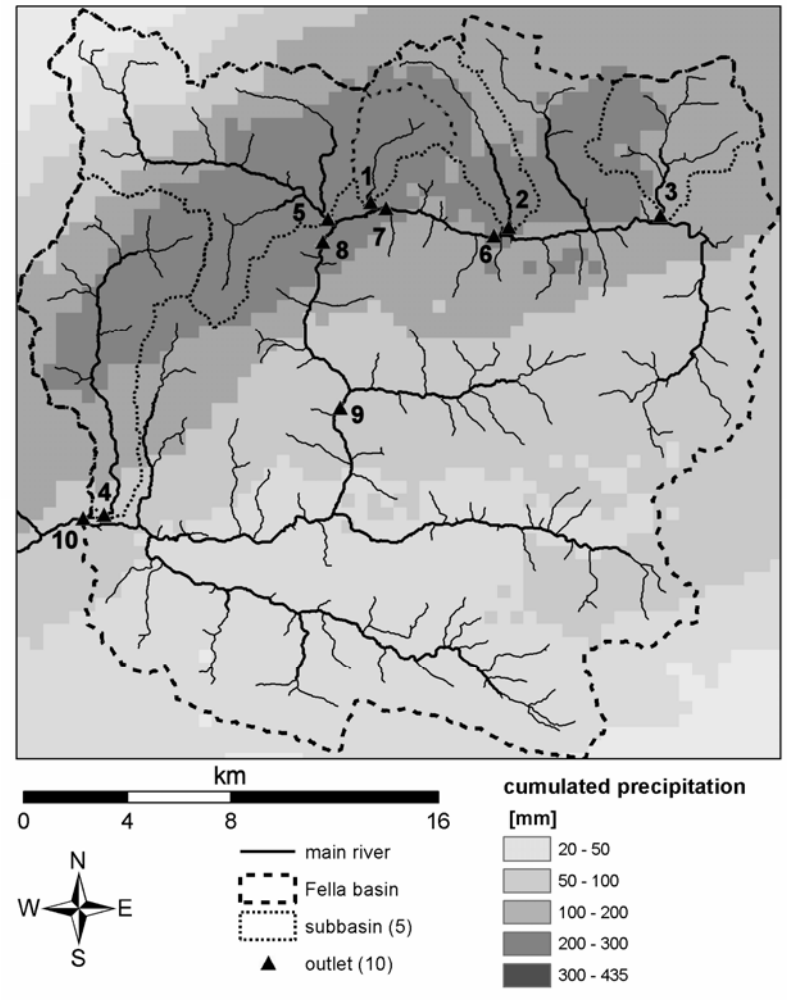

Figure 5.16: Storm total rainfall (mm) for the August 29, 2003 storm on the Fella river basin at Moggio (basin outlet 10, 623km²) with the nine study subbasins: Rio degli Uccelli at Pontebba (1, 10.5km²); Rio Bianco at S. Caterina (2, 17.5km²); Uque at Ugovizza (3, 24km²); Aupa at Moggio Udinese (4, 50km²); Pontebbana at Pontebba (5, 71.2km²); Fella at S.Caterina (6, 139km²); Fella at Pontebba (7, 165km²); Fella at S.Rocco (8, 250km²) and Fella at Dogna (9, 329km²).

Following the August 2003 event, post flood surveys were planned. Surveys were concentrated in the upper Fella basin and included: collection of rainfall data, collection of streamgauge data and execution of indirect peak flood estimation, and postflood interviews. Radar and raingauge observations were used to derive rainfall fields for the August 2003 storm. 5-minute raingauge data were collected at 15 raingauges (Fig.5.15), whereas storm total

rainfall was available at further six daily raingauges. Volume scan reflectivity data from the Doppler, dual-polarised C-band OSMER radar station, located at Fossalon di Grado (Fig.5.15) (time resolution of 5 min and spatial resolution of 250 m in range by 0.9 degree in azimuth), were used to derive radar rainfall rates. Spatially detailed rainfall estimates were obtained by adjusting radar observation accounting for the physics of the radar sensing and incorporating accumulated values of the available raingauge stations.

Streamgauge data and observations from post-event surveys, combined with hydraulic modelling, were used to examine hydrologic response to the storm. Stream gauge data were available at eight sites, including three of the sites considered in this study (Fella at Pontebba, at Dogna and at Moggio) (Fig.5.16). Almost all these gauges are located either close or at bridge crossing sites, where measurements are taken by means of ultrasound sensors. Hydraulic modelling, combined with surveys of the post-flood river section geometry and data about pre- and post-flood geometry, was used to derive stage-discharge relationships at these river sections [Borga et al., 2007]. Furthermore, hydraulic modelling was used to estimate peak discharges based on surveyed high watermarks and postflood channel geometry at another three sites (including the site at the outlet of Uqua basin, Fig.5.16) and to confirm the estimates at the gauged sections. Twenty-two local residents, mostly located close to the Uqua river basin and its fan, were interviewed about the severity of the storm, occurrences of surface flow, and timing of rainfall and stage peaks.

5.4.2 Precipitation analysis

The structure of the rainfall spatial variability has been examined by using the climatological variogram [Berne et al., 2004]. The domain used for this analysis is a 128 km by 64 km region centred on the Fella River basin (Fig.5.15). With the approach based on the climatological variogram, one may take into account information from all the realizations (e.g. rainfall field for successive time steps) assuming the fields to have similar statistical characteristics except for a constant factor. The variogram can therefore be normalised by the respective variance of each field considered and then averaged over all the realizations. Assuming the structure functions have the same shape, the mean normalised variogram obtained, also called climatological variogram, is representative of all the realizations. In particular, we have used here a spherical variogram as a reference spatial structure. The main adjustment factor of this function is the variogram shape and particularly its range (i.e., the decorrelation distance). This allowed us to calibrate a relation between the rainfall accumulation time step Δt (hours) and the range D_R (km) (Fig.5.17a), as follows:

$$D_R = 23.3\Delta t^{0.23} \tag{5.10}$$

Interestingly, this equation is close to the one reported by Berne et al. (2004) for flash flood events observed in France. According to Eq. (5.10), the range of the variogram of half-hourly rain rates is set equal to 19.5 km.

Space and time generation of runoff is controlled mainly by the spatial distribution of the intense rainfall cells. We characterise this spatial distribution by using the concept of the indicator variogram [Barancourt et al., 1992], i.e. by converting the rainfall field into a corresponding binary process. For this, a binary function denoted *i(x,y)*, called the indicator function by Journel [1983], is defined by $i(x,y)=1_{P(x,y)>20\ mm/h}$, i.e.:

i(x,y)=1 if P(x,y)>20 mm/h
i(x,y)=0 otherwise (5.11)

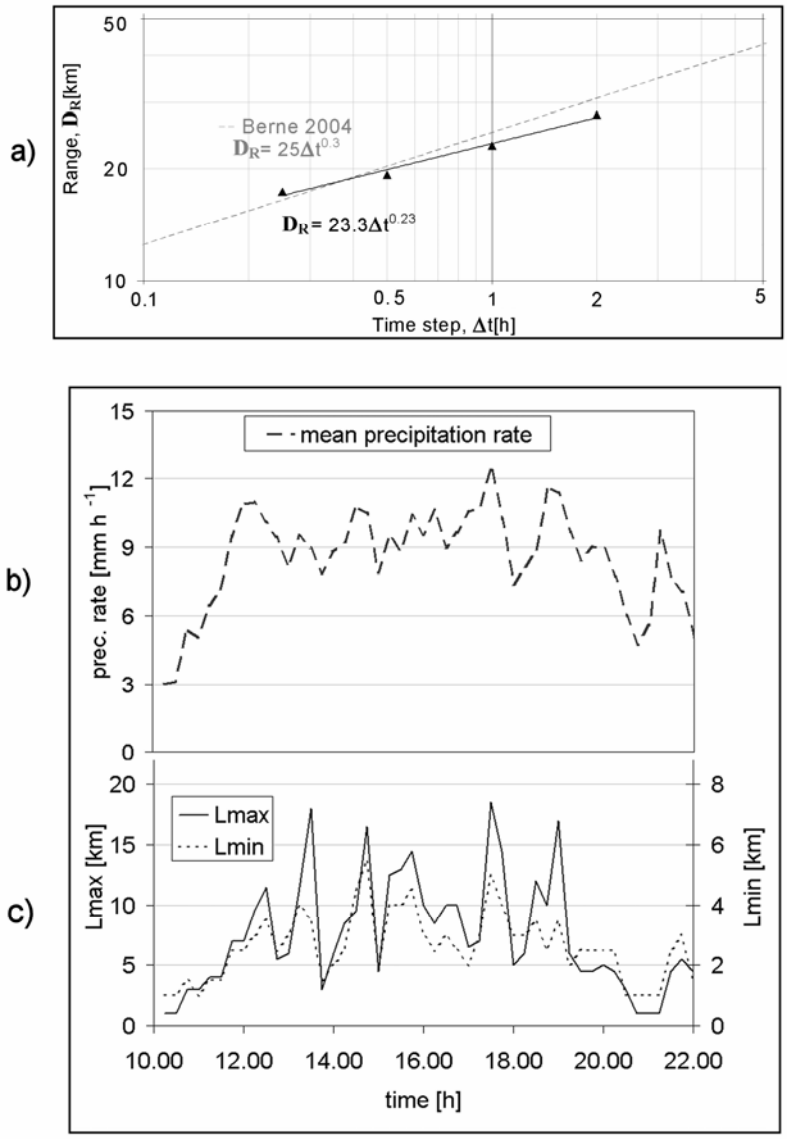

Figure 5.17: Rainfall spatial variability analysis:

a) Range [km], resulting from spatial climatological variogram analysis, versus time step [h]; results are compared with analysis carried out by Berne et al. [2004] (dashed line);
b) Mean precipitation of non zero values inside the rectangle area shown in Figure 1.
c) Lengths of maximum and minimum axis for indicator variogram on binary rainfall fields using 20mmh^{-1} threshold.

The threshold of 20 mm h^{-1} was selected here to isolate the fraction of the basin hit by flood producing rainfall. We analysed the binary field by using the indicator variogram, which show a significant anisotropy with longer correlations in the NE direction. To account for

anisotropy, we conceptualised the range in space as an elliptical field, quantified by the major and minor axes. We describe the temporal evolution of the spatial structure of rainfall accumulate at 30-min time step by reporting the time series of max and min lengths (Fig.5.17c). The indicator variogram analyses highlight the high variability of the storm properties with time. During the period of very intense rainfall occurrence (e.g., between 14:00 and 18:00 CET) the major axis length ranges between 7 and 18 km, whereas minor axis length ranges between 3 and 5 km. This indicates that the shape of the high intense areas is elongated, with the minor axis length equal to 30% of that of the major axis.

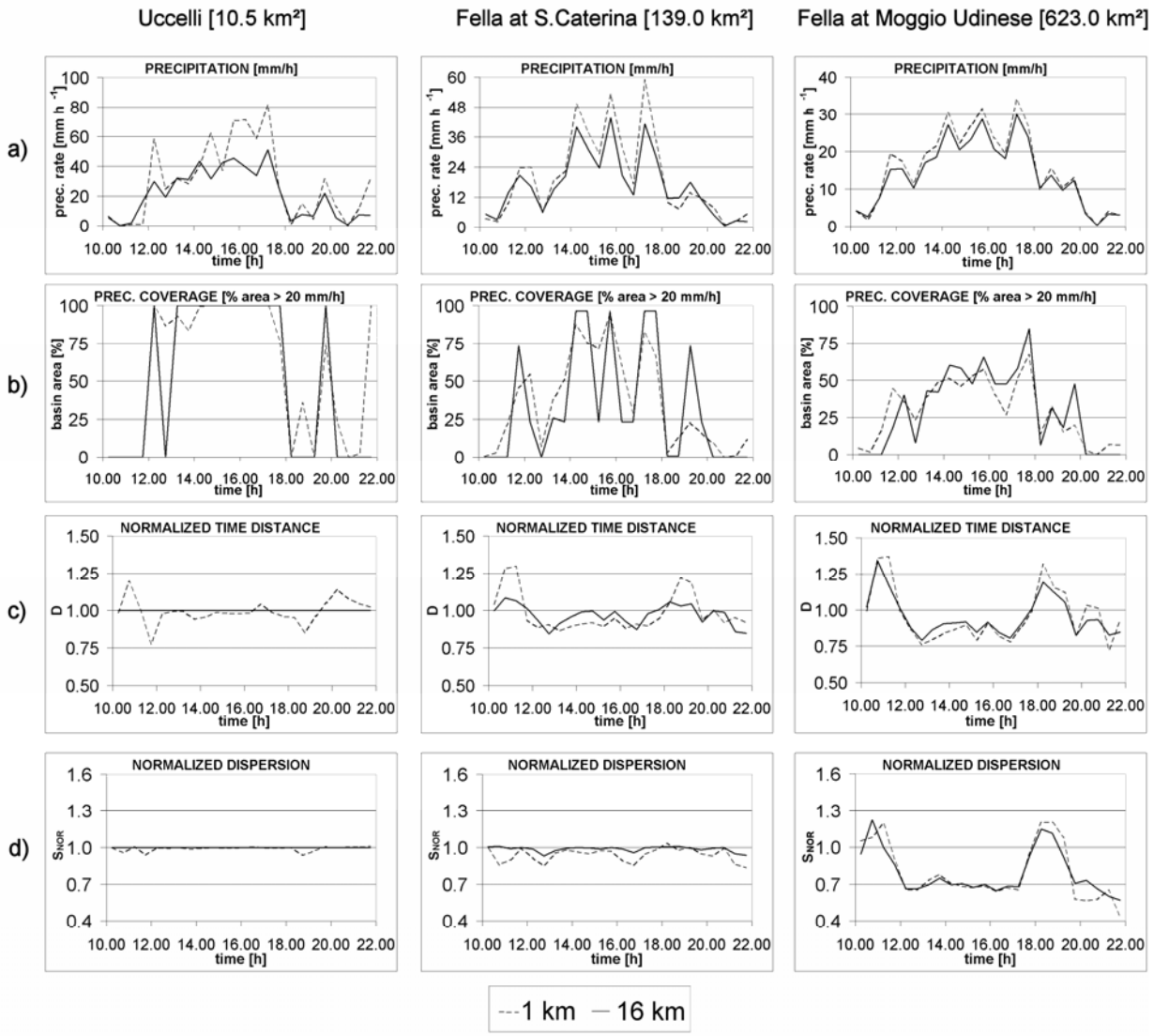

Figure 5.18: Precipitation analysis for three catchments (Uccelli at Pontebba, 10.5km², Fella at S.Caterina, 139 km² and Fella at Moggio Udinese, 623 km²), with two different rainfall grid resolutions (1 km and 16 km):
a) mean rainfall intensity [mm h^{-1}];
b) coverage (for precipitation intensity > 20 mm h^{-1});
c) normalized time distance;
d) normalized time dispersion.

Results of the analysis described in section 5.2 are reported in Fig.5.18 for three catchments: Rio degli Uccelli (10.5 km^2), Fella at S. Caterina (139.0 km^2) and Fella at Moggio (623.0 km^2) and for rainfall fields aggregated over length scales of 1 and 16 km. Rio degli

Uccelli and Fella at Moggio represent the smallest and largest catchment examined in the study, respectively, whereas Fella at S. Caterina represents an intermediate catchment scale. Inspection of mean rainfall intensity shows that aggregation at 16-km scale has relatively less effects over the larger basin (Fella at Moggio), whereas significant smoothing effects (with reductions up to 50%) are recognised over Rio degli Uccelli, particularly for the period 14:00 to 18:00,with intermediate effects for Fella at S. Caterina. Examination of normalised distance highlights different behaviours across the various catchments. Analysis of normalised dispersion over the period of heavy rainfall and at 1-km resolution shows that rainfall concentration translates from the lower portion of the basin to the upper portion and that the dynamics of the normalised distance increases with catchment scale, as expected. Aggregation over 16-km length scale has generally the effect to reduce the dynamics of the normalised distance and has a different impact according to catchment scale. For Rio degli Uccelli, aggregation over 16-km averages out any dynamics, as expected since the rainfall field provided to the catchment at this resolution is completely uniform. If we consider only the period of heavy rainfall, the difference between normalised distances measured at 1-km and at 16-km is emphasised over the Fella at S. Caterina, e.g. at the intermediate catchment scale.

A similar pattern can be recognised for the normalised dispersion, with precipitation exhibiting a unimodal peak for Moggio (at least during the period of extreme precipitation) and a more uniform distribution for the case of Rio degli Uccelli, with S. Caterina being in an intermediate position. There are two main conclusions from this analysis. First, the effect of aggregation on mean rainfall intensity and volumes decreases with catchment scales. Second, the effect of aggregation on the geometrical properties of the rainfall fields is not related to the catchment scales and is emphasised at intermediate catchment scales in the case studies examined here. These results provide a guideline for analysis of influence of rainfall aggregation on flood simulation in the next section.

5.4.3 Influence of rainfall spatial aggregation

The KLEM model has been implemented at 30-min time step and using a 20-m grid size cell for the description of landscape morphology and soil properties, with parameterisation found by Borga et al. [2007], able to describe flash flood dynamics at different scales. Effects of rainfall spatial aggregation on flood response modelling are examined here with reference to the ratio of rainfall resolution to the characteristic basin length (L_r/L_w), taken as the square root of the watershed area. To elucidate the controls of rainfall aggregation on model error, the KLEM model was applied over ten different subbasins ranging from 10.5 km^2 to 623 km^2 (Tab.5.V and Fig.5.18) and by using four different rainfall resolutions: 1-, 4-, 8- and 16-km. This provides 40 different combinations of watershed characteristic lengths and rainfall aggregations.

As shown above, varying the spatial rainfall resolution induces rainfall volume errors, a reduction of the rainfall apparent spatial variability and a distortion of the rainfall geometry

with respect to the flow distance metric. In order to separately address the first two effects we performed numerical experiments in which rainfall depths are rescaled and forced to be exactly preserved at each time step over the range of rainfall resolutions and catchment scales examined.

Basin id number	**Area [km²]**	**Mean areal precipitation [mm]** *using resolution*			
		1km	*4km*	*8km*	*16km*
1	10.5	353	327	314	255
2	17.5	307	303	307	246
3	24	287	279	285	192
4	50	301	284	229	160
5	71.2	246	240	240	222
6	139	241	237	235	203
7	165	247	244	239	211
8	250	253	248	244	216
9	329	237	235	232	224
10	623	189	187	183	170

Table 5.V: Characteristics of the study basins, with catchment area and mean areal cumulated precipitation at four different rainfall resolutions; basin id numbers as reported in Figure 5.16.

Examination of the normalised rainfall volume errors (Fig.5.19a) highlights the impact of the error caused by incorrectly "smoothing rainfall volume" either into or out of the watershed; this generally corresponds to negative errors – i.e. underestimation of the true rainfall volumes (Tab.5.V). These results generalise those reported at the previous section for the catchments of Rio degli Uccelli and Fella at Moggio and examined by using grid resolutions equal to 1 and 16 km. A large rainfall volume error was found for grid size equal to 16 km for the Rio degli Uccelli. This corresponds to L_r/L_w equal to 5.1, for which the normalised rainfall volume error amounts to 27%. On the contrary, the error for the Fella basin at Moggio, for which L_r/L_w is equal to 0.64, amounts to 9%. For the Fella at S. Caterina (L_r/L_w = 1.37), the error amounts to 15%. The figure shows that use of the ratio L_r/L_w is capable to filter out quite effectively the effect of the catchment size on the rainfall volume error. Inspection of the maximum values of the errors shows that the error is up to 0.1 for L_r/L_w equal to 0.4, and then increases to 0.2 for L_r/L_w equal to 1.0 and to 0.5 for L_r/L_w equal to 2.5.

The relationship between the normalised peak discharge error and L_r/L_w, before rainfall volume rescaling, is reported in Fig.5.19b. This figure shows that the rainfall volume error provides a first order control on peak discharge error. Maximum values of the peak discharge error are up to 0.2 for L_r/L_w equal to 0.5 and to 0.33 for L_r/L_w equal to 1.0. The error may reach values up to 0.75 for L_r/L_w equal to 2.3.

Peak discharge errors after rainfall volume rescaling are reported in Fig.5.19c. Comparison between Fig.5.19b and 5.19c allows full appreciation of the impact of rainfall volume error on peak discharge error. Errors in Fig.5.19c are reduced generally by ~50% with reference to Fig.519b, for L_r/L_w <1.0. Reduction ranges from ~40% for L_r/L_w equal to 0.5 to ~60% for L_r/L_w equal to 1.0. For L_r/L_w exceeding 1.0, the reduction may be much larger.

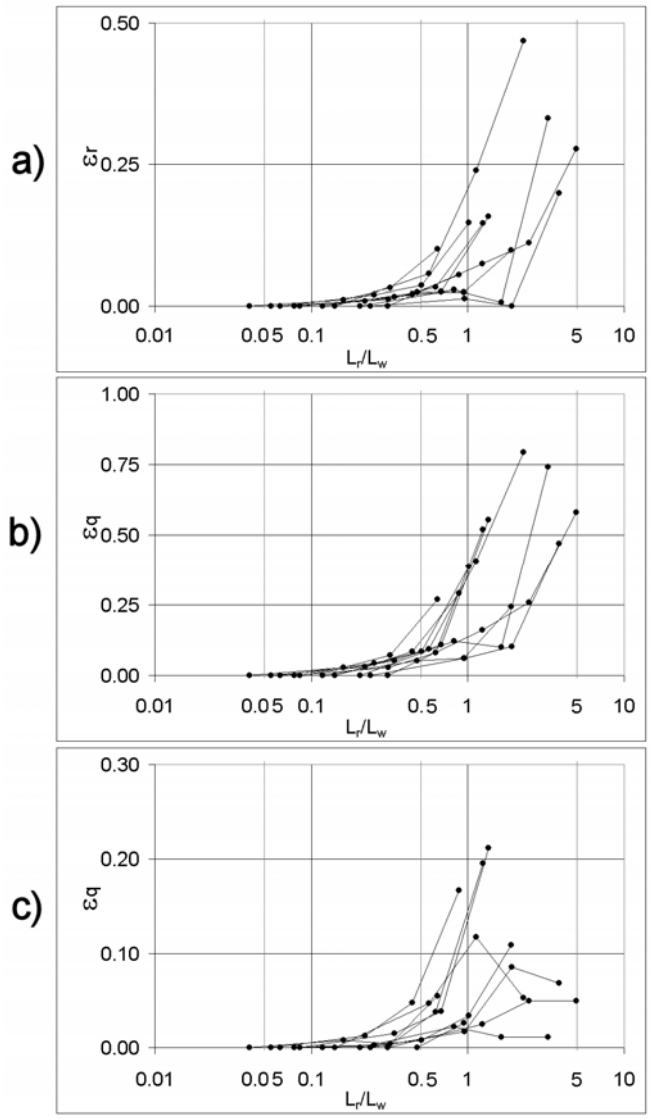

Figure 5.19: Relationship between the ratio L_r/L_w and a) normalised rainfall error; b) normalised peak discharge error before rainfall volume rescaling; c) normalised peak discharge error after rainfall volume rescaling.

We examined the impact of the rainfall spatial resolution on the distortion of rainfall spatial distribution with respect to the river network. To this purpose, we calculated for each subbasin the mean absolute error (MAE) between the normalised time distances computed at 16-km resolution with respect to that computed at 1-km resolution, as follows:

$$MAE = \frac{1}{n}\sum_{i=1}^{n}\left|D_{i,16} - D_{i,1}\right| \tag{5.11}$$

where $D_{i,Lr}$ represents the normalised time distance at time i and at L_r rainfall resolution length, and n is the number of time steps. We restricted the computation of MAE to the period of heavy rainfall (from 14:00 to 18:00 CET). The relationship between the MAE and the normalised peak discharge error is reported in Fig.5.20a,b, before and after rainfall volume rescaling, respectively. Examination of Figures 5.20b shows that the there is a significant

correlation between the MAE and the peak discharge error. This means that increasing rainfall aggregation leads to increased distortion of spatial rainfall variability with respect to the river network, and that this is an important control on peak discharge error – when rainfall volumes are preserved. On the other hand, there is no significant relationship between MAE and peak discharge error before rainfall volume adjustment. The impact of rainfall resolution on distortion of spatial rainfall variability with respect to flow distance emerges only when rainfall volume errors are adjusted for.

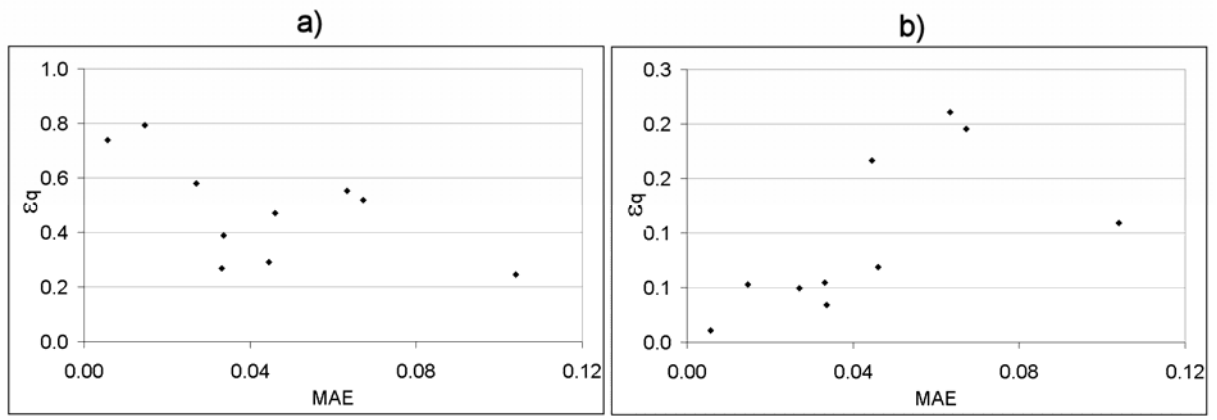

Figure 5.20: Relationship between peak discharge error and Mean Absolute Error (MAE) computed between normalised time distance at 1-km and 16-km rainfall resolution: a) before rainfall volume rescaling, and b) after rainfall volume rescaling.

5. Summary and conclusions

This part of the work focuses on the analysis of the effects of spatial rainfall resolution on runoff simulation for an extreme flash flood event. The increasing availability of radar observations at different spatial resolutions requires examination of the impact of using different aggregation lengths on hydrologic modelling, with specific focus on highly variable flash flood-generating storms. Focus on extreme flash flood events leads, by necessity, to an event-based and opportunistic approach, as opposed to driven by observations from carefully designed field campaigns in experimental watersheds. Extreme, flood-producing storms are spatially and temporally rare and are seldom represented in the observations from experimental watersheds. Accurate post event analyses played an essential role in providing the data required for the present study.

Our evaluations are based on combining fine space-time rainfall observations with a distributed hydrologic modelling based on an empirical infiltration model and a network-based representation of hillslope and channel flow. Radar observations and model analyses are used to evaluate the sensitivity of model results to spatial aggregation of rainfall at various catchment scales ranging from 10.5 km^2 to 623 km^2. Four rainfall spatial resolutions are considered, with grid size equal to 1-, 4-, 8- and 16- km. A dimensionless parameter given by the ratio between length resolution and the square root of the watershed area (L_r/L_w) is used to describe the sensitivity of runoff model.

The analyses are focused on sensitivity of the simulated peak discharges to three different issues: i) rainfall spatial resolution; ii) rainfall volume errors and biased rainfall spatial variability; iii) distortion of rainfall spatial variability with respect to the river network. The principal conclusions of the study are summarized below.

1. Increasing the L_r/L_w parameter induces large errors on the simulated peak discharge. Maximum values of the peak discharge error are up to 0.2 for L_r/L_w equal to 0.5 and to 0.33 for L_r/L_w equal to 1.0. The error may reach values up to 0.75 for L_r/L_w exceeding 2.0. All these errors are negative – i.e. the simulated peak discharge decreases by increasing the L_r/L_w parameter.
2. An important error source related to spatial rainfall aggregation is the rainfall volume error caused by incorrectly "smoothing rainfall volume" either into or out of the watershed. For $L_r/L_w < 1.0$, around 50% of the peak discharge error is due to the rainfall volume error. The remaining error is significantly controlled by the interaction between the attenuated and geometrically biased rainfall spatial variability and the smoothing effects of catchment characteristics.
3. We examined the role of river network geometry in the averaging of space-time rainfall and on simulated peak discharges after rescaling the rainfall fields to preserve rainfall volumes. Increasing the resolution length may lead to a distorted geometry of the rainfall field with respect to the river network. We introduced a metric to account for this effect, and we found that the biased geometry originated by increasing aggregation lengths is significantly correlated with peak discharge errors. This means that increasing rainfall aggregation leads to increased distortion of spatial rainfall variability with respect to the river network, and that this is an important control on peak discharge error – when rainfall volumes are preserved.

Further work might determine whether the results obtained in this investigation apply to other model formulations. The present investigation has obtained illustrative examples of how rainfall variability, as filtered by using different spatial aggregation lengths, feeds through to variability in modelled runoff response at the catchment scale. More extensive investigations would strengthen this understanding and provide additional guidance on the design of radar/raingauge networks for flow forecasting and the spatial resolution requirements for rainfall at different catchment scales. In this framework, future investigations should focus on the sensitivity of the averaging of space-time rainfall fields across locations with equal flow distance coordinates to the rainfall aggregation length and to river network geometry. As shown here, this is a significant and relatively unexplored feature of catchments where rain exhibits significant spatial variability and linear routing through branched channel networks plays a significant role.

Chapter 6 - CONCLUSIONS

The first observation on the analyses carried in this study is that conventional raingauge networks are not able to described rain spatial variability, with appropriate resolution, during convective storms that trigger flash flood event. The use of weather radar doesn't solve the entire problem but it is able to give information about precipitation patters. If these information are correctly collected, elaborated and validated with raingauge comparison and volumetric consideration in hydrological analysis, the chance to reach the ability to answer the basic question "How much did it rained?" considerable increases.

Concerning post event analysis this study includes results about three different event knowledge levels. In Romanian cases, hydrological modelling has been carried on basins where just a rough survey was conducted. This approach doesn't describe completely the analyzed floods and leaves some doubts about the final accuracy. Each analysis contain an accurate elaboration of meteorological data and, where possible, a comparison with available raingauge data. Hydrological quantitative information is quite poor, but it is the usual knowledge on most flash flood events. Model calibration can be used to transfer the parameters and to model the hydrological response at subbasin scale, but this second kind of simulation can't be either validated or rejected since no field data are available. This approach shows a possible path to combine meteorological radar data and distributed hydrological modelling to have a better comprehension of the occurred dynamics and it underlines the problems due to the lack of quantitative and spatial distributed data. With this situation the use of a simplified model is not a limitation, since the main problem is the lack of quantitative and distributed data. These results point the need of collaboration between operational and scientific community: the specific skills of each of the two different approaches can be helpful to data collection and the validation. For this kind of situation, where field data are poor, the simplified KLEM model is suitable for the study: with its simplicity it shows immediately the effect of spatial variability on discharge at different location.

The Slovenian case study is presented as opportunity to combine hydrological modelling and field observations. The KLEM model shows in this case its limitation both for the CN-SCS assumption in runoff generation process and for kinematic wave hypothesis in flood propagation. Computation of effective precipitation through CN-SCS doesn't permit ground deficit recharge, so that at the end of the event the model is very sensible to additional rainfall drenches; the model doesn't admit in its assumption that water can be stored where the topography allows it and so each upstream peak is propagated downstream without attenuation. For these considerations a more realistic and complex model should be used when a great amount of field data are available. Beside that, the study based on *HYDRATE* IPEC in

Slovenia shows how the dynamic understanding process is quite long in time and it requires iterative try and error alternate steps of field observation and flood modelling. The fact that the flood happened not much more than one year ago limits the results as an intermediate step of this process. For final conclusion data will be processed by different hydrological models and probably an additional survey in the region is needed to understand the reasons of some discrepancies between IPEC observations and model results.

August 29, 2003 flash flood validated results at large scale (600km²) have been used to carry a specific analysis on the 0.65 km² Rio Cucco basin. The hydrologic response was simulated using a spatially-distributed, process-based hydrological model. The low initial soil moisture conditions had a remarkable impact of flood formation, causing initial losses exceeding 80 mm. The huge cumulated runoff amounts, together with high rainfall intensities on the time scale of up to one hour, resulted in a flood peak reaching 20 m³/s/km². The major controls of the flood response were the exceptional cumulated rainfall amount, required to exceed the large initial abstractions, and the large rainfall intensities required to generate high flood response. Geomorphic impacts of the event within the drainage basin consisted in intense erosion along the channel network and, locally, in the failure of adjacent slopes. The comparison of the topography of the eroded areas, carried out before and after the event, afforded estimation of the volume of sediments, which estimated amounts from 70'000 to 85'000 m³. A detailed hydrological model (GRISS-2D) was used for the hydrograph estimation and results were combined with solid surveyed volumes to carry out a balance analysis by computing the sediment concentration during the various phases of the event. A particularly high value of sediment concentration was estimated for one of the two surveyed basin: this could be referred to particular dynamics of sediment mobilisation in this sub-basin, in which the failure of temporary channel obstructions and the collapse of the outer channel banks in curves increased the solid concentration of the debris flow.

The studies above described helps to define some suggestions when one is approaching to a flash flood analysis. A detailed spatial distribution may be obtained by an accurate comparison between radar patterns and raingauge data. After validation precipitation field can be used in hydrological analysis to understand flood dynamics. Model results should be compared with spatial distributed data collected in field campaign: precious data comes from cross section peak discharge estimation, accounts from eyewitnesses about timing and flow type during the event, local geomorphologic flood consequences (e.g., debris flow, wood debris, landslide,...).

Chapter 5 aims to examine the role of spatial distribution in flash flood analysis by investigating the effect of spatial aggregation on model results. The literature on the significance of aggregation of rainfall and soil properties for runoff estimation is complex and sometimes contradictory. Effects can be expected to vary depending on the nature of the rainfall, the nature of the catchment, and the spatial scale of the catchment and rainfall. For

temperate regions, the review highlighted the trade-off in terms of catchment response between the impact of spatial variability of rainfall, its aggregation and the smoothing effect due to the heterogeneity of the catchment. The work is motivated by the rapidly expanding body of radar rainfall estimates available for use in flood and flash flood forecasting. The increasing availability of radar observations at different spatial resolutions requires examination of this issue, with specific focus on highly variable flash flood-generating storms. Focus on extreme flash flood events leads, by necessity, to an event-based and opportunistic approach, as opposed to driven by observations from carefully designed field campaigns in experimental watersheds. Extreme, flood-producing storms are spatially and temporally rare and are seldom represented in the observations from experimental watersheds. Accurate post event analyses played an essential role in providing the data required for the present study.

The mountainous areas on the northern border of the Piemonte region and on the Fella river valley in Friuli Venezia Giulia produce some of largest unit discharge peaks in the northern Mediterranean basin and are monitored with a dense network of weather radar, raingauge stations and stream level gauges. This offered an opportunity to examine the impact of spatial aggregation of rainfall and soil properties on extreme flood modelling. Flood response to three extreme storm events, occurred on the Sesia River basin, at four catchment scales ranging from 75 km^2 to 983 km^2, and to one flash flood in Fella basin, at ten subbasin scale from 10.5 to 623km^2 are reproduced by using high resolution radar rainfall estimates.

Four input spatial resolutions are considered, with grid size equal to 1, 4, 8 and 16km, for rainfall and soil properties representation. Two dimensionless parameters given by the ratio between input length aggregation and the square root of the watershed area (L_r/L_w and L_G/L_w for rainfall and soil properties, respectively) are used to describe the sensitivity of the KLEM hydrological model, based on simplistic assumptions: CN-SCS runoff generation method and kinematic wave flood propagation.

The rainfall spatial variability play an important role when rainfall fields are systematically structured across locations with equal flow distance coordinates, as it occurs in the case of orographic effect and when catchments are elongated in the direction perpendicular to the mountainous range. When heavy rainfall lies on a sufficiently narrow range of isochrones, the smoothing effect due to increasing the rainfall aggregation length may result in a significant distortion of the rainfall field geometry with respect to the river network. In these cases, the increase of the spatial rainfall aggregation length leads to a significant deformation of the flood shape, with an anticipation of the simulated flood peak when the precipitation is concentrated towards the periphery of the catchment, and a delay of the simulated flood peak when the precipitation is concentrated towards the outlet of the catchment. These effects are negligible at the small catchment scale and become significant with increasing the catchment size.

When infiltration is ‘switched off’ in the runoff model and all the variability arises due to runoff transport processes, the distortion of the rainfall field geometry with respect to river

network may be an important control on peak discharge error, even at catchment scales less than 500 km^2. Obviously, this distortion has no impact on the runoff volume error, which is in this case completely determined by the rainfall volume error. This volume error arises when rainfall values pertaining to areas just outside the catchment enter the computation of the average rainfall over the basin by increasing the aggregation length. The rainfall volume error is controlled mainly by the ratio L_r/L_w and by the rainfall integral scale; it exerts a dominant impact on peak discharges at small catchment scales, and becomes less significant by increasing the catchment dimension.

Errors on both runoff volumes and peak discharges increase when infiltration is taken into account in the runoff model. This is expected, since the infiltration process injects further spatial variability, both random and structured, into the rainfall-runoff process. The effects of reduced and distorted rainfall spatial variability on peak discharge have been found particularly severe for the flash flood events, with peak errors up to 35% for values of the ratio L_r/L_w around 0.5. Effects are particularly remarkable when significant structured rainfall variability combines with relatively important infiltration rates due to dry initial conditions, as this emphasises the non linear character of the rainfall-runoff transformation. In general, these results confirm that the correct estimate of rainfall volume is not enough for the accurate reproduction of flash flood events characterised by large and structured rainfall spatial variability, even at catchment scales around 250 km^2. However, accurate rainfall volume estimation may suffice for less spatially variable flood events. The results shows also that the rainfall volume errors generally magnify through the rainfall-runoff modelling, at least for the runoff model considered here.

Increasing the soil properties aggregation length exerts similar effects on peak discharge errors as increasing the rainfall aggregation length, for the cases considered here and after rescaling to preserve the rainfall volume. Moreover, peak discharge errors are roughly proportional to runoff volume errors, which indicates that the shape of the flood wave is influenced in a limited way by modifying the detail of the soil property spatial representation. Conversely, rainfall aggregation may exert a pronounced influence on the discharge peak by reshaping the spatial organisation of the runoff volumes and without a comparable impact on the runoff volumes. Even with increasing the soil properties aggregation length, effects are particularly remarkable in those cases characterised by low runoff values and low values of runoff coefficients.

The present investigation has documented how input variability, as filtered by using different spatial aggregation lengths, feeds through to variability in modelled runoff response at the catchment scale. More extensive investigations would strengthen this understanding and provide additional guidance on the design of radar/raingauge networks for flow forecasting and the spatial resolution requirements for rainfall and soil properties at different catchment scales. Further work might determine whether the results obtained in this investigation apply to other model formulations and may be generalised to other hydroclimatic environments.

Future investigations should focus on the sensitivity of the averaging of space-time rainfall fields across locations with equal flow distance coordinates to the rainfall aggregation length and to river network geometry. As shown here, this is a significant and relatively unexplored feature of catchments where rain exhibits significant spatial variability and linear routing through branched channel networks plays a significant role.

REFERENCES

ACTIF (2004): Some research needs for river flood forecasting in FP6, EVK1-CT-2002-80014, www.actif-ec.net.

Agnese C., Baiamonte G. and Corraro C. (2001): A simple model of hillslope response for overland flow generation, *Hydrological processes*, 15, 3225-3238.

AMS: American Meteorological Society (2000): Glossary of Meteorology, T. S. Glickman Ed., 2nd Edition, Boston MA-USA.

Anagnostou M.N., Kalogeros J., Tarolli M., Anagnostou E.N., Borga M., and Papadopoulos A. (2008): Rainfall Measurements of X-band Polarimetric Weather Radar in Complex Terrain, *proceeding for ERAD* - the 5th European conference on radar in meteorology and hydrology.

Andréassian V., Perrin C., Michel C., Usart-Sanchez I. and Lavabre J. (2001): Impact of imperfect rainfall knowledge on the efficiency and the parameters of watershed models, *Journal of Hydrology*, 250, 206-223.

Andrieu H. and Creutin J.D. (1995): Identification of Vertical Profiles of Radar Reflectivity for Hydrological Applications Using an Inverse Method. Part II: Formulation, *Journal of Applied Meteorology*, 240-259.

ARSO (2007): Poročilo o vremenski in hidrološki situaciji18, www.arso.gov.si (in Slovenian).

Bain V., Gaume E. , Marchi L., Sangati M. and Borga M. (2009): Post event analysis of a flash flood on the Selscica Sora River in Slovenia, *HYDRATE document*.

Barancourt C., Creutin J. D., and Rivoirard J. (1992): A Method for Delineating and Estimating Rainfall Fields, *Water Resources Research*, *28*(4), 1133-1144.

Battan L.J. (1973): Radar observation of the atmosphere, University of Chicago Press, 324 pages.

Bell V.A. and Moore R.J. (2000): The sensitivity of catchment runoff models to rainfall data at different spatial scales. *Hydrology and Earth System Sciences*, 4(4), 653-667.

Benson M.A. and Dalrymple T. (1967): General field and office procedures for indirect discharge measurements, U.S. *Geological Survey Tech. Water Resour. Invest.*, Book 3, Chapter A.

Berenguer M., Lee G. W., Sempere-Torres D., and Zawadzki I. (2002): A variational method for attenuation correction of radar signal, *Proceedings for ERAD*, 11-16.

Berne A., Delrieu G., Creutin J.D. and Obled C. (2004): Temporal and spatial resolution of rainfall measurements required for urban hydrology, *Journal of Hydrology*, 299(3-4), 166-179.

Beven K.J. (1982): kinematic subsurface stormflow, *Water Resources Research*, 17(5), 1419-1424.

Beven K.J. and Hornberger G.M. (1982): Assessing the effect of spatial pattern of precipitation in modelling stream flow hydrographs, *Water Resources Bulletin*, 18, 823-829.

Blöschl G. and Sivapalan M. (1995): Scale issues in hydrological modelling: a review, *Hydrological Processes* 9: 251-290.

Bonacci O. (2004): Hazards caused by natural and anthropogenic changes of catchment area in karst, *Hydrogeol. J.*, 4, 655-661.

Borga M., Boscolo P., Zanon F., Sangati M. (2007): Hydrometeorological analysis of the August 29, 2003 flash flood in the eastern Italian Alps*, J. Hydrometeorology*, 8(5), 1049-1067.

Borga M., Gaume E., Creutin J.D., Marchi L. (2008): Surveying flash floods: gauging the ungauged extremes, *Hydrological Processes, 22*(18), 3883-3885**.**

Borga, M., Anagnostou E.N. and Frank E. (2000): On the use of real-time radar rainfall estimates for flood prediction in mountainous basins, *Journal of Geophysical Research*, 105, D2, 2269-2280.

Borga M., Tonelli F., Moore R.J. and Andrieu H. (2002): Long-term assessment of bias adjustment in radar rainfall estimation, *Water Resources Research*, 38(11), 1226.

Borga M., Degli Esposti S. and Norbiato D. (2006): Influence of errors in radar rainfall estimates on hydrological modelling prediction uncertainty, *Water Resources Research, 42*, W08409.

Bouilloud L., Delrieu G. , Boudevillain B., Zanon F. and Borga M. (2009): Radar rainfall estimation for the post-event analysis of a Slovenian flash-flood case: application of the mountain reference technique at C-band frequency, *HYDRATE document*.

Bras R.L. (1990): Hydrology an introduction to hydrologic science, Addison-Wesley, Reading, MA-USA.

Brilly M., Rakovec J. (1996): Use of radar for flood forecasting, Acta Hydrotehnica, University of Ljubljana, Faculty of Civil Engineering and Geodesy, 14/12, Ljubljana.

Bringi V.N., Ran J. and Chandrasekar V. (1998): Polarimetric radar and surface observation of a flash flood, *Geoscience and Remote Sensing Symposium Proceedings*, IGARSS'98, IEEE International, 1:144-146.

Burrell E.M. and Gruntfest E. (2002): Flash flood mitigation: recommendations for research and applications, Global Environmental Change Part B, *Environmental Hazard*, 4(1), 15-22.

Campos E. and Zawadzki I. (2000): Instrumental uncertainties in Z-R relations, *J. Appl. Meteor.*, 39, 1088-1102.

Caroni E., Rosso R. and Siccardi F. (1986): Nonlinearity and time-variance of the hydrologic response of a small mountain creek; in: Gupta V.K. et al. (Eds.), "Scale Problems in Hydrology", D. Reidel Publishing Company, 19-37.

Carraro F., Dal Piaz G.V., Govi M. and Sacchi R. (1969): Il dissesto idrogeologico del 2 novembre 1968 nel bacino della Strona a monte di Cossato, in Studi Geologici nel Vercellese e nella Valle Strona, CNR Torino (in Italian).

Cazorzi F. and Dalla Fontana G. (1992): L'utilizzo dei sistemi informativi geografici nello studio idrologico di bacino, *Quaderni di Idronomia Montana*, 12 (in Italian).

Cazorzi F. and Bincoletto L. (2005): Modellazione dei processi idrologici, in: "La prevenzione del rischio idrogeologico nei piccoli bacini montani della regione: Esperienze e conoscenze acquisite con il progetto *CATCHRISK*", Convegno finale del Progetto CATCHRISK, Udine, 28-29 Giugno 2005, 45-74 (in Italian).

Chow V.T. (1959): Open-chanel hydraulics, McGraw-Hill Book Company.

Costa J.E. (1988): Rheologic, geomorphic, and sedimentologic differentiation of water floods, hyperconcentrated flows, and debris flows, in Flood Geomorphology, Baker V.R., Kochel R.C., Patton P.C., Eds. J. Wiley & Sons: New York; 113-122.

Costa J.E. (1987): Comparison of the largest rainfall-runoff floods in the United States with those of the People 's Republic of China and the world, *Journal of Hydrology*, 96(1-4), 101-115.

Coussot P., Meunier M. (1996): Recognition, classification and mechanical description of debris flows, *Earth-Science Reviews*, 40, 209-227.

Creutin J.D., Borga M. (2003): Radar hydrology modifies the monitoring of flash flood, *Hydrological Processes*, 17, 1453-1456**.**

Da Ros D. and M. Borga, 1997: Use of digital elevation model data for the derivation of the geomorphologic instantaneous unit hydrograph, *Hydrological Processes*, 11, 13-33.

David-Novak H., Morin E., Enzel Y. (2004): Modern extreme storms and the rainfall thresholds for initiating debris flows on the hyperarid western escarpment of the Dead Sea, Israel, *GSA Bulletin*, 116, 718-728.

Delrieu G., Caoudal S. and Creutin J. D. (1997): Feasibility of using mountain return for the correction of ground based X-band weather radar data, *Journal of Atmospheric and Oceanic Technology*, 14, 368-385.

Delrieu G., Ducrocq V., Gaume E., Nicol J., Payrastre O., Yates E., Kirstetter P.E., Andrieu H., Ayral P.A., Bouvier C., Creutin J.D., Livet M., Anquetin S., Lang M., Neppel L., Obled C., du-Châtelet J.P., Saulnier G.M., Walpersdorf A. and Wobrock W. (2005): The catastrophic flash-flood event of 8-9 September 2002 in the Gard Region, France: a first case study for the Cévennes-Vivarais Mediterranean Hydrometeorological Observatory, *J. Hydrometeor.*, 6, 34-52.

Dolinar M. (2000): Abundant precipitation during the 1998 Autumn Floods, Ujma 13, 151-159.

Doswell C.A., Brooks H.E. and Maddox R.A. (1996): Flash flood forecasting: an ingredients-based methodology, *Wea. Forecasting*, 11, 560-581.

Eisbacher G.H., Clague J.J. (1984): Destructive mass movements in high mountains: hazard and management, *Geol. Survey of Canada*, Paper 84-16; 230.

Fabry F. (1995): Vertical profiles of reflectivity and precipitation intensity, *Proceedings of the III International Symposium on Weather Radars*, San Paulo, Brazil.

Fabry F., and Zawadzki I. (1995): Long-term radar observations of the melting layer of precipitation and their interpretation, *J. Atmos. Sci.*, 52, 838-851.

Fiedler F.R. (2004): CE504 Computational Hydrology - Infiltration Equations, www.webs1.uidaho.edu.

Foody G.M., Ghoneim E.M. and Arnell N.W. (2004): Predicting locations sensitive to flash flooding in an arid environment, *Journal of Hydrology*, 292(1-4), 48-58.

Frei C. and Schär C. (1998): A precipitation climatology of the Alps from high-resolution rain-gauge observations, *Int. J. Climatol.*, 18.

Gabet E.J., Bookter A. (2008): A morphometric analysis of gullies scoured by post-fire progressively bulked debris flows in southwest Montana, USA, *Geomorphology* 96, 298-309.

Gaume E., Livet M. and Desbordes M. (2003): Study of the hydrological processes during the Avene river extraordinary flood (south of France): 6-7 October 1997, *Physics and Chemistry of the Earth*, 28, 263-267.

Gaume E. (2006): Post flash flood investigation - Methodological note, www.floddsite.net.

Gaume E., Bain V., Bernardara P. and Borga M.: First Year *HYDRATE* Report Project, WorkPackage 1 on Flash Flood Primary data analysis, *HYDRATE document*.

Georgakakos, K.P. (1986): On the design of national real-time warning systems with capability for site-specific flash flood forecasts, *Bull. Am. Meteorol. Soc.*, 67, 1233-1239.

Ghioca M. (2006): Spatial and temporal variability of Romanian precipitation and river Flows on winter period in connection with the North Atlantic oscillation, National Institute of Hydrology and Water Management, Bucharest, Romania.

Giannoni F., Smith J. A. , Zhang Y. and Roth G. (2003): Hydrologic modelling of extreme floods using radar rainfall estimates, *Adv. Water Resour.,* 26, 195- 200.

Gouldby B., Samuels P., Klijn F., Messner F., van Os A., Sayers P. and Schanze J. (2007): Language of Risk - Project definitions, FLOODsite document, T32-04-01, www.floodsite.com.

Green W.H. and Ampt G.A. (1911): Studies on soil physics, part 1, The flow of air and water through soils, *J. Agric. Sci.*, 4, 1-24.

Gruntfest E., and Huber C.J. (1991): Toward a comprehensive national assessment of flash flooding in the United States, *Episodes*, 14, 26-35.

Gupta V. K., Castro S. and Over T. M. (1996): On scaling exponents of spatial peak flows from rainfall and river network geometry, *Journal of Hydrology*, 187(1-2), 81-104.

Hicks N.S., Smith J.A., Nelson P.A. (2005): Catastrophic flooding from an orographic thunderstorm in the central Appalachians, *Water Resources Research*, 41, W12428.

Hildebrand P.H. (1978): Iterative correction for attenuation of 5 cm radar in rain, *J. Appl. Meteor.*, 17, 508-514.

Hirschboeck K.K. (1987): Catastrophic flooding and atmospheric circulation anomalies, Pp. 23-56 in Catastrophic Flooding, L. Mayer and D. Nash, Eds. Boston: Allen and Unwin.

Hitschfeld W. and Bordan J., (1954): Errors inherent in the radar measurement of rainfall at attenuating wavelengths, *J. Atmos. Sci.*, 11(1), 58-67.

House P.K., and Pearthree P.A. (1995): A geomorphic and hydrologic evaluation of an extraordinary flood discharge estimate: Bronco Creek, Arizona, *Water Resources Research*, 31(12), 3059-3073.

Houze R.A., James C.N. and Medina S., (2001): Radar observations of precipitation and airflow on the Mediterranean side of the Alps: Autumn 1998 and 1999, *Quart. J. Roy. Meteor. Soc.*, 127**,** 2537-2558.

Hubbert J. and Bringi V.N. (1995): An iterative filtering technique for the analysis of copolar differential phase and dual-frequency radar measurements, *J. Atmos. Ocean. Technol.*,12,643-648.

Jakob M., Anderson D., Fuller T., Hungr O., Ayotte D. (2000): An unusually large debris flow at Hummingbird Creek, Mara Lake, British Columbia, *Canadian Geotechnical Journal* 37, 1109-1125.

Jarrett R.D. (1987): Errors in slope-area computations of peak discharges in mountain streams, *Journal of Hydrology*, 96, 53-67.

Jarrett R.D. (1990): Hydrologic and Hydraulic Research in Mountain Rivers, *Water Resources Bulletin*, 26(3), 419-429.

Joss J. and Gori E.G.(1978): Shapes of raindrop size distributions, *J. Appl. Meteor.*, 17,1054-1061.

Joss J. and Waldvogel A. (1968): Raindrop size distribution and sampling size errors, *J. Atmos. Sci.*, 26, 566-569.

Journel A.G. (1983): Non parametric estimation of spatial distributions, *Math. Geol*., 15(3), 445-467.

Journel A.G. and Huijbregts C.J. (1978): Mining geostatistics, Academic Press, London - UK, 600 pp.

Kavvas M.L., Yoon J.Y., Chen Z.Q., Liang L., Dogrul E.C., Ohara N., Aksoy H., Anderson M.L., Reuters J. and Hackley S. (2006): Watershed environmental hydrology model: environmental module and its application to a California watershed, *ASCE Journal of Hydrologic Engineering*, 11(3), 261-272.

Kelsch M., Lanza L., and Caporali E. (2000): Hydrometeorology of flash floods, NATO Advanced Study Institute: Coping With Flash Floods, E. Grunfest and J Handmer ed., Kluuwer Press, The Netherlands, 19-35.

Kolbezen M. (1991): Flooding in Slovenia on November 1, 1990, Ujma No. 5, Ljubljana, 16-18.

Komac B., Natek K. and Zorn M. (2008): Influence of spreading urbanization in flood areas on flood damage, XXIVth Conference of the Danubian Countries on the hydrological forecasting and hydrological bases of water management.

Krajewski W.F. (1995): Rainfall estimation using weather radar and ground stations, *Proceedings of the III International Symposium on Weather Radars*, San Paulo, Brazil.

Le Lay M. and Saulnier G.M. (2007): Exploring the signature of climate and landscape spatial variabilities in flash flood events: Case of the 8-9 September 2002 Cévennes-Vivarais catastrophic event, *Geophys. Res. Lett.*, *34*, L13401.

Lewis H.W., Harrison D.L. and Kitchen M. (2007): Local vertical profile corrections using data from multiple scan elevations, Met. Office, United Kingdom, *Proceedings for 33rd Conference on Radar Meteorology*.

Liljequist G.H. and Cehak K. (1984): Allgemeine Meteorologie, Vieweg Verlag, Braunschweig, Germany (in German).

Lin X. (1999): Flash floods in arid and semi-arid zones, IHP-V Technical Documents in Hydrology, no. 23 (International Hydrological Programme, UNESCO).

Marchi L. and Bain V. (2008): IPEC Report - Intensive Post-Event Campaign in the Selscica Sora river basin, Slovenia, after the flash flood of september 18, 2007, *HYDRATE document*.

Marchi L. and D'Agostino V. (2004): Estimation of debris-flow magnitude in the Eastern Italian Alps, *Earth Surface Processes and Landforms*, 29(2), 207-220.

Marchi L., Pasuto A. (1999): A debris flow in the Dolomites, Northeastern Italy, *Landslide News,* 12, 9-12.

Marchi L., Borga M., Sangati M. and Cavalli M. (2009): Hydrological controls and erosive response of a major alpine debris flow, *Hydrological Processes, under review*.

Marshall J.S. and Palmer W.K. (1948): The distribution of raindrop size to intensity. *J. Meteor.*, 5(165-166).

Marwitz J.D. (1972): The structure and motion of severe hailstorms; part I: supercell storms; part II: multi-cell storms, Part III: severely sheared storms, *J. Appl. Meteor.*, 11, 166-201.

Merz B. and Bardossy A. (1998): Effects of spatial variability on the rainfall runoff process in a small loess catchment, *Journal of Hydrology*, 212-213, 304-317.

Merz, B. and E.J. Plate (1997): An analysis of the effects of spatial variability of soil and soil moisture on runoff, *Water Resour. Res*., 33(12), 2909-2922.

Michaud J.D., Hirschboeck K.K.and Winchel M. (2001): Regional variations in small-basin floods in the United States, *Water Resources Research*, 37, 1405- 1416.

Milly P. and Eagleson, P. (1988): Effects of storm scale on surface runoff volume, *Water Resources Research*, 24, 620-624.

Montandon F. (1933): Chronologie des Grands Eboulements Alpins du début de l'ère chrétienne à nos jours, *Société de Géographie Genève*, Matériaux pour l'étude des calamités, 32, Genève, 271-340 (in French).

Moody J.A. and Kinner D.A. (2005): Spatial structures of stream and hillslope drainage networks following gully erosion after wildfire, *Earth Surface Processes and Landforms*, www.interscience.wiley.com.

Moody J.A. and Martin D.A. (2001): Post-fire, rainfall intensity-peak discharge relations for three mountainous watersheds in the western USA, *Hydrological Processes*, 15(15) 2981-2993.

Moore I.D. (1985): Kinematic overland flow: generalization of Rose's approximation solution, *Journal of Hydrology*, 82, 233-245.

Mortara G., Dutto F., Godone F. (1995): Effetti degli eventi alluvionali nell'ambiente proglaciale: la sovraincisione della morena del ghiacciaio del Mulinet (Stura di Valgrande, Alpi Graie), *Geografia Fisica e Dinamica Quaternaria*, 18(2), 295-304 (in Italian).

Moulin L., Gaume E. and Obled C. (2008): Uncertainties on mean areal precipitation: assessment and impact on streamflow simulations, *Hydrology and Earth System Science Discussion,* 5, 2067-2110.

Naden P.S. (1992): Spatial variability in flood estimation for large catchments: the exploitation of channel network structure, *Hydrol. Sci. J.*, 37, 53-71.

Nicotina L., Alessi Celegon E., Rinaldo A. and Marani M. (2008): On the impact of rainfall patterns on the hydrologic response, *Water Resources Research*, 44, W12401.

Norbiato D., Borga M., Sangati M., Zanon F. (2007): Regional Frequency Analysis of Extreme Precipitation in the eastern Italian Alps and the August 29, 2003 Flash Flood, *Journal of Hydrology*, 345(3-4), 149-166.

Norbiato D., Borga M., Degli Esposti S., Gaume E. and Anquetin S. (2008): Flash flood warning based on rainfall depth-duration thresholds and soil moisture conditions: an assessment for gauged and ungauged basins, *Journal of Hydrology*, 362(3-4).

O'Connor J. E. and Costa J.E. (2004): Spatial distribution of the largest rainfall-runoff floods from basins between 2.6 and 26,000 km² in the United States and Puerto Rico, *Water Resources Research*, 40, W01107.

Obled C., Wendling J. and Beven K. (1994): The sensitivity of hydrological models to spatial rainfall patterns: an evaluation using observed data, *Journal of Hydrology*, 159(1-4), 305-333.

Ogden F.L. and Julien P.Y. (1994): Runoff model sensitivity to radar rainfall resolution, *Journal of Hydrology*, 158, 1-18.

Orlanski I. (1975): A rational subdivision of scales for atmospheric processes, *Bull. Am. Meteorol. Soc.*, 56(5), 527-530.

Payrastre O., Gaume E. and Andrieu H. (2005): Use of historical data to assess the occurrence of floods in small watersheds in the French Mediterranean area, *Advances in Geosciences*, 2, 313-320.

Pellarin T., Delrieu G., Creutin J. D. and Andrieu H. (2000): Hydrologic visibility of weather radars operating in high-mountainous regions: A case study for the Toce catchment

(Italy) during the Mesoscale Alpine Programme, Physics and Chemistry of the Earth, Part B: Hydrology*, Oceans and Atmosphere*, 25, 953-957.

Pessoa M.L., Bras R.L. and Williams E.R. (1993): Use of Weather Radar for Flood Forecasting in the Sieve River Basin: A Sensitivity Analysis, *Journal of Applied Meteorology*, 32, 462-475.

Ponce V.M. and Hawkins R.H. (1996): Runoff curve number: has it reached maturity?, *J. Hydrologic Eng*., 1(1), 11-19.

Rajar R., Zakrajšek M. (1993): Modelling of flood wave, caused by overtopping of landslide created dam, Ujma No 7, Ljubljana, 77-80.

Reid I. and Frostick L.E. (2006): Flow dynamics and suspended sediment properties in arid zone flash floods, *Hydrological Processes*, 1(3), 239-253.

Reya O., (1946): Carte de precipitation's de la Slovenie, Publ. by ZMG, Univ. of Ljubljana (in French).

Rickenmann D., Zimmermann M. (1993): The 1987 debris flows in Switzerland: documentation and analysis, *Geomorphology*, 8, 175-189.

Rinaldo A., Vogel G.K., Rigon R. and Rodriguez-Iturbe I. (1995): Can one gauge the shape of a Basin?, *Water Resources Research*, 31(4), 1119-1127.

Rose C.V., Parlange J.Y., Sander G.C., Campbell S.Y. and Barry D.A. (1983): Kinematic flow approximation to runoff on a plane: an approximate analytical solution, *Journal of Hydrology*, 62, 363-369.

Rosenthal E.M. (1993): The Johnstown Flood, The Journal of American history.

Rosso R. and Serva L. (1998): 9 giugno 1996 - Alluvione in Versilia e Garfagnana, ARTPAT (Agenzia regionale per la protezione ambientale della Toscana) and ANPA (Agenzia nazionale per la protezione dell'ambiente).

Saghafian B. and Julien P.Y. (1995): Time to equilibrium for spatially variable watersheds, *Journal of Hydrology*, 172, 231-245.

Sangati M. and Borga M., 2009: Influence of rainfall spatial resolution on flash flood modelling, *Natural Hazards and Earth System Sciences, under review*.

Sangati M., Borga M., Rabuffetti D. and Bechini R. (2009): Influence of rainfall and soil properties spatial aggregation on extreme flash flood response modelling: an evaluation based on the Sesia river basin, North Western Italy, *Adv. Water Resour.,* doi:10.1016/j.advwatres.2008.12.007.

Segond M.L., Wheater H.S. and Onof C. (2007): The significance of spatial rainfall representation for flood runoff estimation: a numerical evaluation based on the Lee catchment, UK, *Journal of Hydrology*, 347, 116-131.

Sekhon R.S. and Srivastava R.C. (1970): Doppler radar observations of rain drop distributions in a thunderstorm, *J. Atmos. Sci.*, 28:983-994.

Serrar S., Delrieu G., Creutin J. D., and Uijlenhoet R. (2000): Mountain reference technique - The use of mountain returns to calibrate weather radars operating at attenuating wavelengths, *Journal of Geophysical Research*, 105**,** 2281-2290.

Shah S.M.S., O'Connell P.E. and Hosking J.R.M. (1996): Modelling the effects of spatial variability in rainfall on catchment response - 2. Experiments with distributed and lumped models, *Journal of Hydrology*, 175, 89-111.

Šipec S. (2001): Natural and Other Disasters and Incidences in Slovenia in 1999, UJMA, 14-15, 26-28.

Sivapalan M. (2006): Pattern, Process and Function: Elements of a Unified Theory of Hydrology at the Catchment Scale, Encyclopedia of Hydrological Sciences- Part 1. Theory, Organization and Scale.

Skøien, J.O. and Blöschl G. (2006): Scale Effects in Estimating the Variogram and Implications for Soil Hydrology, *Vadose Zone Journal*, 5, 153-167.

Smith J. A., Baeck M.L., Meierdiercks K.L., Nelson P.A., Miller A.J., and Holland E.J. (2005): Field studies of the storm event hydrologic response in an urbanizing watershed, *Water Resources Research*, 41, W10413.

Smith M.B. , Seo D.J., Koren V.I., Reed S.M., Zhang Z., Duan Q., Moreda F. and Cong S., 2004: The distributed model intercomparison project (DMIP): motivation and experiment design, *Journal of Hydrology*, 298, 4-26.

Stancalie G., Oprea C., Irimescu A., Antonescu B., Burcea S., Catana S., Cheval S., Dumitrescu A. and Breza T. (2008): Severe flash flood in Romania - Case studies, EMS8/ECAC7 Abstracts, Vol. 5, EMS2008-A-00253.

Steiner M., Houze R.A., Yuter S.E. (1995): Climatological characterisation of three-dimensional storm structure from operational radar and rain gauge data, *J. Appl. Meteorol.*, 34, 1978-2007.

Stiny J., (1910): Debris flows - An attempted monograph with particular reference to the conditions in the Tyrolean Alps. (Or. title: Die Muren - *Bersuch einer Monographie mit besonderer Berückstichtigung der Berhältnisse in den Tiroler Alpen*. Verlag der Wagnerischen Universitäts - Buchandlung, Innsbruck.) Translated from the German by M. Jakob and N. Skermer, EBA Engineering Consultants Ltd., Vancouver, Canada, 1997, 105 pp.

Tarboton D.G. (2003): Rainfall-Runoff Processes, http://www.webs1.uidaho.edu/ch/notes/intro.pdf.

Thouret J.C., Vivian H., Fabre D. (1995): Instabilité morphodynamique d'un bassin-versant alpin et simulation d'une crise érosive (L'Eglise-Arc 1800, Tarentaise), *Bulletin de la Societé Géologique de France*, 166(5), 587-600 (in French).

Tropeano D., Turconi L., Sanna S. (2004): Debris flows triggered by the 29 August 2003 cloudburst in Val Canale, Eastern Italian Alps, *International Congress Interpraevent 2004*, 1(1), 121-132.

Ulbrich C.W. (1983): Natural variations in the analytical form of the raindrop size distribution, *J. Clim. Appl. Meteor.*, 22, 1764-1775.

U.S. SCS (1986): Urban hydrology for small watersheds, *U.S. Department of Agriculture Tech. Release*, 55, 164 pp.

Vivekanandan J., Yates D.N. and Brandes E.A. (1999): The influence of terrain on rainfall estimates from radar reflectivity and specific propagation phase observations, *J. Atmos. Oceanic Technol.*, 16, 837-845.

Vrhovec T., Cegnar T., Costantini D., Castracane D., Siani A.M. and Palmieri P. (1998): Modelling urban heat island: the case of a Mediterranean town and a continental one, *Proceeding for European Conference on Applied Climatology*.

Waldvogel A. (1974): The N_0 jump of raindrop spectra, *J. Atmos. Sci.*, 31, 1067-1078.

Winchell M., Gupta H., and Sorooshian S. (1998): On the simulation of infiltration- and saturation-excess runoff using radar-based rainfall estimates: effects of algorithm uncertainty and pixel aggregation, *Water Resources Research*, 34(10), 2655-2670.

Wingmosta M.S. and Lettenmaier D.P. (1999): A comparison of simplified methods for routing topographically diven subsurface flow, *Water Resourches Research*, 35(1), 255-264.

Woods R.A. and M. Sivapalan, (1999): A synthesis of space-time variability in storm response: rainfall, runoff generation and routing, *Water Resources Research*, 35(8), 2469-2485.

Woolhiser, D.A., Smith R.E., and Giraldez J.V. (1996): Effects of Spatial Variability of Saturated Hydraulic Conductivity on Hortonian Overland Flow, *Water Resources Research*, 32(3), 671-678.

WMO (World Meteorological Organization) (1994): Guide to hydrological practices, WMO-164, WMO, Geneva (5th edn), WMO-N.168, Geneva, Switzerland.

Yatheendradas S., Wagener T., Gupta H., Unkrich C., Goodrich D., Schaffner M. and Stewart A. (2008): Understanding uncertainty in distributed flash flood forecasting for semiarid regions, *Water Resources Research*, 44, W05S19.

Zhang Y., Smith J.A., and Baeck M.L. (2001): The hydrology and hydrometeorology of extreme floods in the Great Plains of eastern Nebraska, *Adv. Water Resour.,* 24**,** 1037-1050.

www.mcwar.org/articles/types/tstorm_types.html

www.meteogiornale.it/reportages/read.php?id=397